UNIVERSITY
OF TRENTO - Italy
Department of Materials Engineering
and Industrial Technologies

Doctoral School in Materials Engineering – XXII cycle

Cell sheet engineering: smart polymers and self-assembled monolayers

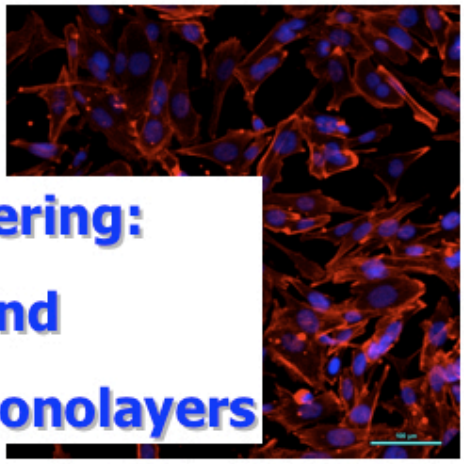

Dario Zeni

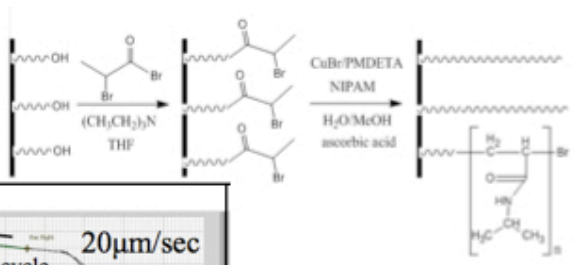

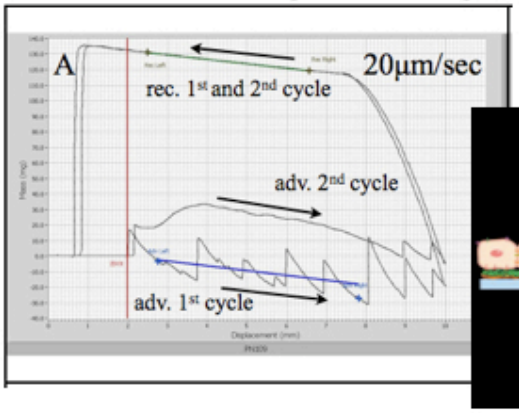

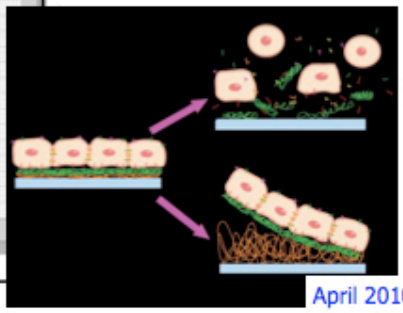

April 2010

“semel in anno *rinsavire* licet”

TABLE of CONTENTS

PREFACE and OBJECTIVES

Cell-based therapies have a relatively long tradition in modern medicine. Since the 70s surgeons tried to treat malignant and non-malignant disease with direct injection of bone marrow cells[1]. Other cell-based therapies have been proposed after these initial achievements, but it was only in the late eighties that a new concept of therapy, based on cells, has been organically developed. In that years, R. Langer, J. and C. Vacanti proposed the combined use of cells and materials (i.e., scaffolds) to repair tissues and organs, so overcoming the several problems associated with the use of transplants[2,3,4]. They coined the term "tissue engineering" as "an interdisciplinary field that applies the principles of engineering and life sciences toward the development of biological substitutes that restore, maintain, or improve tissue function or a whole organ"[3].

The practical application of these concepts started at the Howard Green & Associates with the researches on cultured sheets of autologous epidermis transplanted to patients suffering from different types of skin lesions[1]. Other remarkable examples followed this initial attempt. Autologous osteoblast cells, taken from the periosteum and seeded into coral scaffolds, have been used to reconstruct the traumatically lost thumb of a patient[5]. Occluded pulmonary arteries, replaced with a polycaprolactone-polyglycolic acid copolymers scaffold, seeded with own patient peripheral blood vessels cells, gave positive results[6]. Similarly, isolated vascular smooth muscles and endothelial cells were used to reconstruct arteries[7]. Another example is the attempted substitution of surgical bladder augmentation in favour of tissue engineered bladders made by collagen in which urothelial and smooth muscle cells have been seeded[8].

The therapeutic approaches on which tissue engineering has been initially based can be divided in two major techniques: i) the use of scaffold embedded with cells that adhered and proliferated in it and ii) direct seeding of isolated cells in the injured part to promote

regeneration.

In more recent time, however, an new approach has been developed by a Japanese research group coordinated by prof. Okano. This has been named by him “cell sheet engineering”. The technique is based on the possibility to harvest an undamaged sheet of cells that can be directly transplanted to the injured organ and promote its recovery. Cell sheet engineering possess some advantages over the other techniques as will be clear from the next chapter. Nevertheless, it needs to be improved and, in particular, further studies are necessary to better comprehend the mechanisms by which the cell layer is harvested. This process is based on the behaviour of a “smart polymer” called poly(N-isopropylacrylamide) (PNIPAM) that is capable to trigger cells adhesion simply varying temperature. At 37 °C, cells can adhere and proliferate on substrates grafted with this peculiar polymer, but, once temperature is decreased, it modifies its structure causing cell detachment. If the cells are confluent, then a cell sheet can be harvested and, consequently, used for tissue engineering applications.

The focus of the present work has been the study and characterization of smart substrates employed for cell sheet engineering.

A general overview on tissue engineering and “cell sheet engineering” applications are summarized in the background (Chapter 1).

The state of the art on the different substrates employed and the behaviour of smart polymer are introduced. The general introduction is concluded with the basic concepts on the synthesis route adopted (Chapter 2).

The experimental section is divided in two distinct parts:

1) the first part (Chapter 3) is focused on PNIPAM. A deeper description of the characteristics and the applications for this polymer are presented in a brief introduction. Then, the synthesis and general characterization of the polymer are discussed. The smart properties of tethered PNIPAM are tested by *in vitro* cell cultures and cell sheets, harvested from the obtained samples, characterized. The behaviour of the outermost region of the PNIPAM-coating are deeply investigated by means of Wilhelmy plate technique. A possible model for the evolution of the observed phenomena is given. In the end, an analysis related to the influence of PNIPAM thickness is presented. In particular, the correlation between the polymer chins length and the smart behaviour is investigated by cell culture test and dynamic

contact angle.

2) The second part of the of the work (Chapter 4) is dedicated to a different approach to obtain a cell sheet. In the initial section of the chapter, a possible electroactive substrate is examined as an alternative to PNIPAM. The unexpected results, however, led to a different strategy that is presented. Despite limited to a specific cell line, this method allowed for a simple cell sheet harvesting that is described. A possible application is proposed and the characterization of the substrates used for this approach are exposed. Finally, the biological response and the cell sheets obtained by this method are studied.

Chapter 1

1 GENERAL INTRODUCTION:

Tissue Engineering and Cell Sheet Engineering Background

Chapter 1

Chapter 1

Tissue Engineering and Cell Sheet Engineering Background

Tissue engineering is an emerging multidisciplinary field involving biology, medicine, and engineering that uses cells for either therapeutic or diagnostic applications.

Since the beginning, tissue engineering has proceeded in two distinct main directions: i) the use of scaffolds loaded with cells that adhered and proliferated in it and ii) direct injections of isolated cells to the injured part to promote regeneration.

The former methodology derives from consolidated techniques based on scaffolds that, for many years, have been traditionally implanted in damaged tissue to facilitate organs healing (...). Researchers hoped that the use of polymer biodegradable structures, loaded with proper cells, could lead to faster regeneration, even when the scaffold alone failed. Biodegradable polymers, modelled in the form of an implantable structure, cover a broad range of mechanical or functional properties and have been largely studied. The wide knowledge accumulated during years of *in vitro* and *in vivo* tests greatly helped in combining materials, with the most suitable functional and degradation characteristics, and specific cell lines for the recovery of injured host sites. The basic idea is that, once implanted, the polymer scaffold is reabsorbed by the body, meanwhile cells produce the missing tissue, that is progressively remodelled becoming soon full functional[1,2]. Despite great expectations, for many applications the results are still unsatisfactory and complications limit the rate of success. Yang, Yamato and Okano repeatedly underlined[1,2] that one of the major problems linked to this methodology is a strong inflammatory response that may occur during the polymer degradation[3].

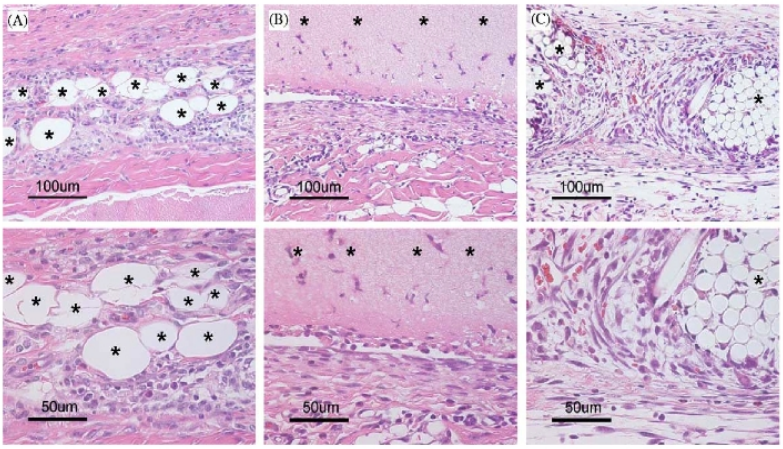

Figure 1.1: Inflammation due to biodegradable scaffolds. Hematoxylin and eosin staining demonstrates non-specific inflammatory responses after the implantation of (A) mannitol-poly(lactic-co-glycolic acid) co-polymer microspheres (45–70 mm in diameter), (B) fibrin gel, and (C) poly(lactic-co- glycolic acid). Asterisks indicate the locations of the implanted polymer materials. Upper and lower panels represent 20 and 40 magnification, respectively[2].

A non-specific inflammation is always expected and even welcomed because is part of the regular process of foreign body integration and of the subsequent healing of a wounded tissue. The use of biological materials as fibrin or collagen gel, can lead to a quasi-natural process but these materials cannot fit all the requirements. Okano et al. stated that many other polymers, despite their interesting characteristics, induced a protracted state of inflammation as consequence of scaffold biodegradation that is not well tolerated, even if the by-products of the reaction are non-toxic (Figure 1.1). In practical terms what happens is the initial migration of activated macrophages and neutrophils with collagenase and elastase activities in the site of the wounded tissue as consequence of body healing response. The environment generated by the cells of the immune system can be of little impact on the polymer scaffold but can severely damage the transplanted cells, including the stem and progenitor populations used for seeding [4]. At the end, the inflammatory state can also result in a failure of the implant. The example of lactic and glycolic acid derived polymers is topical[3,4,5,6]. Considering a polymer of this class, with long-term reabsorption, means a protracted inflammatory response with the appearance inside the scaffold of foreign-body giant cells. The attack lead by macrophages to

the polymer structure can improve its biodegradation but increases also the host response after the initial acute phase of inflammation. This implies that the substances secreted by macrophages come in contact for a prolonged time with the cells loaded in the scaffold and also with the surrounding tissue, with a potentially detrimental situation for the cells seeded in the scaffold and thus representing a limitation for the range of applications in which this polymers can be used. If the kinetics of degradation is fast, even greater problems may arise. Rapidly metabolized polymers like poly(lactic acid) and poly(glycolic acid) produce degradation by-products that induce a decrease in pH due to their acid nature. A scaffold with these characteristics, coupled with the foreign-body response, can damage the transplanted tissue. In fact it has been demonstrated that a decrease in cell viability occurs when cells are cultured on this kind of materials, or on the similar poly(lactic-co-glycolic acid), if compared to standard polystyrene culture substrates[5]. Analogously it is believed that acid environment, as a consequence of degradation, prevents cell integration into the scaffold and is the cause of a decrease in the cell viability at the implant site. An example of these phenomena can be seen after only two weeks from the implantation of smooth muscle cells loaded in this kind of polymer. Inside the scaffold, a rapid polymer degradation induces cell apoptosis as a consequence of a non-physiological condition[2].

In the light of these observations, some limitations have been imposed on the use of these materials. Nowadays, for example, the use of sutures threads made from biodegradable poly(lactic acid) and poly(glycolic acid) is banned in corneal transplantation due to severe inflammatory complications[2].

Alongside the problem of scaffold biodegradation, Okano and al. assert that other drawbacks limit the use of scaffold in tissue engineering[1,2]. As already stated in the ideal evolution of organ regeneration, the scaffold should be reabsorbed by the body and leave the place to new functional tissue. In the practical experience however, a different response has been noticed by the mentioned authors: instead of cells, the space occupied by the polymer has been substituted by large amounts of deposited extra cellular matrix (ECM). This loose cell density structure can be considered as a positive result when relatively isolated cells are surrounded by a considerable volume of ECM like in cartilage or bone[1,2]. On the contrary, human body tissues, with preeminent clinical examples found in heart and liver, possess a high cell density.

This obviously means that, using a biodegradable scaffold, the reconstructed tissue doesn't resemble the native structural anatomy with even the possibility of pathological degeneration in fibrosis [2]. Moreover, the bulky nature of scaffold presents another inconvenience linked to passive diffusion. In fact, in absence of a circulatory system inside the artificial structure, the delivery of nutrients and removal of metabolic wastes in the core of the implant are highly hindered. Consequently we can observe a spread necrosis in the bulk of the scaffold even if in its periphery a healthy and physiologic-like tissue is noticed. Obviously the loss in viability linked to this process leads to unsatisfactory results with poor tissue regeneration[1,2].

A technique that permits to overcome some of the disadvantages of biodegradable polymeric scaffolds is the so-called "single cell suspension". This second methodology conventionally adopted in tissue engineering consists of seeding the isolated cells directly in the damaged tissue with the aims of integrating the injected healthy cells with the injured organ thus inducing a physiological recovery of the lesion. An interesting practical example of this methodology is reported in the treatment of Parkinson's and Huntington's disease[1]. Delivery of neural cells, isolated from aborted foetuses, led to important successes in clinical applications to recover patients affected by these degenerative disorders. Another example of clinical success relates to allogenic hepatocytes transplantation that has been demonstrated to represent a possible future alternative to traditional liver transplantation[1]. Recent results have come also in the treatment of Burger's disease, ischemic hearts and heart failure[1].

In spite of the successes, however, the results are not as expected. The lesion in the tissue often impedes a correct interaction demonstrating that the damaged organ cannot adequately support the seeding of cell suspension[7]. This inevitably leads to a chronic lack of control in size, shape and location (Figure 1.2) of the injected cells[2,7,8]. One of the main reasons for this failure is due to the harvesting methods used to prepare the cell suspension. Great attention has always been paid to methodologies adopted for *in vitro* cells culture but a parallel care in cell detachment doesn't exist at all. Usually proteolytic enzymes are used, with the drawback that substances like trypsin, collagenase or dispase induce the ECM destruction. The protein envelopment that permits cell-cell and cell-environment communication is largely destroyed. Furthermore, there is the possibility that that even cell wall proteins may suffer some degree

of degradation thus leading to loss of differentiated form and function[2,9,10]. The immediate consequence is that the injected cells possess limited potentialities in forming mature cell-cell junctions or to rapidly adhere to the pre-existent injured tissue thus causing severe limitation in tissue regeneration. Moreover, in the event that a peculiar cell conformation is desired, such as specific cell alignment, isolated cells manifest some limitations. They don't usually have the capacity to form such a complex structure in an injured tissue and the result is an organ that doesn't mime the original functionality.

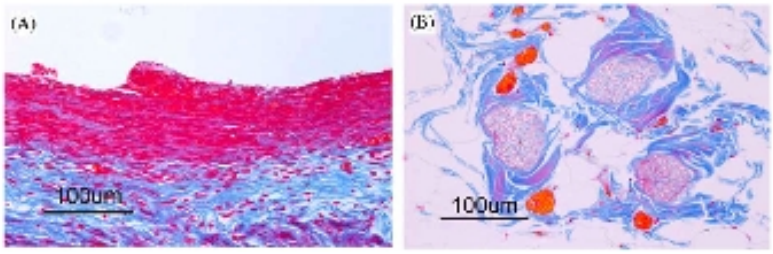

Figure 1.2: Transplanted smooth muscle cells. (A) One week after surgery, azan staining reveals that layered cell sheet constructs form a viable cell-dense structure at the implant site. (B) In contrast, the injection of a smooth muscle cell suspension results in the formation of island-like aggregates with visible necrosis of the injected cells [2].

Research in tissue engineering will be an important part of future medicine and the methodologies based on biodegradable scaffolds and single cell suspension are continuously improving. This will solve some of the problems afflicting these techniques. Nevertheless, sometimes it is necessary to change your point of view to overcome a problem and you have to deal with difficulties on different bases.

This has been the approach of Okano and his research group: in 1990 they first reported a new technique to harvest *in vitro* cultured cells that allowed completely new perspectives in tissue engineering[11]. They understood that it was possible to trigger cells adhesion on their modified substrates just by changing the temperature of the culture medium. This peculiar capability to control cell-substrate interaction was the result of a smart coating with poly(N-isopropylacrylamide) (PNIPAM) (Figure 1.3). Okano perspicaciously saw in this phenomenon

the possibility to open a new outlook on tissue engineering. In fact, he was able to show to the scientific community the great potential of his discovery harvesting undamaged layers of cells with this method and then using these sheets in surgery to repair injured tissue. This new approach has been named by him "cell sheet engineering"[12,13] and the success of this idea is emphasized in over 300 publications concerning only biological cell release from PNIPAM substrates[14].

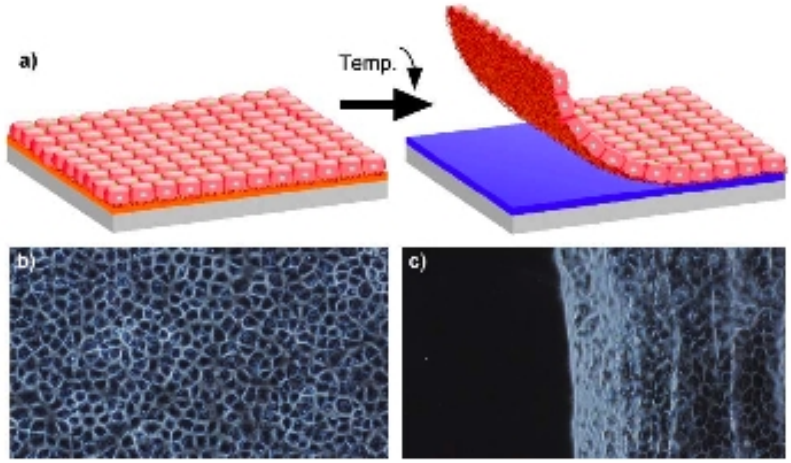

Figure 1.3: Cell sheet engineering using PIPAAm-grafted surfaces. (a) Schematic illustration for temperature-induced recovery of intact monolayer cultures. (b) Confluent culture of endothelial cells on PIPAAm-grafted dishes at 37 °C. (c) Detaching endothelial cell sheet by lowering culture temperature to 20 °C[32].

This peculiar polymer, when dissolved in bulk solution, is highly hydrated at low temperature but as a result of temperature-dependent molecular interactions (principally intra/inter-molecular hydrogen bonding and hydrophobic interaction), the water becomes a bad solvent once a threshold point is exceeded leading to an abrupt polymer chains collapse. The transition is reversible. Decreasing the temperature PNIPAM, the chains return to the original solvated state. The process of swelling and coiling follows the mechanism of a true second order thermodynamic transition and this happens at a specific temperature, known as low critical solution temperature (LCST). In the case of PNIPAM it lies between 30 and 35 °C depending on the molecular structural properties. The proximity of PNIPAM LCST with body

temperature explains why this polymer is so interesting in biological terms[15]. Many different applications have been proposed to exploit the behaviour manifested by PNIPAM but the solution adopted by Okano is probably the most successful, at least from a scientific point of view. He, in fact, was the first to report the double nature of this polymer when interacts with cells. When cultured at body temperature, cells can adhere on the modified culture dish as on a standard polystyrene substrate, but when the temperature is decreased to room temperature the consequent polymer swelling induces a passive and an active process that finally leads to cell detachment[8,14]. In the case of confluent cells the cell-cell junctions and the ECM are maintained perfectly intact[16,17,18,19,20] and thus, once the detachment process is concluded, a layer of cells in the form of a sheet can be observed floating in the medium. Since the process causes only the disruption of the interactions between adhesive proteins, on the basal side of the cell sheet, and the polymer surface (Figure 1.4), cells can rapidly re-adhere to a new surface or a living tissue with nearly 100% efficiency of delivery to the host site, if conditions are maintained[1].

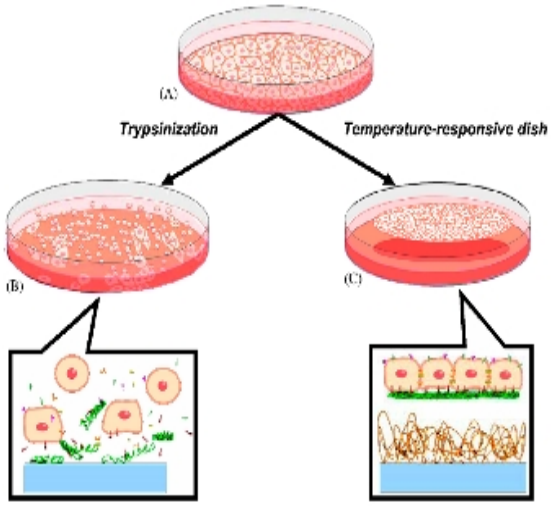

Figure 1.4: Temperature-responsive culture dishes. (A) During cell culture, cells deposit extracellular matrix (ECM) molecules and form cell-to-cell junctions. (B) With typical proteolytic harvest by trypsinization, both ECM and cell-to-cell junction proteins are degraded for cell recovery. (C) In contrast, cells harvested from temperature-responsive dishes are recovered as intact sheets along with their deposited ECM, by simple temperature reduction.[2]

A further section will be devoted to explain the detailed physical process underlying cell detachment, the general PNIPAM properties and the questions arisen on the behaviour of this polymer when tethered on a surface. Instead, in the last part of this introduction a brief summary of the results reported in the literature regarding tissue-engineering applications of PNIPAM will be presented.

One of the main reasons why Okano and his group believed in the cell sheet engineering potential is that parenchyma and epithelia of many tissues generally consist of closely associated cell layers, with comparatively little associated ECM[1]. On the contrary bone tissue engineering for bone or cartilage where few and relatively isolated cells in a structure made of ECM are required, in the majority of the mammalian tissues, cells form a dense system strictly similar to the sheets harvested from PNIPAM coated culture dish.

One of the most noticeable results has been obtained repairing damaged corneal tissue[20,21,22]. Sumide et al. conducted preliminary tests on rabbits. Human corneal endothelial cell sheets were transplanted to the animals' eyes and after only 5 minutes a complete adhesion with the underlying stroma was reported[23]. Finally an improved corneal transparency was noticed with a significant reduced swelling of the eyes. Similarly Nishida et al.[24] transplanted cell sheets over the entire corneal surface of rabbit eyes and, apart from a normal transparency, cells were found to express keratin. After these trials Nishida et al.[23] conducted tests on humans suffering from bilateral corneal epithelial stem cell deficiency. They isolated autologous epithelial stem cells from the patients' oral mucosa that where subsequently expanded until confluence on PNIPAM grafted dish. The detached sheet was successfully transplanted to the patients' eyes. No sutures or scaffolds to support cells have been used to great advantage for the patients who recovered a good eyesight and long-term maintenance of healthy ocular surface. Thanks to these good results in eye disease recovery, Okano and his collaborators have recently tested the possibility to adopt cell sheet engineering to aid post-operative recovery after refractive surgery[13]. The tests are actually limited to animals but results are promising and near future applications of this technique to human patients are planned (Figure 1.5)[25].

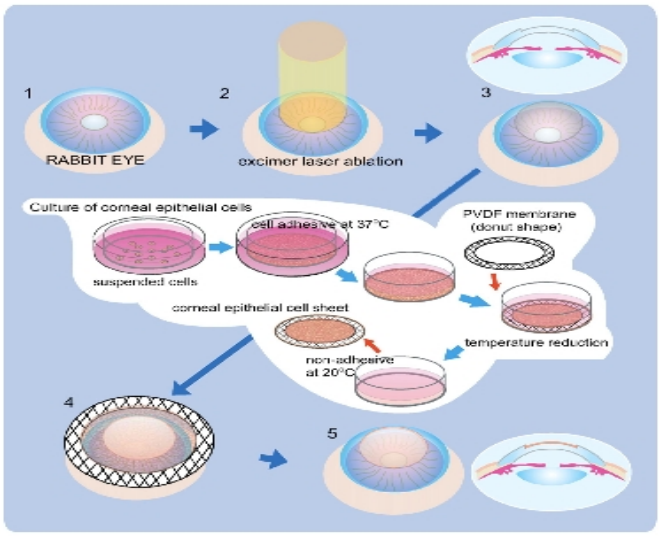

Figure 1.5: Refractive surgery and epithelial cell sheet transplantation. Corneal epithelial cells were cultured for 2 weeks on temperature-responsive culture surfaces. After excimer laser photoablation, the cell sheets are harvested by temperature reduction to 20 °C for 30 min and transplanted to the ablated stromal bed using a donut-shaped support membrane. [25]

Another source of success is in cardiac tissue transplantation. Shimizu et al. and Memon et al.[14] demonstrated the possibility to layer cell sheets composed of neonatal rat ventricular myocytes. The groups reported simultaneous and spontaneous pulsation of the tissue, sign of established electrical connections[26,27]. Further research confirmed that this layered sheets, subcutaneously transplanted in a rat, still showed spontaneous pulsations with neovascularization and morphological characteristics that resemble heart tissue[26,28,29]. These results confirmed the retained ability of cells to rapidly adhere to the new tissue, or to other sheets, thanks to the presence of adhesive proteins on the basal side of the layer not damaged during the detachment[27]. The subsequent step was to repair myocardium damage in a rat with the implantation of a sheet of myoblasts[30,23]. Some cell layers were overlaid and applied to the host site (Figure 1.6). This thick cardiac patch was able to induce myocardial fibrosis reduction with scar tissue replaced by new cells and the formation of new capillaries[13,23].

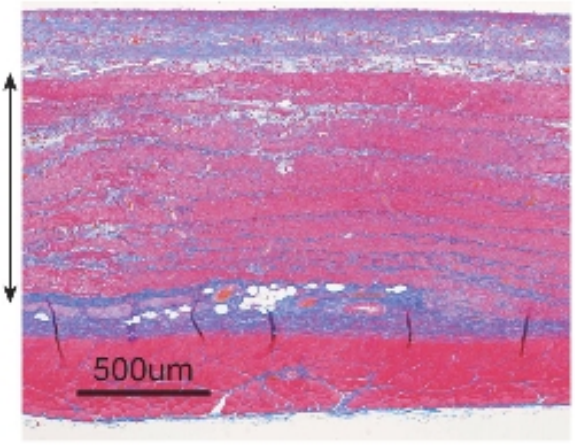

Figure 1.6: Engineering of 1mm thick cardiac tissues using polysurgery. Using10 times repeated transplantations, approximately 1mm thick synchronously beating cardiac tissues with well-organized microvascular networks could be engineered in the subcutaneous space.[30]

Interesting results were obtained also for skin lesions. Specific autologous cell sheets demonstrated that this technique can satisfactory be adopted in plastic reconstructive surgery[11]. Similar treatments have also been developed to enhance wound healing after esophageal cancer resection[23]. In a canine model, an autologous oral mucosal epithelial cell sheet has been transplanted to the postoperative ulcerative area. The sheet tightly adhered to the host site without the need of sutures or carrier materials. These interesting results indicate that this technique should prevent painful esophageal constriction and stenosis with significant effects on patients' postoperative quality life.

These results show how Okano collaborated for more than 10 years with many colleagues to implement this technique and to discover new approaches and applications for cell sheet engineering. Brilliant results have been obtained but much more work is still to be done. Actually the frontiers of this technique are facing the problem of three-dimensional tissues. When more than three layers of cells are superimposed, the thickness reaches a value of circa 100 μm, a critical parameter for passive diffusion[30]. Beyond this thickness, as it happens for biodegradable scaffolds, the nutrients can't reach the cells and the metabolic wastes can't be

eliminated with consequent cells apoptosis. The ideas to overcome this limits are essentially two. In the first approach Okano et al. opted for a poly-surgery methodology. They noted that rapid neovascularization takes place in cell sheets transplanted *in vivo*[28], thereafter the idea to pile up many "triple-layered" sheets of cardiomyocytes at intervals of some days until reaching the considerable total thickness of 1 mm of functional tissue (Figure 1.7)[30]. The second approach is to implant a tissue at least partly prevascularized employing co-culture of specific cells, such as cardiomyocytes or hepatocytes, with endothelial cells that should form the microvascular network before the implantation, also with the aid of growth factors and bioreactors[2].

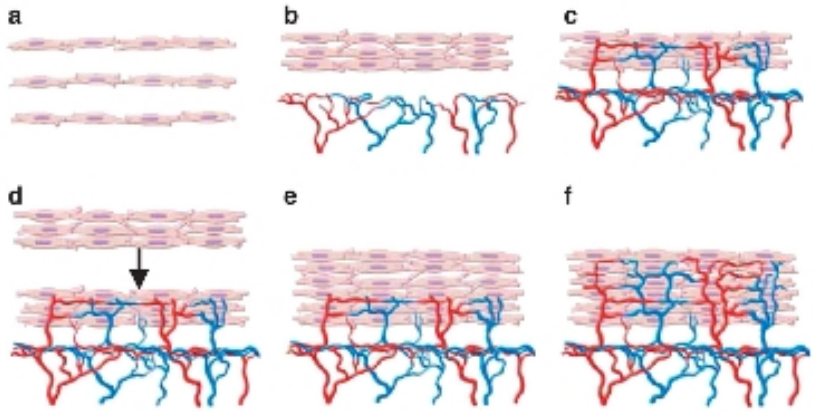

Figure 1.7: Polysurgery to create thick, vascularized myocardial tissues. (a) Individual cardiomyocyte sheets are harvested from temperature-responsive culture dishes and stacked to create layered constructs. (b) Triple-layer myocardial grafts are transplanted subcutaneously. (c) After transplantation, neovascularization occurs within the bioengineered tissues. (d) After sufficient neovascularization has occurred, a second triple-layer myocardial graft is transplanted directly over the first construct. (e) Neovascularization of the second graft occurs through the first construct, creating thick tissues that can overcome the limits of passive diffusion. [30]

In general terms, the future of medical treatments will be closely linked to tissue engineering and surely cell sheet engineering will play a consistent part in it. Drawbacks have to be solved but up to now this field of biomedicine is as promising as ever and the results exposed in this brief introduction are just a small tribute to this process.

Despite the successes obtained in biological matters there is however a parallel process that has always to be taken into account: a good knowledge on PNIPAM has been accumulated in decades of hard work but as some recent reviews reported some questions are still open. Unravelling this controversial matter generates positive consequences on a broad range of technologies and particularly for regenerative medicine that would surely benefit from a better understanding of phenomena involved in the behaviour of PNIPA[14,31]. A note on this key factor could be made by the fact that in about 90% of the publications concerning biological cell release only possible applications are taken into account with little attention paid to detachment mechanism or cell-substrate interactions. As Cooperstein and Canavan underline, the popularity of this smart polymer with regard to cell sheet engineering and "the sheer number of publications in literature may have led many to certain misunderstandings regarding cell detachment from PNIPAM, namely, that the sole application for which cell release from PNIPAM is used, is tissue engineering, that the mechanism by which cell release is achieved is a well-understood phenomenon, and that there is a standard set of procedures that researchers follow to yield predictable release from PNIPAM"[14]. This problem has been precisely the focal intent of this work: to investigate PNIPAM properties trying to contribute to the knowledge of this polymer and possibly to find other ways helpful in cell sheet engineering research.

2 BACKGROUND:

Substrates Background and Synthesis Approach

Chapter 2

2.1 Self-Assembled Monolayers

During this thesis work different approaches have been followed to obtain surfaces suitable for cell sheet engineering. Then the choice of a standard substrate, with well known, homogeneous and reproducible characteristics, has been a crucial aspect to consider. A substrate with similar behaviour allows to better compare results, at least within a sufficient degree of reliability. At the same time it is possible to reduce the variables to a feasible minimum, permitting a clearer understanding of the process involved during tests. Hence, among the available approaches, the most convenient and flexible choice has been the utilization of self-assembled monolayer (SAM) surfaces.

These films can be defined as organic assemblies formed by the absorption of molecules onto a solid surface (or in regular arrays on the surface of a liquid). Moreover the specific feature of SAM is that the constituents of the organic layer are able to spontaneously organize into crystalline or semicrystalline domains (Figure 2.1.1).

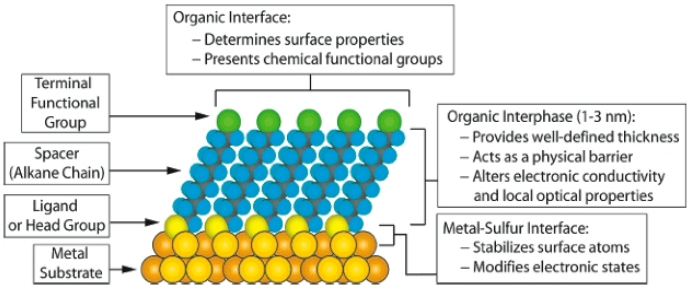

Figure 2.1.1: Schematic diagram of an ideal, single-crystalline SAM of alkanethiolates supported on a gold surface with a (111) texture. The anatomy and characteristics of the SAM are highlighted[3].

The substrates studied in the present context can be divided into two major groups: substrates composed by SAMs alone, with their own specific characteristics, and substrates constituted by SAMs utilized as initiators for polymer grafting. Obviously in both cases the SAM molecules played a significant role in the features of the substrates, even if they were simply the starting point for a polymerization. It is crucial then to briefly present how they form and some of the properties that make this class of surfaces so attractive, especially in the biomedical field.

SAMs have been widely studied since the eighties. In the first years the investigations of these particular films focused primarily on the practical procedures to obtain reliable and organized surfaces. Other aspects investigated related with thermodynamics and kinetics of the assembling on the substrate, and obviously some of the physical characteristics of these unique films[1,2,3].

Researches identified various molecules capable of self-assemble, all of them constituted by three main parts: the "headgrop" and the terminal group divided by a more or less large molecule chain. The extremity of the molecule usually known as headgroup reacts with the substrate forming a tight bond that greatly contributes to the stability of the assembled structure as a whole. Many different headgroups have been identified with affinity for different substrates: the list is broad and comprises alkyl silanes on hydroxylate surfaces (commonly silicon oxide), alkyl carboxylates on various metals, phosphates on metal oxide and on semiconductors and alkyl thiols and alkyl sulfides on different metals. Since the beginning, the most studied types of molecules were organosulfur compounds, with particular attention paid for thiols. These molecules are characterized by a sulfur-hydrogen group that possess a high affinity for gold[4,5] and other noble metals[3,6]

In the present work the attention has been precisely focalized on alkyl thiols assembled on gold (Figure 2.1.1). The reasons for this choice are various but the fact that their formation and properties are well known played a considerable part in it. Moreover, as consequence of this "popularity", a broad range of molecules is now available on the market thus leading to a high degree of versatility.

As stated, on the opposite extremity of the sulfur-hydrogen atoms, the molecule chain-end with the so-called "terminal group" (despite some authors prefer to use an inverse

nomenclature for head and terminal groups) (Figure 2.1.1). This is usually the most characterizing part of the molecule. It is in fact this chemical group that is exposed toward the external environment once the assembling has been completed and thus representing the key factor by which surfaces can be tailored.

The flexibility to "construct" a surface with the desired functionality in a relatively simple manner has been the driving force that attracted the attention of many scientists working with living organisms. Cells and other biological systems are extremely complex in their nature and SAMs represented an alternative to systematically study the interactions of biological environments with matter. SAMs have been used as a model surfaces with well defined composition providing a useful tools for the study of the physical-organic chemistry occurring in biological systems. SAMs in fact possess many of the characteristics sought for a surface model (Figure 2.1.2). The possibility to be tailored at a molecular level with a high degree of order and homogeneity and the possibility to present a wide range of organic functionalities (potentially resistant or promoting cell adhesion) with the desired density represented an interesting way to elucidate cells-substrate interactions. Moreover SAMs can be easily and reliably prepared and, due to the type of substrate commonly employed, are already suited for a relatively wide number of analytical techniques, ensuring then a remarkable advantage over other surface typologies.

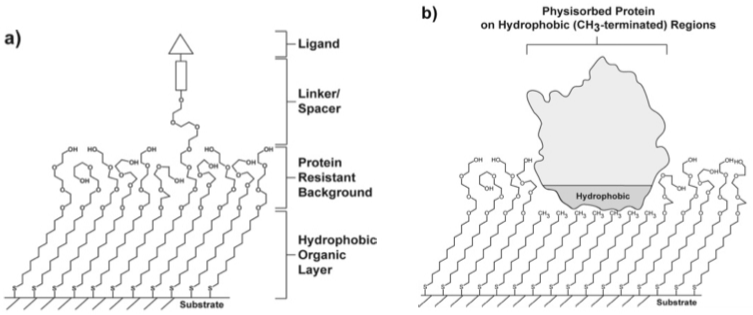

Figure 2.1.2: Schematic illustrations of (a) a mixed SAM and (b) a patterned SAM. Both types are used as surface models for applications in biology and biochemistry[3].

Chapter 2

In the following paragraphs a brief description of materials and process involving the self-assembling of thiols is presented.

To accomplish this task, it has been decided to start from the substrate that commonly is constituted by a silicon wafer, or a mica or common glass, coated with gold. These kinds of samples are a quasi-standardized surface, not solely for the investigation of thiol SAMs. The reason derives from some consolidated considerations linked to the characteristics of the gold coating. By means of widespread technologies, this metal is in fact easily obtained in form of films or colloids bestowing it a good versatility. Furthermore gold is considered a unique material thanks to its reasonable inertness with the majority of chemical substances, particularly oxygen. This confers to such a substrates an "easy handling" with the possibility to work also in atmospheric condition or even worst environmental situations while other metals need more sophisticated procedures. It is then obvious the reason of a wide utilization of gold that consequently has become a "standard" in many applications particularly in spectroscopic and analytical techniques. Given the great affinity with sulphur compounds, gold has also represented the most logic alternative to prepare thiol SAMs particularly for applications related to biological investigation. In form of a film, this noble metal is in fact non-toxic for cells and thiol SAMs formed on it are long-term stable in culture media. These considerations are the base of the decision to utilize this kind of substrates also in the present study.

Gold is typically obtained by physical vapour deposition and forms a polycrystalline film with a dominant (111) crystalline habit. Then the surface on which thiols adhere is organized in an fcc structure with a hexagonal atoms disposition[5,6]. The grain size can vary considerably depending on the deposition technique, and subsequent treatments

One of the key factors in the production of good SAMs is the cleanliness of the substrate. It is well known that a metal surface adsorbs adventitious organic materials as consequence of free energy equilibrium with atmospheric air or environment in general. The adsorbates in fact are able to lower the surface energy and consequently induce an alteration of the interfacial properties of the metal[7]. However most of these physisorbed materials can be displaced by thiols that, thanks to their affinity for gold, form a more stable covalent bond with the metal. Nevertheless the more dirty the surface is, the more the organosulfur are hindered in their

formation process, finally leading to a SAM with a high concentration of defects. To overcome the problem different procedures are reported in the literature[3],[7]. The most common methodologies are a strongly oxidizing solution named piranha (2/3 of sulphuric acid and 1/3 of hydrogen peroxide) or a treatment in a radio frequency oxygen plasma.

Immediately after the cleaning process the gold-coated silicon wafers are usually immersed in a solution containing the thiols so that the process of SAM formation could start. During the formation process many factors may influence the assembling.

Firstly it is important to use an appropriate solvent in which dilute the thiols. The effect of different solvents is poorly understood and dynamic interactions that occur between solvent, surface, thiols and adsorbate impurities are still obscure and matter of complex studies. Polar solvents are widely employed and able to reduce assembling defects and promote densely packed monolayers[8,9]. However SAM formation is reported also using environmental-friendly aqueous solution[10] or hydrocarbon solvents with a low molecular weight that offer some interesting advantage like a higher kinetics[11]. Polar solvent remains nevertheless the most utilized. These liquids poorly solubilize alkanethiols inducing the segregation of these on the metal surface favouring SAM growth. On the contrary polar solvents possess a high affinity for physisorbed hydrocarbons and consequently tend to displace impurities from gold.

Other useful properties sought for a good solvent are inexpensiveness, availability in high purity and the least possible toxicity. In consideration of the mentioned specifications ethanol represented the most convenient formula and through the years the use of an ethanol solution with a dilute concentration of thiols has become a consolidated practice[4].

Usually the amount of the assembling molecules in solution ranged between 1 mM and 10 mM. This concentration is sufficient to form a SAM in 12-18 hours[3].

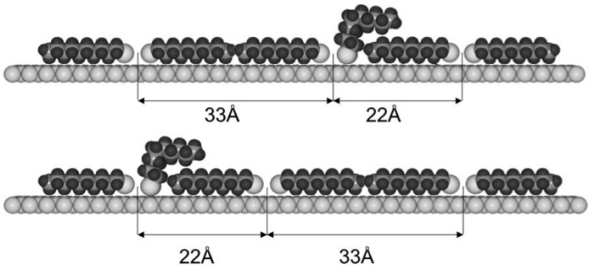

Figure 2.1.3: model structures of the mixed striped phase showing a 33–22 A° and a 22–33 A° stripe sequence, respectively[25].

An increase in the soaking time (literature report data until around 10 days) can promote an evolution of the structure that promotes a decrease in pinhole defects and in conformational defects. However the kinetics of this process is very slow and the differences in properties negligible. This fact limits the practise of long formation period to only some specific applications[3].

Assembling time depends also on the molarity of thiols in solution. An inverse relation has been in fact observed between time and molecule concentration[4,12]. A 1 μM solution takes a longer time to form an organized SAM and even after a week the film doesn't possess the same characteristics obtained in "standard" conditions. Despite that solution in the mM range exceeds many times the necessary amount of molecules to form a monolayer (alkanethiolates on gold are credited of a maximum of circa $4{,}5*10^{14}$ molecules/cm^2, thus a 1 μM solution should be sufficient to meet the scope[5]), impurities, kinetics and thermodynamics occurring during the process hinder the assembling phenomena to such an extent that extremely diluted solutions are avoided.

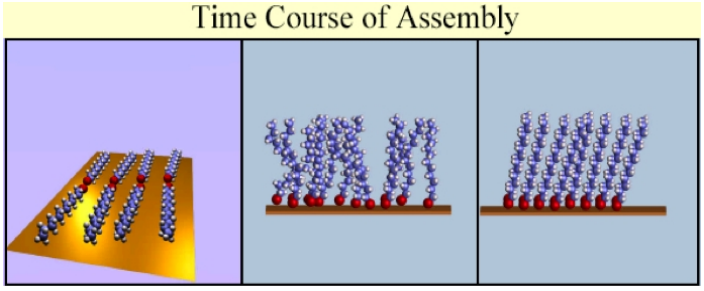

Figure 2.1.4: from left to right: after the striped phase, the nucleation and growth of the semicrystalline domains takes place.

As mentioned above, once the gold substrate is immersed in the solution the process of SAM growth immediately starts.

The steps occurring during the self assembling from solution are clear only from a qualitative point of view and still lack of quantitatively details[13]. Furthermore some phenomena are controversial and not deeply understood due to the complexity of the system[13].

To reduce the variables affecting the system, theoretical studies of complex terminal groups have been avoided in favour of simpler n-alkanethiols. It is speculated that the assembly follows a kinetic progression that has a functional form resembling the Langmuir adsorption model[3].

Further details however have been drawn only hypothesizing that a similar evolution takes place from solution and gas phase. The latter methodology of assembling allows in fact for a more suitable investigation with current analytical and spectroscopic equipments.

The first step of SAM growth is the so-called striped phase (Figure 2.1.3). Alkanethiol molecules are adsorbed on the surface and arrange in an ordered assembly lying flat on the gold substrate[5,13]. During thiols physisorpotion and organization in a characteristic regular structure, the S-H bonds start to dissociate in thiolates tied to gold surface. It is speculated that H_2 is formed as by-product of the process though this assumption is controversial and subject of debate[14,15].

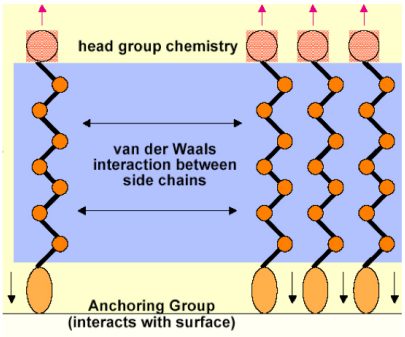

Figure 2.1.5: schematic view of the lateral chains interaction among the n-alkanthiolate molecules that promotes an ordered self-assembling

Thereafter the proper phase of nucleation and growth of the semicrystalline domains takes place (Figure 2.1.4). The higher coverage in an upright structure is the most critic passage in the self-assembling. This is especially true for long chains due to steric effects and interaction with the substrate that hinder growth kinetics.

This passage is poorly understood but it is driven by two main inter-playing forces: the thiolate bond, that links the molecule to the surface, and the non-covalent lateral interaction (mainly van der Waals[16] and hydrogen bonding[17,18]) among the organic chains that tends to maximize the molecular density and the organization in characteristic semicrystalline structures (Figure 2.1.5).

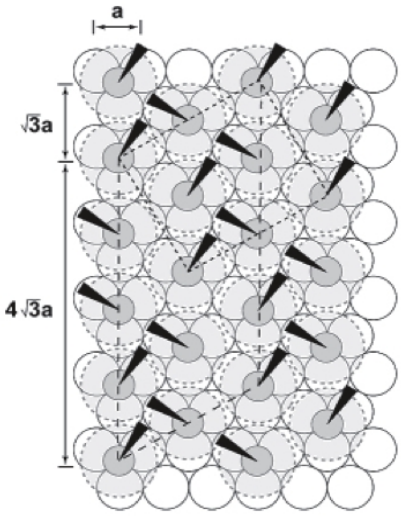

Figure 2.1.6: Schematic diagram depicting the arrangement of decanethiolates on Au(111) lattice when maximum coverage of the thiolates is attained. Structural model of the commensurate adlayer formed by thiols on the gold lattice. The arrangement shown is a (√3 X √3)R30° structure where the sulfur atoms (dark grey circles) are positioned in the 3-fold hollows of the gold lattice (white circles, a = 2.88 Å). The light grey circles with the dashed lines indicate the approximate projected surface area occupied by each alkane chain; the dark wedges indicate the projection of the CCC plane of the alkane chain onto the surface. Note the alternating orientation of the alkanechains defines a c(4 X 2) superlattice structure. The formal c(4 X 2) unit cell is marked (long dashes); an equivalent2√3 X 3 unit cell is marked by lines with short dashes. The alkane chains tilt in the direction of their next-nearest neighbours[3].

Typically n-alkanethiols assume on (111) gold a (√3x√3)-R30° lattice structure[5,13] (Figure 2.1.6). This conventional nomenclature means that thiols are assembled with the maximum possible order in a hexagonal close packed crystal lattice with the sulphur atoms occupying the 3-fold hollows of the (111) gold crystal structure[19,20]. The acronym R30° refers to the value of tilt angle (α) away from the surface normal assumed by the linear backbone of the molecule that in the case of alkane chains is rotated (=R) of 30°. The tilt angle is associated to the steric effect of the molecule and the lattice structure assumed by sulphur headgroups on gold atoms (3-fold hollows structure). The latter create a space among polymer chains that n-alkanethiols can't fill in a configuration perpendicular to the surface due to a modest molecular volume.

Different terminal groups means obviously new dissimilar tilt angle assumed by the backbone chain. The force that regulates tilt angle organization is the same attractive lateral interaction that leads to the self-assembling of the molecules (the energy contribution of for each methylene group in the chain been ~1.0 kcal/mol[5]).

The complex mechanism of interaction induces also a rotation (β) of the molecules about the long axis of the backbone. Likewise in the former case, rotation is characteristic for each

molecule and substrate characteristics. An angle of about 50° has been determined for n-alkanethiols on (111) gold[21] (Figure 2.1.7, a). This disposition of the molecules is usually identified as a secondary organization in a superlattice structure that in the case of n-alkanethiols is a c(4x2).

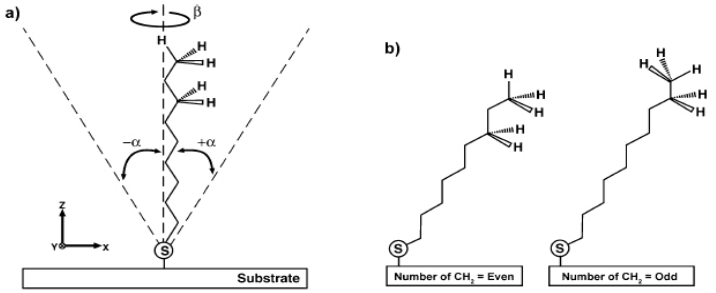

Figure 2.1.7: (a) Schematic view of an all-trans conformer of a single, long-chain alkanethiolate adsorbed on a surface. The tilt angle (α) is defined with respect to the surface normal direction. The twist angle (β) describes the rotation of the CCC bond plane relative to the plane of the surface normal and the tilted chain. (b) Schematic views of single,long-chain alkanethiolates (with even and odd numbers of methylene groups) adsorbed on gold. The conserved value of R for each produces different projections of the terminal methyl group on the surface[3].

The theoretical model of n-alkanethiols assembling is finally determined by a last parameter that highly influences also the SAM macroscopic properties. It is usually defined as the "odd-even" effect, a name that derives from the number of carbon atoms composing the alkyl chain of the thiol. This characteristic is important because induces a different orientation of the hydrogen atoms of the terminal methyl group (for n-alkanethiols) and is absolutely independent from α and β angles (Figure 2.1.7, b). The different methyl conformation influences the chemical behaviours of SAM to such an extent that dissimilar wetting property are reported as consequence of a slightly higher free energy for chains with odd compared to even methylene number[22,23].

The ideal description of SAM is however quite far from the real surface. It is important to keep in mind that all this phenomena are regulated by thermodynamic laws, then a certain degree of imperfections is expected as result of entropic contribution and pre-existent

substrate defects.

SAM imperfections have substantially two origins. Intrinsic defects[24] (especially for polycrystalline gold substrates) but also extrinsic factors induce the formation of many imperfections that greatly contribute to compromise SAM stability on long term. Hence cleanliness of the substrate, purity of the chemical compounds used and other aspects during the preparation procedure have to be controlled as much as possible to obtain reliable results (Figure 2.1.8). Moreover when large molecules (steric bulk $\geq$ 0,25 nm^2) or terminal groups with particular functionalities are employed, the self organization of thiols may considerably differ from the exposed process leading to a large numbers of pinholes and other defects[3] or even to a loss in long range organization.

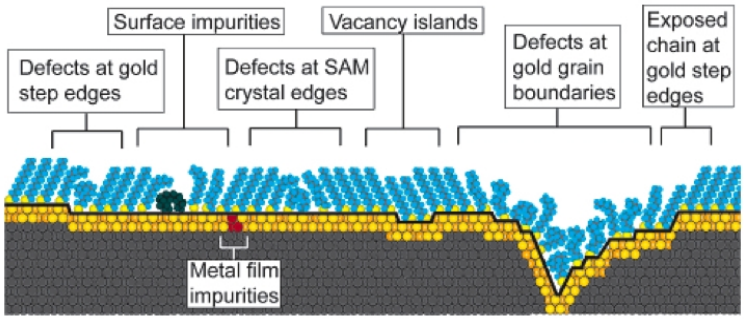

Figure 2.1.8: Schematic illustration of some of the intrinsic and extrinsic defects found in SAMs formed on polycrystalline substrates. The dark line at the metal-sulfur interface is a visual guide for the reader and indicates the changing topography of the substrate itself[3].

Despite "real" SAMs may considerably differ from the ideal surface usually described in modelling studies, SAMs represent one of the most promising substrates in several different fields and biotechnology is surely one of the most prominent. But the application of SAMs doesn't limit to a direct employment. These films are in fact a common and flexible substrate for the grafting of polymer brushes, many of which found interesting applications in tissue engineering.

2.2 Smart polymers

Smart polymers, also known as stimulus-responsive polymers, can "undergo reversible large, physical or chemical changes in response to a small environmental variation"[1] (Figure 2.2.1). The adjective "smart" or "intelligent" is reminiscent of the distinctive properties of living systems and is attributed to these polymers in contrast to the intrinsically "static" behaviour of common materials. In fact cells, and life in general, share many aspects with organic chemistry and, in particular responsive polymers. Many of the remarkable components of living creatures are in fact polymers: proteins, carbohydrates and nucleic acids. Starting from these simple structures, nature developed complex mechanisms capable of interacting and even modifing the surrounding environment (Figure 2.2.2). Often responsive polymers are the consequence of direct observation and imitation of these mechanisms, but, despite the great efforts spent to mimic nature, they are still evidently less complex than most living systems[2].
As biopolymers they possess a highly non-linear (or all-or-nothing) response to external changes. In other terms, large and abrupt variations occur only at a distinctive threshold point, otherwise little to no change take place in the smart system regardless of the extent of external stimulus. Furthermore, like the majority of the natural process the transition is reversible: when the stimulus ends and the environment returns to the initial conditions the polymer turns to its original state[3].

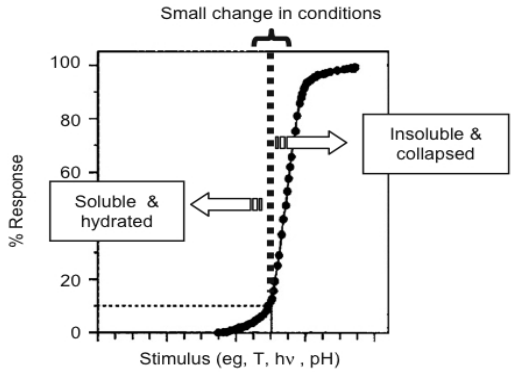

Figure 2.2.1: Schematic showing the special behaviour of smart polymers[39]

As observed, one of the distinctive feature of a non-linear mechanism is that the transition happens within a narrow interval of the external stimulus variation and once the change is completed the polymer is mostly non-responsive to further alterations. This non-linear response is the result of a highly cooperative interaction among the polymer chains. Although any single interaction has a modest value, the huge number of functional groups undergoing the process leads to significant driving forces with considerable macroscopic effects. The chemical nature of these interactions that trigger the smart transition can vary considerably.

The most common are a change in efficiency of hydrogen bonding due to a temperature or ionic strength variation[4], a collapse of hydrogels and interpenetrating polymer networks[5], the neutralization of charged groups by either a pH shift[6] or the addition of an oppositely charged polymer[7].

All these parameters can be directly controlled to trigger smart properties; however, sometimes it is more convenient to adopt an indirect pathway to modulate interactions. A paradigmatic example of such a pathway is thermoresponsive polymers coupled with magnetic particles. The latter are able to transform magnetic impulses in thermal energy. Consequently, it is sufficient to modulate an electromagnetic field to tune the properties of the smart polymer. This simple example gives an idea of the great versatility that these systems possess thanks to the possibility to directly or indirectly control environmental parameters.

Further, and even more interesting, developments can derive from the study of living systems.

It is reasonable to expect that a large part of the next generation of smart functionalities will be directly modeled from biological systems. But at the same time, life sciences are also one of the most promising fields of application for artificial smart polymers. The majority of the intelligent behaviours that distinguish responsive polymers occur in aqueous media, with only few exceptions in organic solvents or polymers blends[8]. This represents a promising development for biotechnology where medicine and researchers are consequently devoting more attention toward these smart mechanisms to actively interact with living systems.

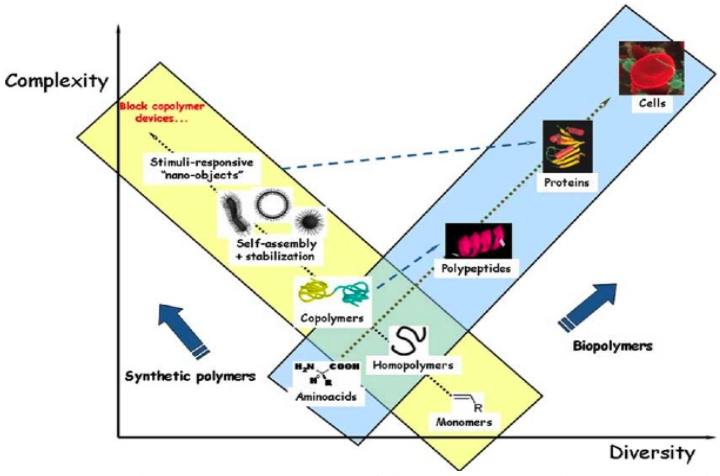

Figure 2.2.2: schematic representation of diversity vs. complexity in natural and syntetic polymers[41].

As elucidated earlier, different environmental stimuli like temperature, pH, electromagnetic field, ionic strength and light have been used to trigger the behaviour of smart polymers.
Macroscopically the smart properties can manifest in different ways, more specifically as the formation of precipitate from a solution (Figure 2.2.3 i), an order-of-magnitude change in the size and water content of hydrogels (Figure 2.2.3 ii), or the variation of surface wettability (Figure 2.2.3 iii).
However, at a molecular level the principle at the base of transition mechanism is a change in microstructure from a hydrophilic to a hydrophobic state (and vice-versa). It is therefore believed that an appropriate balance of hydrophobic and hydrophilic molecular groups is

fundamental to obtain the phase transition.

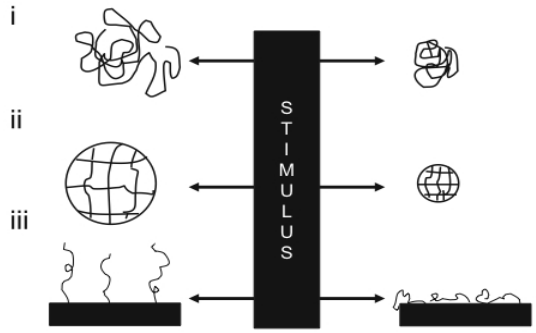

Figure 2.2.3: Classification of the polymers by their physical form: (i)linear free chains in solution where polymer undergoes a reversible collapse after an external stimulus is applied; (ii)covalently cross-linked reversible gels where swelling or shrinking of the gels can be triggered by environmental change; and (iii)chain adsorbed or surface-grafted form, where the polymer reversibly swells or collapses on surface, once an external parameter is changed[40].

In the following sections, a brief summary of the principal smart polymer will be given. To give a more intelligible account the various smart polymers has been grouped as function of their active stimuli.

Temperature controlled switching

Temperature sensitive polymers are the most studied class among stimulus responsive systems and a broad range of applications have been reported in the literature with a particularly large number of publications devoted to the biomedical field[9].

The phase separation, usually observed in water, is linked to a swelled-to-coiled transition exhibited at a characteristic temperature known as the critical solution temperature.

Two different systems have been reported. The first possess an upper critical solution temperature (UCST) meaning a uniform solution above it and phase separation below this threshold point, the second exhibits an exactly opposite behaviour. A monophase below the

threshold point and two distinct phases above a temperature usually define the low critical solution temperature (LCST). The latter system is by far the most investigated among the smart polymers[10] with particular attention to poly(N-isopropylacrylamide) (PNIPAM)[11] which displays a LCST at approximately 32°C.

As noted earlier, thermoresponsive polymers are characterized by a LCST that can be better defined as the critical threshold point at which the polymer solution undergoes a transition from one phase (isotropic state) to two phases (anisotropic state) constituted by the solvent and the precipitated polymer[9]. The swelled-to-coiled transition, and vice versa, is regulated by an enthalpy-entropy equilibrium. Below the LCST the hydrogen bonding term, related to enthalpy, dominates with solvated polymer chains thanks to water molecule hydration. On the contrary, when the temperature rises above the threshold point, hydrogen bonding ceases to be stable and water becomes a bad solvent for PNIPAM. Consequently, hydrophobic interactions, linked to entropy, became responsible for polymer coiling and phase separation.

The smart behaviour of PNIPAM has been studied for many years[12] and today this polymer is so widely known that it can be considered the smart polymer *par excellence*. Moreover, in recent times it has considerably attracted the attention of many scientists involved in biomedical research because its LCST is close to body temperature. Scientists in fact understood that it was possible to employ PNIAPM in many useful biotechnological applications e.g. drug delivery systems, bioseparation and cell sheet engineering. Due to the fact that this polymer has been the base of a significant part of this work, a separate introductory section (Chapter 3) will be devoted exclusively to it in the next pages, and the authors refer the reader to this section for further information about PNIPAM.

The next paragraph will discuss other thermoresponsive polymer prevalently used in biomedical fields.

In the N-alkyl substituted polyacrylamides family, other polymers are known to exhibit thermosensitive characteristics such as poly(N,N-diethylacrylamide)[13,14]. Smart thermal properties are reported also for chemically similar structures as poly(N-substituted amino acids), poly(N-vinylalkylamides), poly(N-vinylcaprolactam) and polyalcohols[14,15]. Among the latter, the most studied are poly(2-hydroxyethylvinylether), poly(2-isopropyl-2-oxazolines) and poly(4-hydroxybutyl vinylether).

It is known that poly(ethylene oxide) (PEO) and poly(propylene oxide) (PPO) also possess a LCST, but, for biotechnological thermoresponsive applications, they have been predominantly studied in the from of copolymers. One of the first copolymer investigated was a terpolymer composed of segments of (PEO-PPO-PEO) that was found to undergo intermolecular association and consequent micelle formation above a critical micelle temperature (CMT)[16]. This, and other similar copolymers, still based on PEO and PPO, has been commercialized with brand names such as Pluronics® or Poloxamer and Tetronics® (Figure 2.2.4). As stated previously, in these products the process that leads to phase separation is the result of intermolecular association, which can be observed macroscopically by a sol-gel transition close or below the body temperature subsequently followed by a gel-sol transition at approximatively 50°C and a LCST[17]. As usual, it is possible to modulate these transitions by adding hydrophobic or hydrophilic moieties as side chains. By modifying the hydrophobic-hydrophilic balance it is also possible to decrease the necessary amount of copolymer in solution to induce the sol-gel transition as it has been done with poly(acrylic acid) (PAA) grafted segments which promoted a physical cross-linking and subsequent micelle formation at a lower concentration compared to an unmodified copolymer (73c).

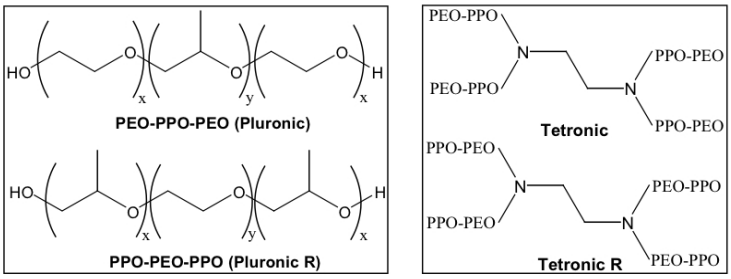

Figure 2.2.4: Schematic structure of polymers with amphiphilic balance[1]

Some of the Pluronics® and Tetronics® block copolymers have also been approved by FDA and EPA for food, pharmaceutical, drug delivery applications and as injectable systems for tissue engineering[18]. A remarkable medical application has been demonstrated using Pluronic F127 in treatment of injured skin of human patients[1]. Another example is Poloxamer 407

hydrogels that, embedded with isolated chondrocytes, has been used as an injectable cartilage substitute. Histological examinations revealed that the hydrogel injected subcutaneously in mice promoted the formation of new cartilage[1].

However, one of the most interesting applications for this class of polymer is in the drug delivery. Hydrogels of the Poloxamer family has been tested for the release of proteins and peptides like insulin, urease and growth factors. Unfortunaley the actual formulation of this copolymer, due to rapid dissolution in water, is suitable only for delivery on short periods, nevertheless good results are expected in the next years[19].

Chemically similar to Pluronic family is the triblock copolymer composed of poly(DL lactic acid-co-glycolic acid) (PLGA) and PEO. This class of copolymer presents an UCST useful for injectable drug delivery systems that jellifies once in the body[19]. PLGA-PEO-PLGA copolymers have been tested also as injectable bandages for corneal wound repair showing enhanced lesion repair and minimization of scar formation[15].

A final group of temperature responsive polymers that deserves attention are natural polypeptides[20,21]. Some of these are investigated because natural polymers, besides thermal switching, can be engineered with a high level of specificity. Many biopolymers have evolved an high degree of specificity thanks to natural selection. A remarkable example is elastine-like polypeptides (ELPs)[22,23] that naturally show pH and temperature sensitivity and have been modified with photoresponsive molecules to cover a wide range of properties[1]. A practical exemplification of elastine-like potentiality has been demonstrated in cancer treatments. An ELP with a smart transition slightly above the body temperature (41°C) was implanted in nude mice to verify tumor-targeting capability. Researchers noted that the engineered polymer allowed a physiological blood circulation at 37°C while accumulating at the site of locally heated cancerous tissue[24,25].

pH-controlled switching

As noted above some thermoresponsive polymers, such as PNIPAM and ELPs, present also smart properties linked to pH variation; nevertheless, the most studied polymers that respond to acidic or basic environments are polyelectrolytes bearing weak acidic or weak basic

moieties in the polymer chains (Figure 2.2.5).

These chemical groups accept or release protons as consequence of changes in pH which then affects the solubility of polymer as a whole. Ionized groups, with like charges, tend to increase the hydrodynamic volume of polymer chains in response to electrostatic repulsion. On the contrary, in a well-engineered polymer with accurately balanced hydrophilic and hydrophobic moieties, when ionisable groups loose their charge, the polymer chains collapse as consequence of prevailing hydrophobic interaction of the polymer backbone. By selecting the right pKa of the ionizable moieties it is possible to modulate the smart properties in order to match the desired pH range of solvation. At the same time, the addition of the proper hydrophobic groups lead to tuneable hydrophobic interactions with the result that the coiling force can be, at least to some extent tailored.

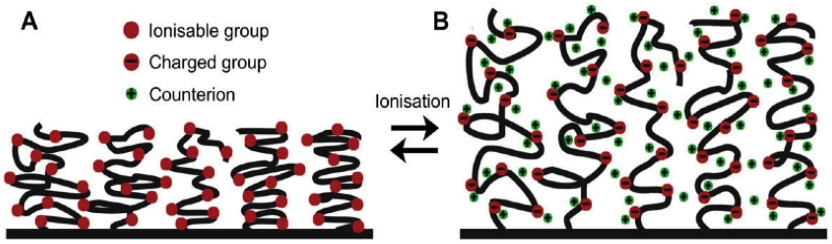

Figure 2.2.5: Polyelectrolyte brush coating exhibiting neutral collapsed (A) and ionised expanded state (B)[15].

Grafted copolymers have been synthesized utilizing monomer with acidic and basic groups (polyampholytes) demonstrating the possibility to have swelled brushes in acidic and basic environments but a collapsed structure at intermediate pH[26,27]. At low pH, in fact, the acid groups are protonated while the basic moieties are charged and induce the stretching of the polymer chains due to electrostatic repulsion. Similarly, at high pH the basic moieties are neutral but the net charge deriving from anionic groups again induce polymer swelling. On the contrary, at intermediate pH both types of moieties are ionized and reach an isoelectric point. In this particular state the anionic groups equal cationic groups and mutual charge neutralization is observed. The consequent prevalence of hydrophobic interactions, due to

backbone brushes, induces the collapse of polymer chains.

In the literature the most studied example is PAA poly(methacrylic acid) (PMAA) copolymerized with poly(2-(diethylamino) ethyl methacrylate) (PDMAEMA), and poly(2-vinylpyridine) (PVP)[26].

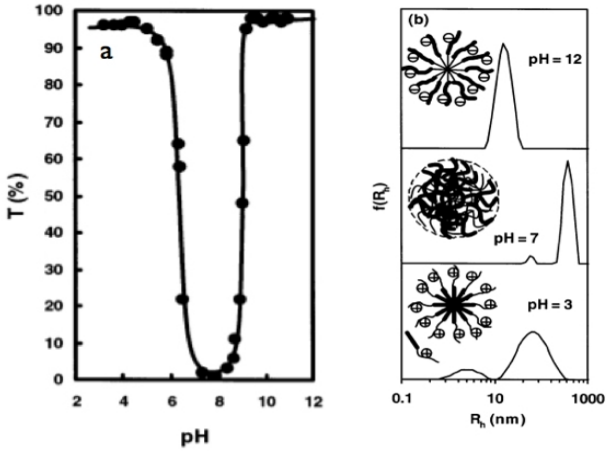

Figure 2.2.6: (a) The UV-visible transmittance of the P(MAA-b-DEAEMA) aqueous solutions at different pH values. (b) The hydrodynamic radius distributions and possible structures of P(MAA-b-DEAEMA) at different pH values[26].

Despite the interesting characteristics presented by polyampholytes, a larger part of literature on pH responsive polymers is focused on polyacidic and polybasic polymers.

The former is based on polymers with anionic groups that precipitate at low pH when all the ionizable moieties are protonated. On the contrary, when pH is higher than the characteristic pKa of the acidic groups the polymer swells in response of the developed net charge (Figure 2.2.5). Typical examples are poly(carboxylic acid) as PAA or PMAA[1,28]. Less common but more versatile are the polysulfonamides. The pKa of these weak polyacids can in fact be tailored on wide range of values by simply modifying the substituent on the nitrogen atom[29].

Similar in principle, but with opposite behavior are polybasic polymers which precipitate at high pH but swell when it decreases. Common examples are PDMAEMA, PVP or the biopolymers poly(lysine) and chitosan.

Usually pH responsive polymers present some limits for *in vitro* and *in vivo* biomedical applications since most of the living systems survive only in a relatively narrow range of pH and ionic strength. Moreover, reversible pH tuning is usually not obtained as easily as in the case of other switching modalities such as temperature or light. Often it is required that the aqueous solution be replaced or added to in order to induce the phase transition. This is one of the main reasons why these polymers are uncommon for cell base applications and preferably employed for drug delivery systems like in biological host sites with severe pH conditions as the digestive apparatus. In the gastrointestinal tract pH may range from the acid environment of the stomach to neutral or slightly basic condition in the colon. Despite the variance in pH range among individuals and physiological states, promising results has been observed for specific drug release in the colon tract utilizing polymers that resist degradation at low pH but release drugs in basic environment[30].

A more sophisticated design is required for insulin release. Drug release for diabetic patients has always been a complex task because the hormone has to be delivered only when needed and in the exact amount. Different mechanisms have been developed employing pH sensitive polymers that respond to the oxidation of glucose[8]. The principle at the base of this mechanism is a decrease in pH that takes place when a high amount of glucose is present in the blood. Gluconic acid is, in fact, the byproduct, catalyzed by glucose oxidase, of glucose oxidation that starts when the monosaccharide reaches a certain amount (Figure 2.2.7).

Another way to use pH sensitive polymers is in specific reactions that require the use of reversibly soluble biocatalysts. Enzymes, covalently coupled to smart polymers, can be alternatively masked or exposed to the environment as consequence of polymer shrink or swell. A direct modification, or consequence, of enzyme-catalyzed reactions can change pH environmental conditions which triggers the catalyst activity[8].

One of the most promising applications for this class of polymers is in the gene therapy. The development of non-viral gene delivery systems able to condense DNA and to transfect it through cell phospholipid membranes is a key factor for future pharmacological therapies. Poly(ethylenimine) and poly(L-lysine) have been tested as gene carriers to introduce specific DNA sequences inside cells[31] and demonstrated to be one of the most promising candidates. Other studies confirm that smart polymers sensitive to pH can transfect DNA inside cells with

a high degree of efficiency[1].

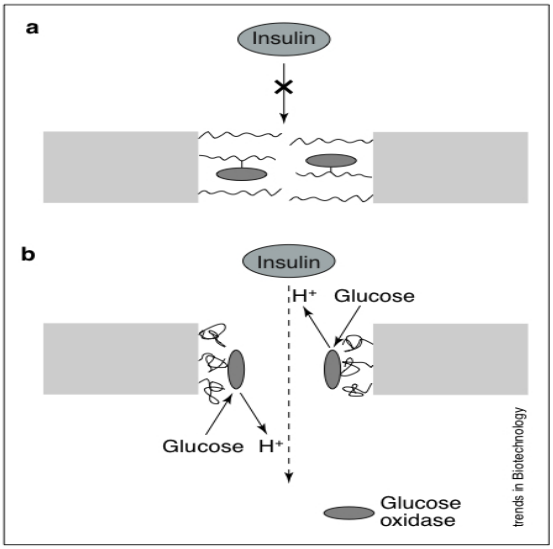

Figure 2.2.7: Schematic presentation of a 'chemical valve'. Glucose oxidase is immobilized on pH-responsive polyacrylic acid, which is grafted onto a porous polycarbonate membrane. (a) Poly(acrylic acid) is in an expanded conformation blocking insulin transport. (b) The oxidation of glucose is accompanied by a decrease in pH and the transition of poly(acrylic acid) into a compact conformation, resulting in the opening of the pores and the transport of insulin[8].

Lastly a brief summary on the application of pH-responsive polymers as biomimetic actuators will be presented. Intriguing solutions have been developed to mimic the typically efficient conversion of chemical energy into mechanical energy of living systems. Researchers have combined ionic hydrogels, sensitive to pH, with electrical circuits. An electrical stimulus was then applied to the system to induce a pH shift inside the polymers. The pH variation caused in turn a large volume modification of the ionic hydrogels. In the proper condition the phenomenon can develop significant forces and thus easily employed to manipulate objects. Interesting solutions are reported in literature using appropriately modelled hydrogels to move or handle items simply modifying an electrical potential[8,32].

Electrochemical and electrically driven switching

Most of the efforts in the development of electrochemical smart surfaces are directed toward SAMs. These kinds of surfaces, in fact, have been long studied to modify electrodes, and the large knowledge accumulated has facilitated the step toward smart applications.

Molecules capable to self assemble and undergo electrochemical bond cleavages have been studied for different purposes. A group of researchers was able, for example, to obtain a marked shift in wettability applying an electrical potential to a SAM and thus causing the desorption of hydrophobic molecules[33]. In other studies, a confined ferrocene group, capable to repeatedly oxidize and reduce in response to voltage variation, was again used to modify wettability[33,34].

One of the most studied molecules known to reversibly undergo reduction/oxidation reactions is hydroquinone and its derivatives. In particular, Mrksich extensively employed this moiety for biomedical applications. They demonstrated that hydroxyquinone derived molecules were able to trigger cell adhesion thus allowing the possibility to study cell migration. Unfortunately the system is not reversible and presented some limitations but this will be argument for a further section of this thesis work (Chapter 4).

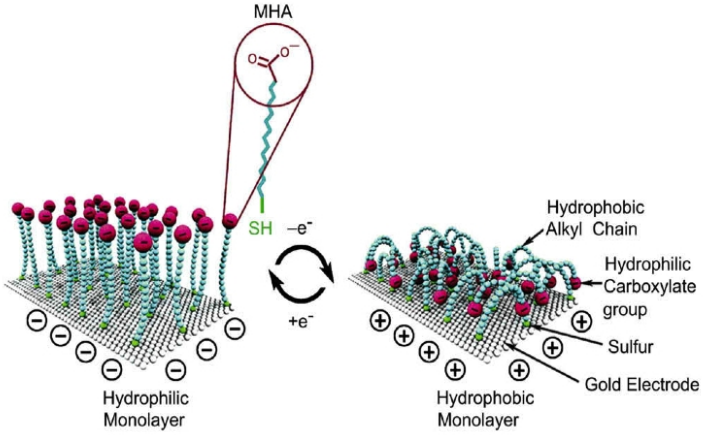

Figure 2.2.8: Idealized representation of the transition between straight (hydrophilic) and bent(hydrophobic) molecular conformations. Ions and solvent molecules are not shown. MHA is16-mercapto-hexadecanoic acid[35].

A different adopted strategy is the use of Coulomb force generated on an electrode coated with smart polymers to modify surface properties. Electric fields are in fact known to cause the bending/collapse (or stretching) of molecules or tethered polyelectrolytes. Lahann et al. invented one of the most famous examples in this science field to control the wettability of an electrode (Figure 2.2.8). They were able to develop a low density SAM on gold composed of thiol with a sufficient spatial freedom for the molecules to bend. The terminal group of the thiols was a carboxylic acid that was attracted or repulsed by the metal surface when applying the proper electrical potential. When carboxylic groups were repulsed the molecules resulted in a stretched state which then exposed the hydrophilic acidic moieties. On the contrary, when the thiols were in a bent conformation, as consequence of carboxylic acid attraction to the surface, only the alkyl chains were exposed toward the environment thus turning the surface to a hydrophobic state[35]. After this elegant experiment, similar approaches, but with different designs, have been reported in literature[36,37].

Photoinduced switching

In conventional and solid state synthesis, photocleavable protecting groups are commonly used and studied. As a result, a direct employment of these moieties for smart applications was relatively short to undertake[15].

Some experiments were also set up for biomedical applications demonstrating that some degree of control over proteins adsorption and subsequent cell attachment could be achieved following this strategy[15]. Despite promising results, this system remains substantially as an on-off switch, and therefore with relatively few applications.

Consequently, other approaches have been investigated with particular attention toward photoisomerization. This method sought to modify surface wettability through a conformational change of chromophores. Hydrophobic/hydrophilic transition was achieved inducing the trans/cis photoisomerization of a diazobenzene group by means of near-UV light[15]. This wettability change proved to be sufficient to regulate cell attachment but only to a partial extent. Similar results have been reported with spiropyran stimulated with UV light to cause photoisomerization of the molecule[15].

The use of light leads to a high degree of versatility in particular when a patterned surface is required. Modifying the path or the shape of a pattern would be in fact extremely easy, for example by means of a simple mask. In the biomedical field, however, some obstacles have still to be overcome in order to find useful applications. A change in wettability is not *per se* sufficient to tune cell adhesion, and, moreover, the use of UV light has to be strictly controlled and limited in time[15].

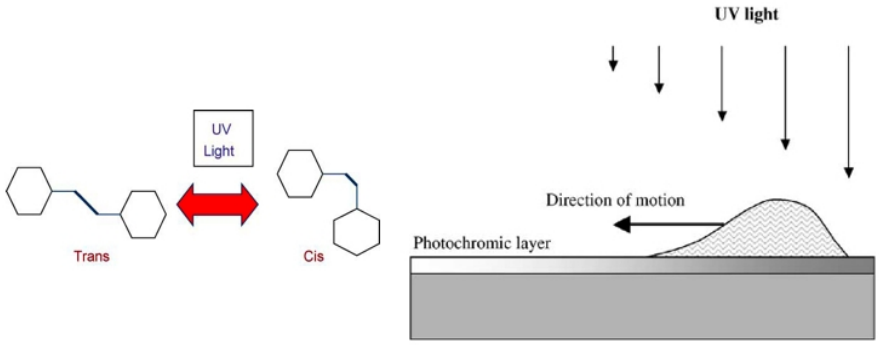

Figure 2.2.9: Asymmetric shape of the liquid droplet moving on agradient surface created by gradient UV-illumination of azobenzenesurface layer[38].

In other fields of application, however, photoinduced switching maintains its potential as demonstrated by Ichimura[38]. He used a diazobenzene moiety to tune wettability and create a gradient in surface free energy that induced the motion of a water droplet on the substrate (Figure 2.2.9). By tuning steepness and direction of light he was able to manipulate the speed of the droplet on a desired path.

2.3 Atom Transfer Radical Polymerization

More than 50 years ago, precisely in 1956, two papers published by Michael Szwarc revolutionized synthetic polymer chemistry presenting the first living polymerization[1].

Those publications have been considered the birth of a number of techniques based on the concepts exposed by Szwarc for his living anionic polymerization. This is defined as a synthesis method without chain-breaking reactions in contrast with traditional free radical polymerization.

The technique marked a turning point because it prompted the development of other methodologies for the synthesis of well-defined copolymers. Despite, from a theoretical point of view, in the latter controlled/living systems chain-breaking reactions were observed, these new synthesis methods were clearly the continuance of Szwarc's work.

The possibility to synthesize well-defined polymers with a precise molecular architecture meant not only major developments in polymer chemistry but also a key factor in polymer physics[1]. As stated, Szwarc's discovery was the keystone for many other achievements in the subsequent years defining a breakthrough for scientists that started to search for new conditions in a variety of systems in which chains termination and transfer could be eliminated.

Different techniques has been discovered and implemented until, in the nineties, a new family of controlled/living polymerization have been devised. As controlled/living radical polymerization (CRP) mechanisms in general, these are based on the co-existence in a dynamic equilibrium of active and inactive species. Thanks to the fact that the latter (also known as "dormant") by far surpass the former in number the reaction proceeds with a smooth and controlled process.

Among the controlled radical polymerization methods developed in the last decades, there are some that have taken a preeminent position thanks to their advantages in producing a wide range of polymers and copolymers with relatively high molecular weight, a low polydispersity index and engineered structure without the need for stringent process conditions.

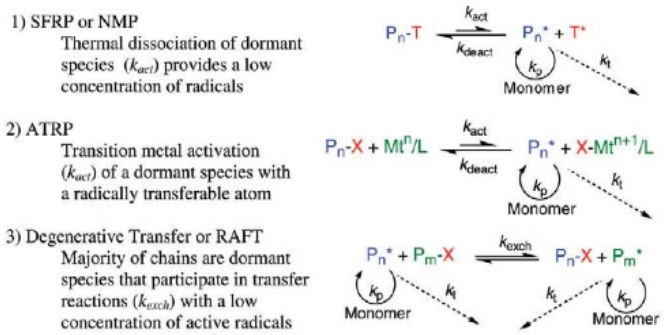

Scheme 2.3.1: the three main CRP methods[2].

These techniques are nitroxide mediated polymerization (NPM)[2] (the most employed example of stable free radical polymerization (SFRP)), degenerative transfer with dithioesters via reversible addition-fragmentation chain transfer (RAFT)[2] and transition-metal-catalyzed atom transfer radical polymerization (ATRP)[2,3,4] (Scheme 2.3.1). In this thesis work the latter has been extensively used to synthesize the desired polymers, then a brief summary of the main concepts at the base this methods are presented.

As noticed, ATRP is the product of years of research in controlled/living polymerization systems but its basic mechanism derives directly from a traditional free-radical polymerization developed in the early 1940s by Kharasch. This was the atom transfer radical addition (ATRA) (or Kharasch addition), a reaction that proceeded through the addition of a reagent across a carbon-carbon double bond by means of a radical process that involved a halogenated specie[5]. Further development in the subsequent years established that the technique could be better controlled using transition metals complexes to catalyze ATRA and new developed halogenated compounds[5] (Scheme 2.3.2).

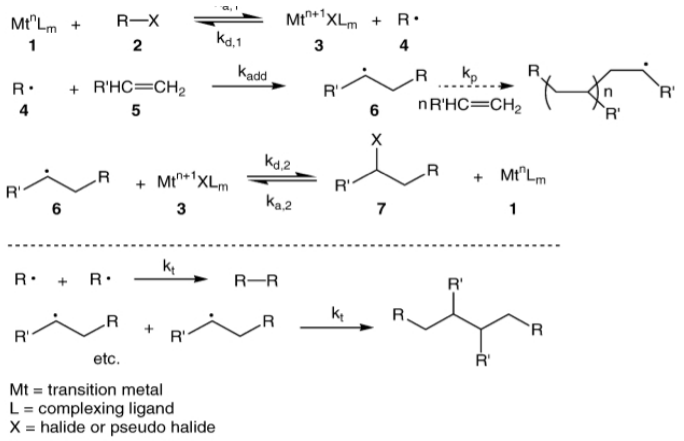

Scheme 2.3.2: proposed mechanism for the transition metal catalysed ATRA[5].

Moreover a series of commercially important olefins were found to be employable monomers in the process leading to a vast utilization of this reaction method[5].

Similarly to transition metals catalyzed ATRA, ATRP adopts transition metals complexes as halogen transfer agent however it avoids many of the drawbacks of the former technique thanks to the improvements promoted by the mentioned controlled/living polymerization (Scheme 2.3.1).

The principal features that lead to great advantages of controlled/living radical polymerization over traditional radical polymerization can be summarized in few points[6].

First, assumed that initiation is fast, the logarithmic concentration of monomer is a linear function with time. This is the consequence of a negligible chain termination and consequently a constant concentration of propagating radicals that "consume" the monomer[6]. A similar trend could be also seen for traditional free radical polymerization but in this case is the result of a dynamic equilibrium between radical formation and termination. On the contrary, in the living polymerization a pure control over the reaction is observed thanks to an equilibrium established between activation and deactivation processes of propagating radicals that allows for a rate of initiation far greater than the rate of propagation[6].

Another important aspect is the linear growth of degree of polymerization with monomer conversion that is the consequence of a constant number of chains during the polymerization.

This peculiarity of controlled radical polymerization is ensured when all the chain should start growing at the same time as result of a sufficiently fast initiation. Moreover the number of chains have to remain constant, thus chain transfer as well as coupling reaction have to be avoided to limit the chain termination process[6].

A consequence of the latter feature is the persistence of long-lived polymer chains. This means that once the monomer is completely consumed, its further addition is sufficient to restart the reaction. Furthermore this is the basic concept for block copolymer synthesis[6].

In real conditions it is, however, impossible to completely stop termination of chains. Nevertheless it is possible to drastically reduce it maintaining a high percentage of dormant species that can opportunely be reconverted to radical propagating chains[6].

At the same time, to maintain control over the reaction it is necessary that exchange between active and inactive species be fast, leading to an equal probability for dormant species to be reactivated. It is important to highlight that a large degree of inactive specie doesn't mean a slow rate of polymerization, besides permit a narrow polydisperity index[7,8].

To achieve a narrow molar mass distribution it is however necessary to accomplish other conditions fundamental also for the other discussed features of controlled radical polymerization. Briefly: 1) an homogeneous system, 2) a fast initiation rate, so that all chains simultaneously start to growth, 3) a depropagation rate negligible compared to propagation, meaning an irreversible polymerization and that all active species possess the same probability to react with monomer for an uniform propagation.

Scheme 2.3.1 (case 2, ATRP) describes the proposed mechanisms for ATRP synthesis[5,9,10]. The propagation process starts when a homolytic cleavage of the alkyl-halogen bond (R-X) by a transition metal complex in the lower oxidation state (Mt^n-Y/ligand) generates an alkyl radical (R•) and a transition metal complex in the higher oxidation state (X-Mt^{n+1}-Y/ligand). The formed radicals can initiate the polymerization by adding across the double bond of a vinyl monomer, propagate, terminate by either coupling or disproportionation, or be reversibly deactivated by the transition metal complex in the higher oxidation state[5].

The formation of radicals during the ATRP process is reversible. Moreover, as already mentioned, termination reaction is reduced by a shift to the left-hand side of reaction (scheme

X, activation (k_a) << deactivation (k_d)) with the consequence that a low stationary concentration of radicals is observed. This equilibrium is commonly named persistent radical effect (PRE) [6,11,12,13] and it is at the base of a successfully controlled ATRP.

One of the interesting features of ATRP is that PRE can be appropriately adjusted to adapt to different necessity[14,15]. This versatility has been employed in the synthesis of different monomer to produce polymers and copolymers with a well-defined composition and architecture. Styrenes, (meth)acrylates, acrylonitriles and acrylamides have been successfully produced[5].

In order to optimize the reaction to different scientific and industrial necessities, various formulations has been developed starting from common commercially available alkyl halides as initiators. Moreover numerous nitrogen based ligands have been successfully tested such as different transition metals comprising Ti, Mo, Re, Fe, Ru, Rh, Ni beside the traditionally utilized Cu[5].

Despite the brilliant achievements some drawbacks still represent a problem in the technology transfer to industry. The major difficulty to overcome is the elimination of the transition metals once the synthesis is completed. In traditional ATRP it may amount to even 0.1-1% of the reaction mixture. It is thus easily understandable the great efforts made to resolve this inconvenience.

The basic idea to overcome the problem has been to increase the activity of the catalyst so that its quantity could be reduced[16]. The mechanism thought to accomplish the goal is to reduce the catalyst sensitivity toward oxygen and oxidant molecules. These species always present in the reaction mixture are in fact responsible for the transition metal inactivation.

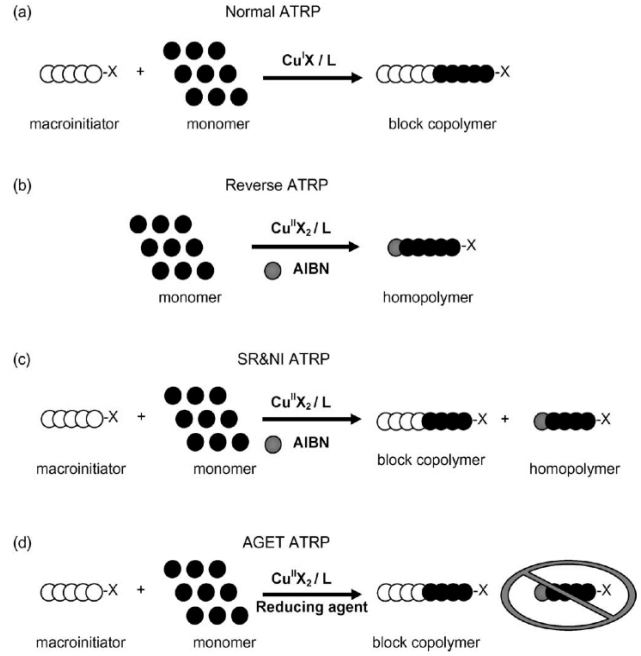

Scheme 2.3.3: methods for conducting ATRP[14].

Reverse ATRP[17] has been one first developed solution. It employs a conventional radical initiator and a transition metal in the oxidized state that react to generate the ATRP initiator and the transition metal activator (Scheme 2.3.3, b). The advantage in this case resides in a less sensitiveness of initial components to oxygen.

With this technique, however, several drawbacks persist and research was directed toward other more suitable routes. A first step has been taken with simultaneous reverse and normal initiation (SR&NI) ATRP[18] that combine traditional and reverse ATRP to improve the technique (Scheme 2.3.3, c). This enhances the activation of the catalyst but is still affect by several complications.

Further improvements have been undertaken with activator generator by electron transfer (AGET) ATRP[19]. The key factor in this method is an electron transfer to generate a lower oxidation state for transition metal complex, instead of traditional organic radicals. The basic idea (Scheme 2.3.3, d) is to substitute the radical initiator with a reducing agent to obtain

similar effects. The improvement allows to produce pure copolymers avoiding the side effect of homopolymers present in the reaction mixture as happened in the case of SR&NI ATRP.

From AGET ATRP derived the so-called activators regenerated by electron transfer (ARGET) ATRP[20] as a further progress toward industrialization of the process. The reaction starts as a normal ATRP but whenever transition metal deactivators accumulate due to oxidation, the reducing agent intervenes to restore the equilibrium between active and inactive species (Scheme 2.3.4).

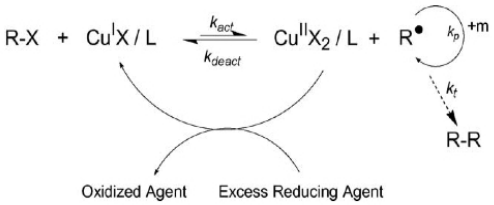

Scheme 2.3.4: proposed mechanism for ARGET ATRP[20].

The progressive formation of oxidized catalyst complexes is a consequence of radical termination reactions in accordance with the PRE process and lead to a polymerization halt. Hence the addition of the reducing agent induces the regeneration of the catalyst, therefore restoring a normal ATRP reaction.

This method has drastic effects on the possibility to lower the amount of catalyst needed to a successful reaction with obvious economical and environmental impacts for industrial application. Moreover, an excess of the reducing agents can remove dissolved oxygen from the polymerization systems then requiring less stringent environmental conditions for efficient reactions. The typical catalyst amount used in standard and ARGET ATRP gives a better idea of the improvement. With the former methods around 1000 ppm of catalyst were needed while for the latter 10 ppm can be sufficient. Moreover, common reducing agent are FDA approved compounds such as ascorbic acid or tin(II)2-ethylhexanoate[14].

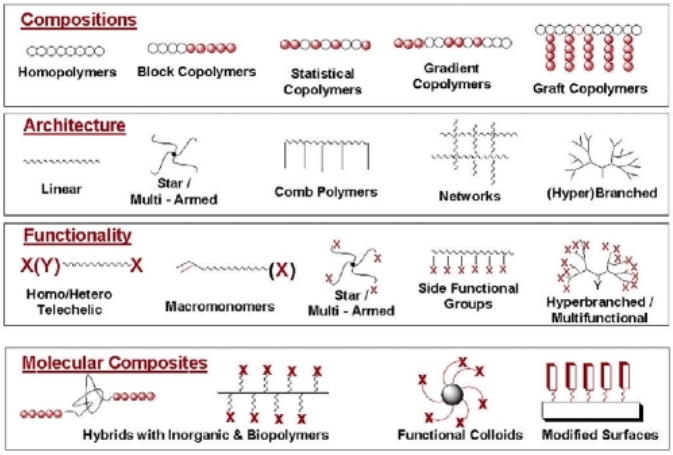

Figure 2.3.1: examples of molecular structures attained through ATRP[2].

The possibility to easily obtain control of topologies, compositions, microstructures and functionalities[21,22] over a wide range of monomers (Figure 2.3.1) and the continuous improvement in the technique are the reason for the tremendous spread of ATRP in scientific and industrial research . Hundreds of papers have already been published on the argument[23] and the trend is for a further increase.

In the present study ATRP played an important role since it is one of the few methods that permits to synthesize PNIPAM and other smart polymers controlling their macromolecular architecture without the need for expensive laboratory equipments.

PNIPAM has been studied since many years for its smart characteristics. Nevertheless, the improvements in synthesis technique introduced by ATRP allowed for a better comprehension of the behaviour of this polymer especially when tethered on a surface. This arguments and a more general description of the PNIPAM characteristics will precisely be the subject of the next section.

3 Thermal-Responsive PNIPAM:

Chapter 3

3.1 Background

In this chapter, a brief summary of the literature on PNIPAM behaviour is provided before the results obtained during this thesis work are presented.

A brief, qualitative, description of thermoresponsive systems has already been reported in a previous section (Chapter 2), here, a more detailed description of PNIPAM behaviour is reported focusing the attention on the fundamental aspects related to the thesis topics.

The smart behaviour of PNIPAM is critically related to the molecular structure of this polymer (Figure 3.1.1). When synthesized in form of single chains, PNIPAM is composed of a n-alkane backbone from which amide moieties depart terminating with an isopropyl group. The chemical structure is thus a balance of hydrophilic and hydrophobic moieties that differently interact with polar solvents[1].

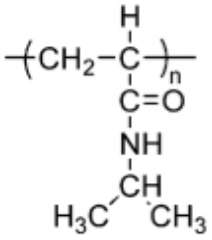

PNIPAM

Figure 3.1.1: schematic structures of PNIPAM

The amide moieties are particularly important since they are able to form hydrogen bonds

with water molecules. The coordination of strongly interacting solvents with the amides groups causes, in fact, the polymer solvation. At the same time, however, Schild and Tirrell evidenced that the formation of this hydrogen bonds is strongly hindered since a specific molecular orientation is required[2,3]. Hence, in the energy balance that regulate the polymer behaviour, it is necessary to take in account two distinct parameter: the enthalpic and the entropic contributions. The former (H) is linked to the hydrogen bonds between water and polymer moieties that promote dissolution. The latter (S) is connected to the unfavourable molecules organization necessary to achieve the bond formation. The final balance of these two thermodynamic parameters determines the free energy of dissolution ($\Delta H - T*\Delta S$) and ultimately the solvation degree of polymer chains[4]. As evidenced by the equation, the key factor that moves the equilibrium balance from negative equation terms (dissolution favoured) to positive values (unfavourable to solubility) is the temperature (T). It is then explained the thermodynamic mechanism by which, increasing the temperature of the system, PNIPAM precipitates when the two terms of the equation are equivalent. This critic value occurs at a threshold temperature defined as the low critical solubility temperature (LCST) that " corresponds to the region in the phase diagram where the enthalpy contribution of the water hydrogen bonded to the polymer chain becomes less than the entropic gain of the system as a whole"[4].

As stated before, the solvated polymer interacts with water forming an organized structure with side chains (Figure 3.1.2): specifically with both amide and isopropyl groups. When, as consequence of temperature increase, the LCST is reached, the free-energy balance changes and water molecules associated with the side moieties are expelled into the bulk water replaced by intra/inter molecular bonds among the amide groups. In the new system conditions, the hydrophobic effect, controlled by entropy, prevails on hydrophilicity with the result that the polymer precipitates and, to minimize the contact with water, turns to a coiled conformation.

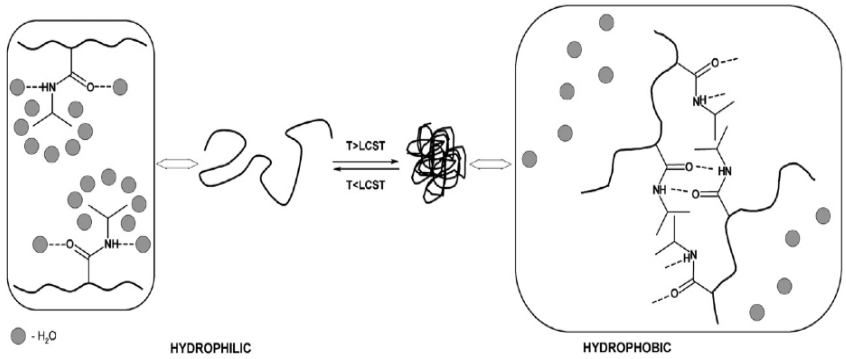

Figure 3.1.2: Illustration of temperature induced PNIPAM phase transition[4].

The transition from a monophase solution to an anisotropic phases is easily observable since the light scattering, caused by the formation of the coiled polymer chains, induces a loss of transparency (Figure 3.1.3). This phase transition has been traditionally named cloud point and, obviously, it occurs at the LCST that in the case of PNIPAM lies between approximately 30 °C and 35 °C, depending on detailed microstructure of the macromolecule[2].

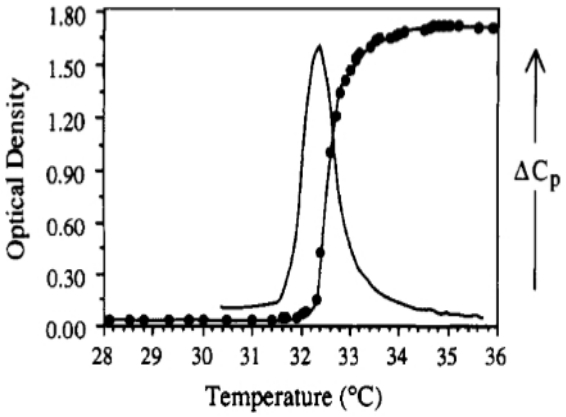

Figure 3.1.3: Cloud point temperature curve and microcalorimetric endotherm of PNIPAM[2].

The interesting behaviour of PNIPAM has been employed in various filed of science and technology as, for example, in rheology[2] and optics[5].

The major field of investigation, however, has been, and still remains, focused on biological applications. PNIPAM has been for example widely studied for drug delivery.

Membranes composed of PNIPAM[6,7] have been used to regulate the release of drugs while hydrogels of this polymer have been tested as drug delivery systems[2]. During this investigation it has been observed that the architecture is fundamental parameter for PNIPAM homopolymer. An example it the discovery that a comb-like structure is more responsive than a crosslinked hydrogel. This structure allows in fact for a greater mobility of PNIPAM chains that enhances the coiling/stretching effect[8].

In the studies on drug delivery, PNIPAM has been extensively used also copolymerized with other monomers. An interesting aspect of PNIPAM copolymerization is that changing the composition of the copolymer can modulate the phase transition of these systems. It is well known that adding a hydrophilic moiety induces a shift of the LCST toward higher temperature while hydrophobic moieties has the opposite behaviour[4,9,10,11] (Figure 3.1.4).

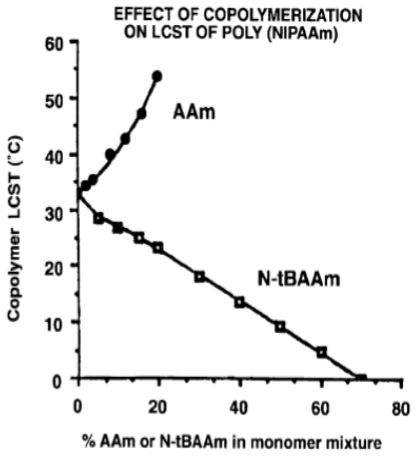

Figure 3.1.4: Effect of copolymerization of poly(N-isopropylacrylamide) with acryl amide (AAm, a more hydrophilic co-monomer) and N-test butylacrylamide (N-tBAAm, a more hydrophobic co-monomer) on the LCST[10].

Moreover, when synthesized in form of hydrogels, the added functionalities influence the swelling/deswelling response both in terms of kinetics and water uptake[12]. The addition of hydrophilic acrylic acid in the network structure, for example, leads to a rapid deswelling[13]. At the same time, another aspect to take in consideration when new moieties are added, is the final copolymer structure. In fact, the new functionalities interact more efficiently when linked as end-groups then in a hydrogels obtained by means of random copolymerization[12].

In drug delivery research, one of the main issues has always been insulin release. PNIPAM has been tested also for this purpose but combined with hydrophobic moieties. NIPAM was copolymerized with butyl methacrylate to lower the LCST to about 25°C and the hormone delivery, in a temperature on-off profile, was investigated with interesting results[14].

Other ways to modify the copolymer compositions have been studied to overcome the limits on biodegradability of PNIPAM. An example are hydrogel microparticles of PNIPAM dispersed in a gelatine matrix that have been proposed specifically as drug delivery system[15].

A completely different approach of NIPAM copolymerization has been proposed for immobilized biocatalyst applications. A gel of poly(NIPAM-co-acylamide) has been functionalized with invertase, an enzyme responsible for sucrose hydrolysis. The system was also embedded with γ-Fe2O3 nanoparticles that are able to generate heat when exposed to a magnetic field. As expected, an increase in temperature induced by the nanopartilces, caused the collapse of the thermosensitive hydrogel and consequently a sharp decrease in the sugar hydrolysis was observed[16].

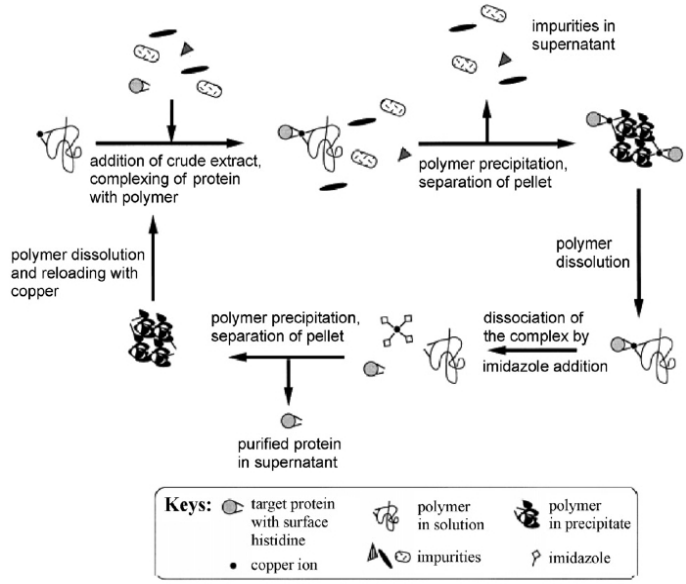

Figure 3.1.5: Scheme of metal chelate affinity precipitation of proteins for bioseparation techniques[44].

The utilization of PNIAPM covalently coupled with specific ligands for proteins was instead adopted as an alternative bioseparation method (Figure 3.1.5). Different systems have been devised to induce the formation of complexes between ligands and target molecules dispersed in solution[2,16]. The phase separation of PNIPAM, induced by an increase in temperature, caused the co-precipitation of the proteins "captured" by the ligands. The technique confirmed to be an efficient method to selectively concentrate the desired molecular species.

A similar concept was also at the base of PNIPAM utilization in chromatography. Grafted on a chromatographic column, the temperature sensitive polymer has been reported to adsorb peptides and proteins from aqueous solution when in a coiled state. A subsequent decrease in temperature leads to the release of the entrapped species demonstrating the possibility of future uses of PNIAPM for this analytical technique[17,18].

Despite the wide utilization of PNIPAM in different scientific research fields, the most intriguing and studied method to use this smart polymer is, probably, in tissue engineering.

The interesting results obtained by Okano and other scientists with the cell sheet engineering

technique has been already discussed in a previous section (Chapter 1). But the physical and biological phenomena occurring during cell detachment has not yet been presented. Despite many works have been published on the subject, this argument can be described mostly in qualitative terms since it remains largely not understood[19].

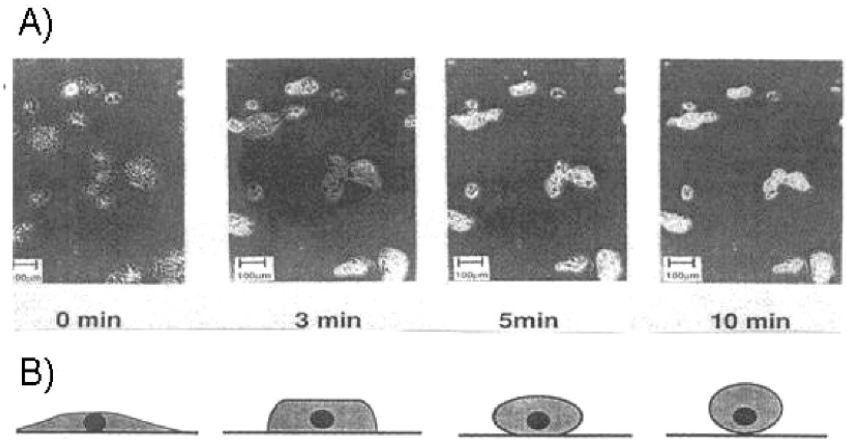

Figure 3.1.6: Phase-contrast micrographs (top row) and a schematic representation (bottom row) of the mechanism of cell sheet detachmentfrom pNIPAM-coated surfaces. Bars are 100 μm. Cells are hepatocytes[20].

During detachment (Figure 3.1.6), cells have been observed to change their morphology from a physiologic spread shape to a more spherical appearance, followed by the final detachment from the PNIPAM coated substrate. Investigating the metabolism of cells, Okano et al. proposed a two-step mechanism[20]. When culture medium temperature is decreased below the LCST of PNIPAM, the polymer swelling induces a first passive phase of detachment. The hydration of tethered brushed is in fact supposed to behave like an anti-fouling surfaces that, due to an entropic repulsion of protein adsorption, prevents cells adhesion[9]. The first step causes also the start of the second phase that has been described as active since it directly involves cells metabolic processes that induce the observed morphological change in cell appearance. This fact has been indirectly confirmed studying cellular activity during the detachment at different temperatures[20]. At 4°C, in fact, the lift-off process was partially suppressed, if compared to the same phenomenon occurring at higher temperature.

Further direct evidences have come adding to the culture medium sodium azide, a compound that inhibits the physiological ATP generation[20]. The so artificially inhibited activities of cells caused a decrease in detachment confirming, once again, the existence of an active involvement of cells during the lift-off. Other detailed studies on this aspect revealed that the active phase was linked to cytoskeletal dynamics. The tensile forces exerted by the cytoskeleton were in fact found to be at the base of cell release[21], while chemical cellular activity was negligible such as the formation of new proteins[22].

Investigating the amount of collagen type IV left on the substrate after the detachment, it was also possible to hypothesize that the lift-off process starts with an active separation from the ECM at the edge of cells[19]. After this initial phase, ECM is largely retained by cells and detaches with them from the substrate. This is a crucial aspect to assess since the ECM that envelops cells after detachment is the distinguishing feature of cell sheet engineering. It in fact permits a full and rapid integration once transplanted in the injured host tissue.

Despite these interesting results, the cell lift-off presents some aspects that are still under investigation. In particular, the amount and type of ECM left on the substrate after detachment is still debated[19].

Another concept that has been criticized in recent reviews[9,19], as regard the detachment process, is the misleading idea that cell lift-off is induced by a change in wettability. These authors observed that the shift in contact angle, as consequence of polymer hydration, is usually modest (20 or less degrees). Moreover, it has to be considered that mammalian cells are usually able to adhere on solid surfaces with a relatively wide range of wettability[9]. Suitable contact angles for this kind of cells can in fact extend from 33° to 96°, a range that encompasses the common contact angles for PNIPAM under both swelled and coiled conditions. Then, it has been suggested that cells were not sensitive to contact angle variation but to the hydration of the polymer chains. It is known that polymers like poly(ethylene glycol) or poly(hydroxyethylmethacrylate), when highly hydrated, resist to cell adhesion due to entropic repulsion of cell-adhesive glycoproteins[9]. Moreover the high water uptake makes the surface so soft that cells cannot tightly adhere on it[23]. In the extended conformation, PNIPAM is similarly hydrated and can consequently manifest antifouling characteristics. On the contrary, when collapsed, it is assimilable to common solid polymer surfaces, thus

permitting cell adhesion and proliferation. Current literature data propose then the view that bio-adhesiveness of PNIPAM has to be thought in terms of hydration and mechanical properties instead of the wettability.

Cole and Canavan, then, evidenced that misunderstanding as regard cell detachment and the physical mechanisms by which cells are released by PNIPAM are often underestimated while the attentions are focused on possible applications. A similar problem has been noticed by Cole also as regard the swelling/coiling process of PNIPAM brushes.

At the beginning of this section it has been briefly summarized the phase separation process for single PNIPAM chains dispersed in bulk solution. The polymer used for cell sheet engineering is, nevertheless, tethered on a substrate and, in this case, the behaviour of the smart polymer has been found to change. While the diving forces that lead to solvation and precipitation are the same as the polymer in bulk solution (hydrogen bonding and hydrophobic effect), once PNIPAM chains are tethered to a surface, the dense packaging of brushes and the interactions with the substrate lead to an alteration of the transition process.

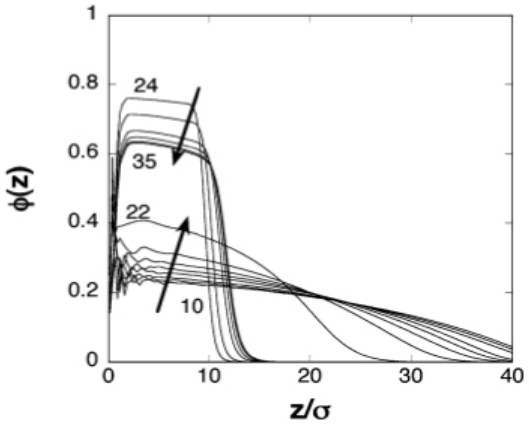

Figure 3.1.7: Example of computational modelling for swelled-to-coiled transition of tethered PNIPAM. Polymer volume fraction profiles (in ordinate) versus the distance from the surface (in abscissa) over a series of temperatures (10° to 35 °C) are shown. The arrows point in direction of increasing temperature[26].

Theoretical and computational modellings for densely grafted and high molecular weight brushes of PNIPAM have been used to predict the polymer behaviour. While similar approaches for swelled-to-coiled transition of single chains in dilute solution are well understood[24,25], the results on grafted brushes are in continuous evolution. The modelling is particularly demanding since issues of confinement, surface wetting and cooperativity are still poorly understood[9]. However, it seems generally accepted that the polymer undergoes a gradual collapse[26,27,28] instead of a sharp phase separation that follows a true second order thermodynamic transition[29]. Usually a strong dependence of this phenomenon on surface coverage has been observed such as a decrease in LCST as consequence of a higher grafting density. In particular, when the latter condition is accomplished, the temperature increase causes the decrease in solvent quality and the brushes tend to gradually shrink starting from the outermost region of the chains. Finally, brushes collapse on the substrate expelling the remaining water[26] (Figure 3.1.7). The transition of tethered brushes is, then, more gradual if compared to the case of polymer in bulk solution and extents over a broader temperature range.

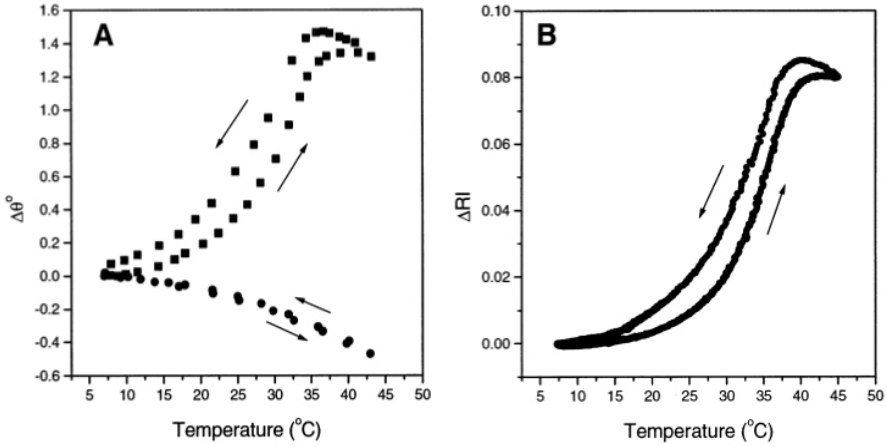

Figure 3.1.8: Temperature-dependent SPR measurement on tethered PNIPAM. (A) Change in the minimum of the SPR curve (Δθ) for the PNIPAM layer (■) and for the control surface (a SAM formed from 11-mercaptoundecane) (●) as a function of temperature. (B) Real-time measurement of change in the reflected intensity at a constant angle (74.5°) for the PNIPAM layer as a function of temperature[29].

Experimental tests confirmed the computational modellings. Surface plasmon resonance (SPR) (Figure 3.1.8) analyses showed a more or less smooth decrease in the layer thickness[29,30] during temperature increase. Similarly, other experiments, based on quartz crystal microbalance (Figure 3.1.9) and neutron reflection measurements, confirmed the hypothesis of a gradual dehydration of the polymer chains as consequence of inter/intra-molecular bound formation[30,31,32,33].

An interesting aspect related to this process is that a dependence on molecular weight has been often reported[34,32,33]. This testifies, once again, the differences in comparison to the single chains in bulk solution. Despite in the latter case an increase in molecular weight has been reported to lower the LCST[32,34], this phenomenon seems more pronounced for the tethered polymer. Some authors even reported the complete absence of transition for low molecular weight PNIPAM[34]. The mechanism is, nevertheless, argument of discussion since no systematic studies have been published yet. As regard the mismatching data, Cole and Canavan speculate that these may be the consequence of different chain density or molecular microstructure[9].

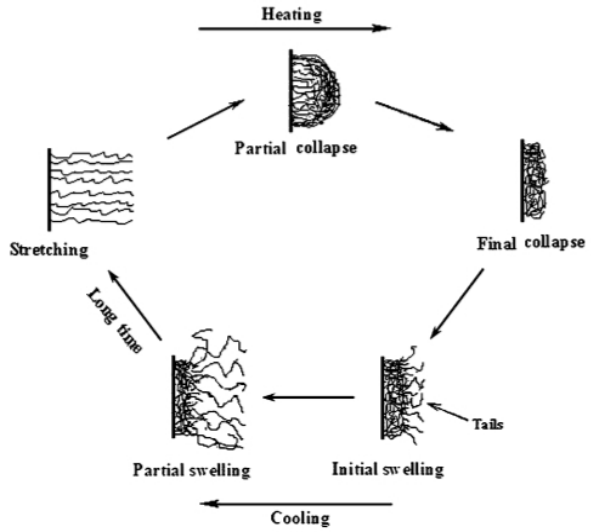

Figure 3.1.9: Schematic illustration of collapse and swelling of PNIPAM brushes[30].

Importantly, this uncertainty is reflected also on cell sheet experiments leading to an unclear detachment dependence upon PNIPAM thickness[9,35,36].

An aspect that, probably, has never received a great deal of attention is related to the outermost region of the brushes. This superficial part is of crucial importance for biomedical application of PNIPAM. Clearly, cell detachment occurs when the entire coating swells, but biological moieties and cells came in contact, and directly interact, principally with the external region of the brushes during all the cell culture period. Thus, it appears necessary to deeply analyze the outermost surface characteristics of the tethered smart polymer. In this sense, contact angle measurement represents one of the most common and versatile method to analyze superficial properties.

Results on static or advancing/receding contact angles have already been reported in literature but no detailed study on the contact angle kinetics has been published before. By means of this technique, the authors usually noticed a behaviour that resembles the PNIPAM phase separation in free bulk solution with a sharp hydrophobic/hydrophilic transition observed at the LCST[29,37,38]. On the contrary, in some cases a more gradual increase in contact angle has been reported[37,39,40,41,42].

As mentioned before, a deep knowledge on the superficial characteristics of a culture substrate is a strategical factor. Consequently, during this thesis work, it has been decided to focus the attention on the investigation of PNIAPM surface characteristics.

This has been accomplished by means of a Wilhelmy plate microbalance. This technique has been developed by Andrade et al. as an effective and powerful tool for characterizing polymer surface dynamics[38]. This method provides, in fact, reliable advancing and receding contact angles but it permits also to record other useful information related to processes occurring on the surface.

The first part of this chapter will deal with a general characterization of PNIAPM-coated samples, then, the attention will move to the analysis of the superficial properties of this thermoresponsive polymer. Finally, a possible interpretations of the observed phenomena will be proposed.

3.2 Experimental section. PNIPAM-Grafted Surfaces

As stated before, in this part of the chapter, the physical and biological characterization of PNIPAM-coated samples has been assessed. To evaluate the effectiveness of the synthesis process, non-grafted PNIPAM has been polymerized and subsequently characterized by different techniques (FTIR, NMR, cloud point test).

Then, once the synthesis method has been validated, the ATRP has been used to grow the smart polymer with a “grafted from” process on SAMs modified as surface initiator. Controls at intermediate steps of the process has been carried out by means of contact angle measurements, while, at the end of the process, grazing angle FTIR measurements confirmed the reaction success. A first physical proof of the smart behaviour of the grafted PNIPAM has been obtained by AFM measurements. In fact, the instrument recorded a different polymer thickness and stiffness for the same sample immersed in water at a temperature below and above LCST. Furthermore, ellipsometric measurements gave a more precise thickness of the PNIPAm film in the dry state.

Various biological tests have been carried out to assess the non-cytotoxicity of the obtained surfaces and to confirm the possibility for cells to adhere on the smart polymer while in a coiled state (at temperature above the LCST). Finally, the known characteristic of PNIPAM to tune cell adhesion has been proved. Cell detachment, in the form of a cell sheet, has been carried out simply decreasing the temperature of the culture medium and consequently inducing the polymer swelling.

As observed in the background part of this chapter, the physical principle that induce cell detachment is not as known in details as reputed before. In this thesis work, it has been then investigated, in different test conditions, the PNIPAM behaviour in the outermost film region during the transition. The results revealed interesting phenomena never reported before. The

collected data has been finally merged in a model to explain the polymer behaviour.

Materials and Methods

Substrate. Silicon gold coated substrates, used for PNIPAM grafting, were obtained from FBK (Fondazione Bruno Kessler, Italy). The samples were prepared starting from a Si (100) wafer on which 20 nm of chromium were deposited to improve the adhesion of the final polycrystalline gold (99.9999% pure) layer approximately 150 nm tick. Silicon thickness ranged from 0,3 mm to 1 mm depending on test methods.

Chemical products. N-Isopropylacrylamide (NIPAM, 97%), Ethyl α-bromoisobutyrate (Ebib, 98%), 11-mercapto-1-undecanol (97%), 2-bromoporpionyl bromide (>97%), triethylamine (≥99,5%), CuBr (99,999%), 1,1,4,7,7-Pentamethyldiethylenetriamine (PMDETA, 99%) and tetrahydrofuran anhydrous (THF, ≥99,9%), ascorbic acid (≥99,5%) were obtained from Sigma Aldrich.

non-grafted PNIPAM polymerization. Free polymer chains were synthesized by atom transfer radical polymerization (ATRP) with the following procedure: in a sealed schlenk flask a solution of methanol and milli-Q water (12 ml 1:1) was subjected to three freeze-pump-thaw cycles. The solution was added to a second schlenk flask where 40 mmol of NIPAM, 0,4 mmol of CuBr, 0,2 mmol of ascorbic acid and 0,13 mmol of Ebib free iniziator. The solution was stirred for 10 minutes before 1,2 mmol of PMDETA was added to start the reaction. The ascorbic acid was added as reducing agent to limit the oxidation of the copper in accordance with activators re-generated by electron transfer (ARGET) ATRP procedures[1,2]. The reaction lasted for 2 hours at room temperature and during all the period the flask was maintained under a constant nitrogen flux. PNIPAM was precipitated in hot water. The precipitate was then solubilised in water and filtered by means of an ultrafiltration-stirred cell (1 kDa membrane). PNIPAM was finally re-precipitated and dried in vacuum.

Infrared reflection absorption spectroscopy. Attenuated total reflectance Fourier transform

infrared reflection absorption spectroscopy (ATR-FTIR) was carried out on non-grafted PNIPAM with a Spectrum One (PerkinElmer). For each sample 8 scans were collected with a 4 cm-1 resolution.

Solid state NMR. Solid state NMR analyses were carried out with a Bruker 400WB instrument applying a carrier frequency of 400.13 MHz (1H). 1D experiments were based on single pulse sequence under the following conditions: 13C at 100.07 MHz, π/2 3.5 μs at -1.7 dB, 5.3 μs decoupling pulse and 10 s delay time and cross polarization experiment with delay time 5s, contact time 200 μs, decoupling and excitation pulse -4.2 μs. Samples were packed in 4 mm-zirconia rotors, which were spun at 10 kHz under air flow.

Cloud point test. Commercial PNIPAM (avarege M_n 20000-25000, Sigma) and the non-grafted PNIAPM were separately dissolved in 25 ml of Milli-Q water with a concentration of 1,5 g/l. The solutions were heated with a thermostatic bath and the cloud point of the two solution was verified.

Self assembled monolayer (SAM) preparation. Tethered PNIPAM brushes were synthesized by a "grafting from" technique utilizing the gold-coated silicon wafer covered with a modified SAM as substrate. Samples obtained by FBK have been immersed for 10min in piranha solution (70:30 H2SO4/H2O2) for a first cleaning treatment. The substrates were then rinsed with Milli-Q water and subsequently with ethanol and finally dried under nitrogen. A final treatment in RF plasma (15 sec in a low vacuum glow discharge plasma at 200 W with 40 mL/min oxygen flux) was performed to obtain a clean surface. At the end of the cleaning process AFM measurements evidenced an average surface roughness of 5,2 ± 0,4 nm with a mean grain dimension comprised between 0,5 μm and 0,1 μm (Figure 3.2.1). Immediately after these treatments the samples were soaked in a 2 mM ethanol solution of 11-mercapto-1-undecanol for 48 h. Once removed from solution, the samples were rinsed with ethanol in order to remove the physisorbed thiols and subsequently dried under nitrogen.

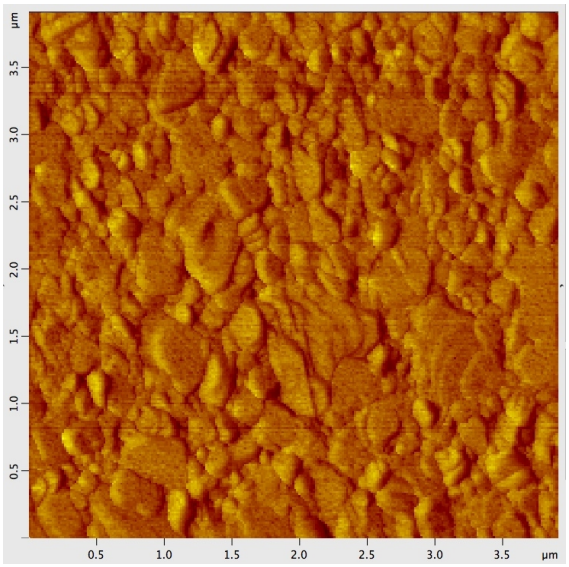

Figure 3.2.1: AFM topography of the polycrystalline gold substrate after cleaning

SAM modification into initiator. The hydroxyl terminated SAM were immersed in 8 ml of anhydrous terahydrofuran. 2-bromopropionyl bromide (0.1 M) was added drop-wise in the presence of triethylamine (0.12 M) for 2–3 min at room temperature. The sample was dipped in the solution only for a short time since a thiol SAM could be unstable in acid bromide. The reaction was done in an inert nitrogen atmosphere because the acid bromides are moisture sensitive, especially in presence of an organic base.

Static contact angle. Static contact angle on SAM and SAM modified surfaces have been performed by means of a custom made goniometer using a 3 µl drop of milli-Q water as probing liquid. For each sample, at least three measurements from different surface locations were averaged.

Surface-initiated PNIPAM polymerization. After the SAM modification, the samples were abundantly rinsed in ethanol and dried under a flux of nitrogen. The polymer was subsequently synthesized via a "grafting from" process using an atom transfer radical

polymerization (ATRP) with the following procedure: in a sealed schlenk flask a solution of methanol and milli-Q water (12 ml 1:1) was subjected to three freeze-pump-thaw cycles. The solution was added to a second schlenk flask where 40 mmol of NIPAM, 0.4 mmol of CuBr, 0.2mmol of ascorbic acid and the samples were previously added and degassed. The solution was stirred for 10 minutes before the addition of 1,2 mmol of PMDETA to start the reaction. The reaction lasted for 0,5 hours at room temperature and during all the period the flask was maintained under a constant nitrogen flux. The reaction was stopped transferring the samples in a flask containing methanol and milli-Q water (1:1). Finally the samples were abundantly rinsed with ethanol and, subsequently, stored in ethanol.

Infrared reflection absorption spectroscopy in grazing angle. Attenuated total reflectance Fourier transform infrared reflection absorption spectroscopy (ATR-FTIR) was carried out with a Spectrum One (PerkinElmer) coupled with a VeeMax II Accessory (PIKE) for grazing angle (GA) measurements. The source light was p-polarized and spectra were collected at 65° in grazing angle reflection mode. For each sample 128 scans were collected with a 4 cm-1 resolution. In order to have the best signal-to-noise ratio for this test the synthesis reaction time has been prolonged to 5 hours.

Atomic force microscopy (AFM) measurements. The AFM system used in this study was a NT-MDT scanning prob microscopy solver P47H equipped with a S7 scanner (scanning by sample). The measurements were performed in the contact mode with samples immersed in milli-Q water at the set temperature. A Si cantilever with a spring constant of 0.03 N/m and a tip radius of 10 nm was used (scanning rate 0.6-1 Hz). All images (512 _ 512 pixels) were collected over a 4x4 μm scan area in the “height mode”, which kept the force constant. The roughness value was the average calculated on at least three different regions for each sample. Subsequently the AFM tip has been repeatedly approached and retreated from the surface in the same position to study the mechanical response of the tethered brashes at different temperature (above and below the LCST). A precise control of temperature was not possible due to the instrument limits. The cantilever deflection, proportional to the force opposed by the material, is registered by the instrument as a current variation. However, a conversion of

this parameter to real deflection values was not possible with the available configuration. Moreover, a calculation of the real force, generated by the material during the compression with the AFM tip, is subjected to error due to an inaccurate value of the spring constant of the cantilever. Thus, it has been plotted the obtained value as a current variation (nevertheless $\propto$ to force) against the z-position of the AFM tip. The zero, on the z-position axis, has been arbitrary taken as the point where the elastic response of the rigid gold substrate starts.

Film thickness measurements by ellipsometry. Ellipsometry measurements were obtained with an UVISEL 800 (Horiba) ellipsometer at fixed incident angle of 45°. A gold-coated wafer, cleaned in piranha, was used to determine the optical constants of the bare gold substrate. A SAM modified with the halogen initiator of ATRP was used to determine the SAM thickness (approximately 1,7 nm). The polymer film data were then fit to a two-layer model with gold and the SAM as substrate covered by the PNIPAM layer.

Cell culture. Before cell culture, all samples have been disinfected by immersion in ethanol 70% followed by washing with sterile phosphate buffer solution (PBS) and finally placed in a 24-wells plates. 1 ml of cell suspension of human osteosarcoma cells (MG63, passage 109, obtained from Istituto Zooprofilattico di Brescia) was seeded in each well at a concentration of $0{,}5x10^5$ cells/ml ($\sim$300 cells/mm^2). Minimum essential medium (MEM, Invitrogen) supplemented with 10% heat inactivated Fetal Bovine Serum (FBS), sodium piruvate (1mM, Euroclone), L-glutamine (4mM, Euroclone), 1% vitamins, 1% non essential aminoacids, 1% Penicillin was used as culture medium. As a control test the cells were also seeded in an empty culture well. Cells were incubated at 37ºC in a 5% CO_2 atmosphere incubator, changing the medium one day after the seeding and subsequently every two days. In order to verify cells initial adhesion after 24 hours from the seeding, three samples have been fixed in a formaldehyde solution (4% in PBS) with 0.2% TritonX for permeabilization. The samples were then stained with rhodamine phalloidin (cell cytoskeleton, red) and DAPI (cell nucleus, blue) according to the manufacturers' protocol (Molecular Probes Inc., Oregon, USA). Finally the morphology of cells has been observed by confocal microscopy (Nikon confocal

microscopy A1) and the cell number has been determined taking nine pictures on a 3x3 mm^2 regular grid for each samples. The so obtained images have been analyzed counting the nuclei number and, finally, the mean cell number per square centimetres has been calculated. After 3 days of culture, cells confluence was reached and cell sheet detachment has been tested. The samples were kept under a laminar hood at room temperature to induce the cell sheet detachment. After the completion of the process, a viability test on the cell sheets has been carried out. Samples stained with fluorescein diacetate–propidium iodide (FDA–PI) (Molecular Probes Inc., Oregon, USA) were observed at the confocal laser microscope. FDA stains viable cells green, while PI stains necrotic and secondary apoptotic cells red. The assay was performed according with previously published methods[3]. Cell morphology after detachment was also observed by confocal microscope. The samples have been stained with rhodamine phalloidin (cell cytoskeleton, red) and DAPI (cell nucleus, blue) as described before. To check cell ability to re-adhere in a sheet-form, the detached layers of cells have been placed in a new culture well and few microliters of culture medium were added to maintain the cells alive but avoiding cell sheets to float. New culture medium was added at regular intervals (1 h) during the first five hours so that cells could adhere to the bottom of the well. At the end of this first step the sheets were found completely adherent to the bottom of the well and it was then possible to add 1 ml of culture medium. After two days, in order to verify cells viability, the cells were stained with FDA–PI and successively observed at the confocal laser microscopy.

Wilhemy plate experiments. Dynamic contact angles have been measured at different temperature using a Cahn 322 microbalance equipped with a circulating temperature bath. The test liquid (Milli-Q water, resistivity of >18 MΩ cm-1) was kept at +/-0.2 °C the set temperature. At the same time, also the temperature and the humidity of the environment has been continuously checked. The samples were kept above the bath for two minutes before the test so that a better thermal equilibrium could be reached. The immersion speed ranged from 20 μm/s to 160 μm/s. For this test specific silicon wafers coated with gold on both sides have been used. Samples size where 10x15 mm with a thickness of 300 μm in order to have

negligible surfaces not covered by PNIPAM. Two subsequent immersion cycles in water have been carried out for each sample. Samples have been also tested at 2 μm/s, in this case only one cycle has been performed due to acquisition limits of the instrument. Advancing and receding contact angle values have been calculated as the average of three independent runs. Before each test the samples have been dried under a dry nitrogen flux, while, once the experiment ended, they have been stored in pure ethanol.

Results

The synthesis of non-grafted PNIPAM has been used to control the chemical composition of the obtained polymer.

After the purification procedure, the reaction product has been characterized by FTIR spectroscopy to assess the effective PNIPAM synthesis. The measurement gave the spectra of Figure 3.2.2 (Synthesized) where the specific absorption peaks of the polymer are recognizable. In particular it is possible to identify the stretch vibration of the secondary amide group (-NH) at ～3300 cm-1, while the peak at 2971 cm-1 has been assigned to the asymmetric stretching vibration of methyl group (-CH3, but also C-H). The asymmetric bending deformation of the same group lay at 1459 cm-1. The most intense and characteristic peaks at 1647 cm-1 and 1547 cm-1 are assigned to the amide I and amide II bands, respectively. The former correspond principally to the carbonyl (-C=O) stretch, while the latter to mostly -NH in-plane deformation[4,5]. The two nearly symmetric peaks at 1387 cm-1 and 1367 cm-1 are representative of the two methyl groups in the isopropyl functionality.

Comparing the spectra of the synthesized polymer with a commercial product (Sigma) (Figure 3.2.2, commercial product), it is possible to note the practically perfect superposition of the two plots.

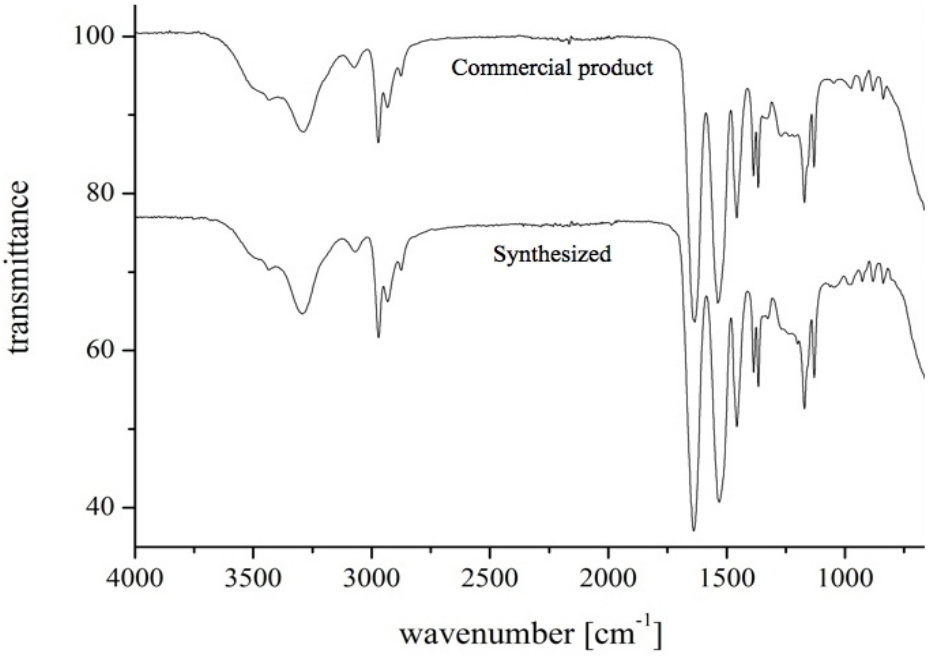

Figure 3.2.2: ATR-FTIR spectra of commercial PNIPAM (commercial product) and non-grafted PNIPAM synthesized by ARGET ATRP (Synthesized)

NMR spectrum gave further confirmation of the results obtained by FTIR (Figure 3.2.3).

The first peak (starting from right) has been assigned to the two methyl groups of the isopropyl functionality (a, b). The broad peak, that starts at approximately 30 ppm and becomes the shoulder of the peak positioned at around 42 ppm, has been associated with the tertiary carbon atom of the polymer backbone (e) and the tertiary carbon atom of the isopropyl group (c). The shoulder is particularly broad since the tertiary carbon atom peak of the isopropyl group presents a shift induced by the near nitrogen atom. The sharp peak at approximately 42 ppm corresponds to the CH2 atoms of the chain backbone (f) while the peak at 175 ppm is the signal relative to the carbonyl group (d). The two small peaks at 75 and 165 ppm are spinning side bands.

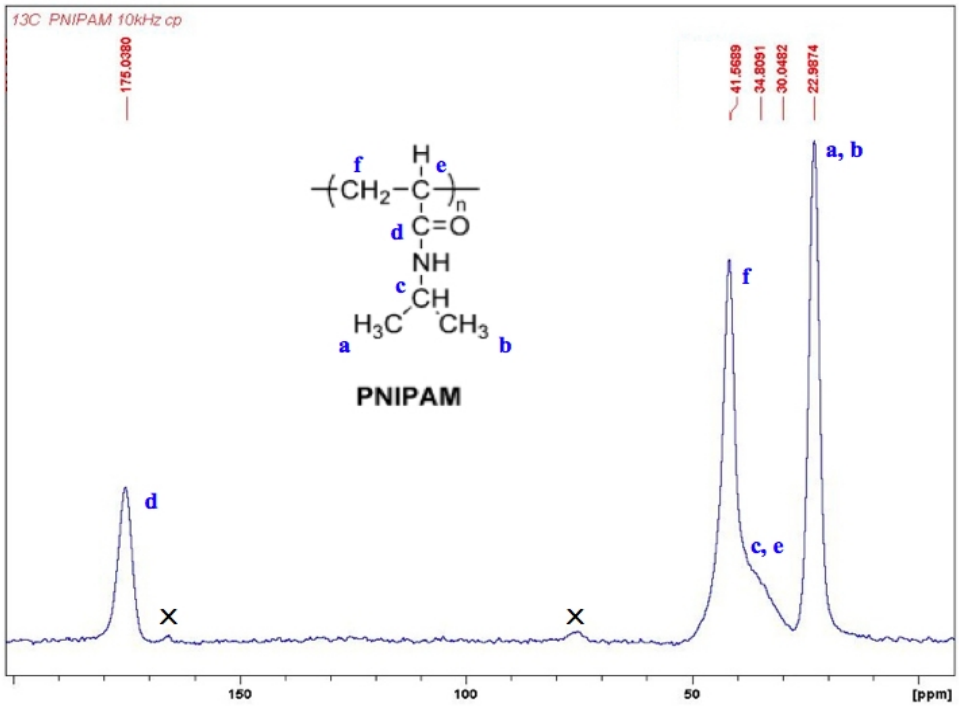

Figure 3.2.3: Solid state 13C NMR spectrum of non-grafted PNIPAM. X represents the spinning side bands.

The temperature transition of the non-grafted PNIPAM has been evaluated by means of the so-called cloud point test. This is a simple method to verify the temperature at which the phase separation takes place by observing the transparency of a PNIPAM aqueous solution at the variation of temperature. At 25 °C the solution is perfectly transparent (Figure 3.2.4, left) but, heating the solution, when the LCST is reached the liquid suddenly becomes opaque due to the light scattering caused by the phase separation of PNIPAM microparticles (Figure 3.2.4, right). The non-grafted PNIPAM displayed a LCST at 34,5 °C while for the commercial polymer the transition occurred at 34 °C.

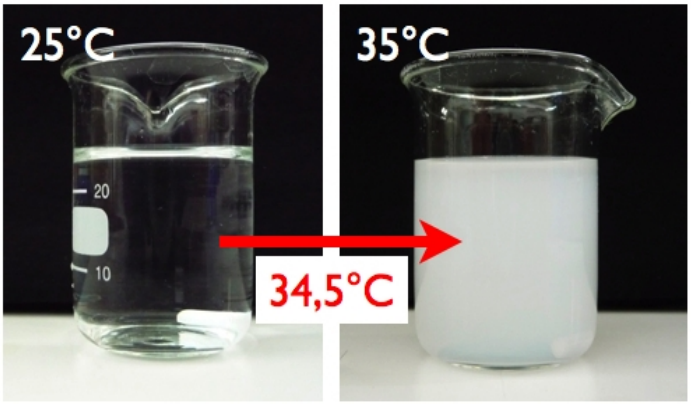

Figure 3.2.4: Cloud point test: 37,5 mg of synthesized PNIPAM has been dissolved in 25 ml at 25 °C (left). Increasing the temperature above the LCST (34,5 °C) the solution becomes turbid (right) due to PNIPAM precipitation.

Once the synthesis procedure has been validated, it has been proceeded with the grafting of PNIPAM on modified SAM surfaces. Following the described procedures (Scheme 3.2.1), the hydroxyl terminated SAM has been obtained and subsequently modified into the polymerization initiator (Figure 3.2.5).

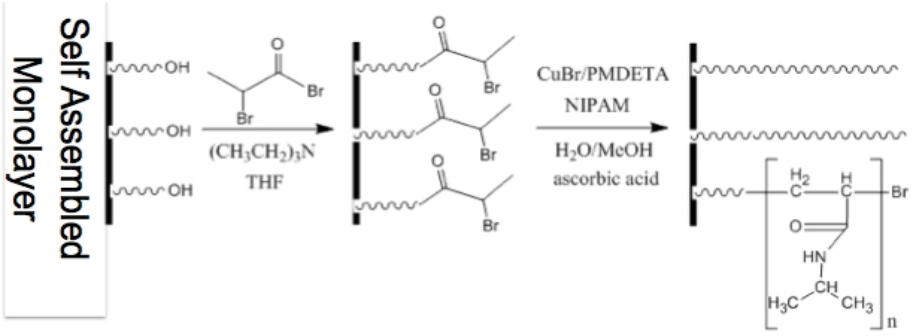

Scheme 3.2.1: grafted "from" reaction scheme: the hydroxyl terminated SAM has been modified into the polymerization initiator. Subsequently the ATRP of NIPAM has been carried out

After each step the process was indirectly controlled measuring the static contact angle of the surfaces. On hydroxyl terminated SAM a static contact angle of 13,1° ± 3,7° (Figure 3.2.5,

left) has been measured while on the modified SAM the contact angle value increased to 78,7° ± 2,5° (Figure 3.2.5, right). The latter result is consistent with the literature data[6] and testifies a marked decrease in wettability as consequence of the new hydrophobic moieties covalently linked to the surface.

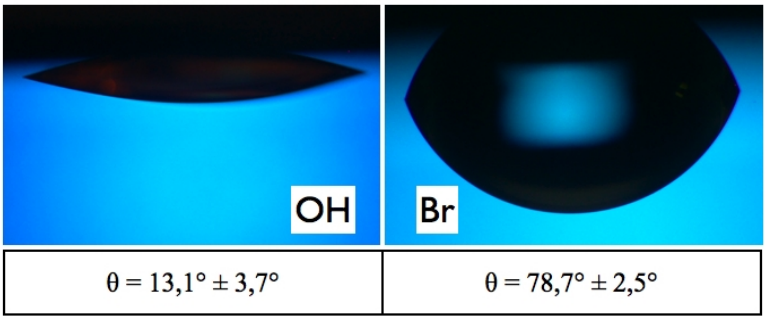

Figure 3.2.5: static contact angle (θ) of hydroxyl terminated SAM (OH) and modified in the bromine-terminated polymerization initiator (Br)

The halogen terminated SAMs have been then used to start the the synthesis procedure of PNIPAM (Scheme 3.2.1). The results were checked firstly by means of ATR-FTIR analysis (Figure 3.2.6). Despite the limits of the equipment in grazing angle lead to a noisy graph in spectrum region above approximately 3000 cm^{-1}, all the fingerprints of PNPAM are clearly distinguishable and comparable with the data obtained for non-grafted PNIPAM (Figure 3.2.2) and the literature[4,5].

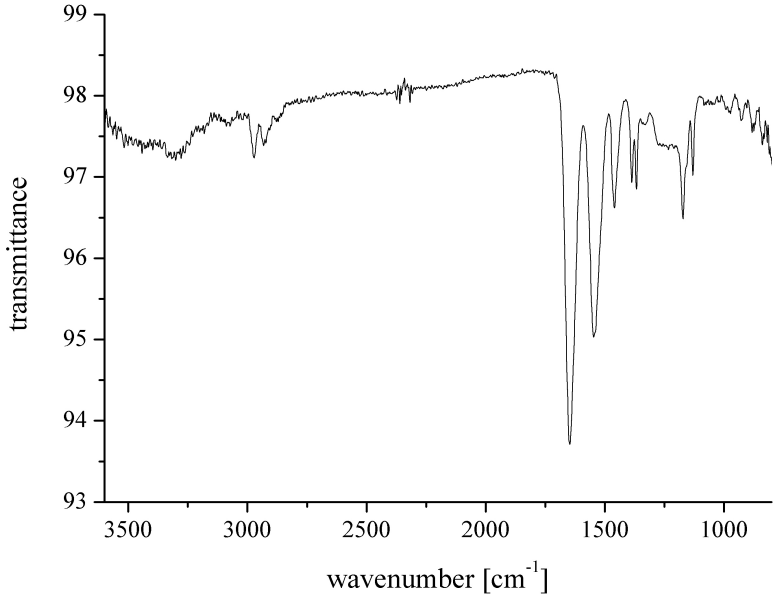

Figure 3.2.6: ATR-FTIR-GA spectrum of grafted PNIPAM

Samples topography has been characterized by means of AFM above and below the LCST (Figure 3.2.7 and Figure 3.2.8, respectively below and above LCST).

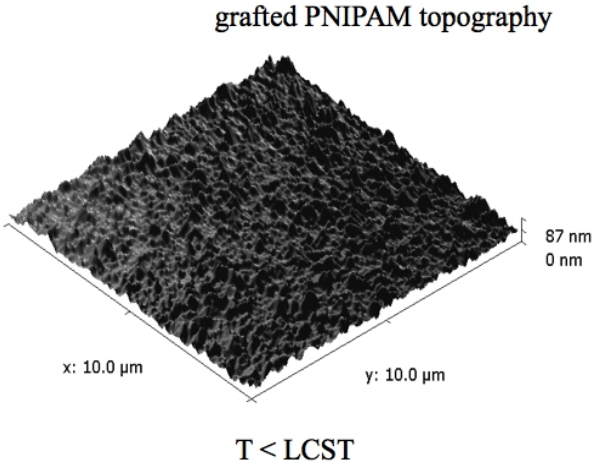

Figure 3.2.7: AFM topography of grafted PNIPAM at a temperature below the LCST

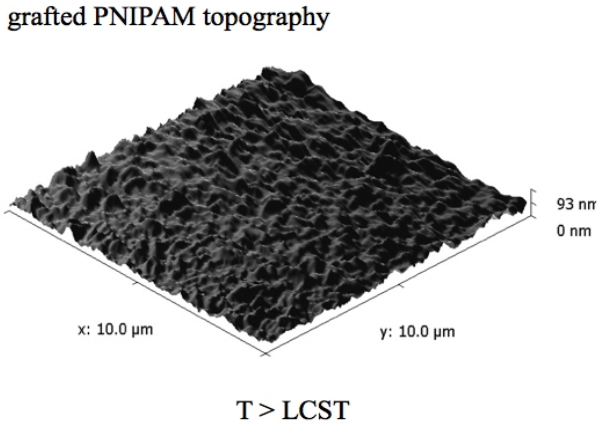

Figure 3.2.8: AFM topography of grafted PNIPAM at a temperature above the LCST

Despite a similar average roughness (7,8 nm above LCST and 7,6 nm below LCST) the surface topography observed at temperature below the LCST appears more corrugated. Subsequently, the AFM tip has been used as an "indenter" to probe the PNIPAM brushes response in the swollen and in the coiled state.

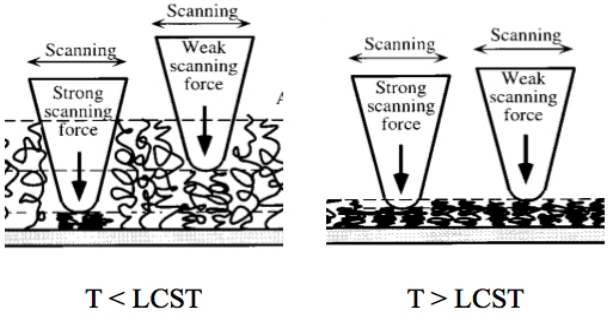

Figure 3.2.9: schematic representation of the compression test performed by AFM tip at a temperature below (left) and above (right) the LCST[7]

Figure 3.2.9 displays a schematic representation of the test with the AFM tip while compressing the tethered polymer chains. During the test, the instrument indirectly registered the AFM cantilever deflection as consequence of the opposing force generated by the brushes

to tip penetration (refer to materials and methods for further elucidations). These approach/retreat curves clearly displayed a different cantilever deflection in response to temperature change (Figure 3.2.10).

At high temperature, the instrument started to register the brushes residence to penetration close to the zero value of z-position (determined as the point where the linear elastic response of the rigid gold substratum starts), while the interaction of AFM tips with the PNIPAM chains in a swelled state started further from the surface. Moreover, the force opposed to the penetration grew more slowly at temperature below the LCST indicating that, in this state, the material is softer. From these plots it has been also possible to indirectly measure the film thickness in the swelled and coiled state but the values have to be considered as an approximation since the AFM tip is not sufficiently sensible to measure the real swelled thickness[7].

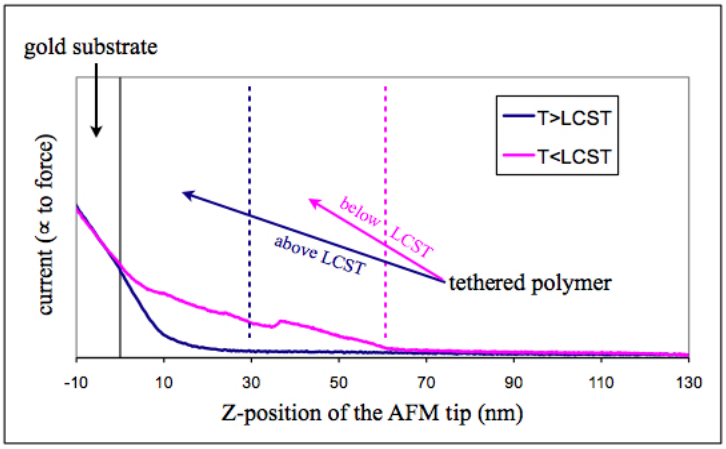

Figure 3.2.10: compression test performed by the AFM. The magenta line represents the force opposed by brushes to AFF tip penetration at a temperature below LCST. The dark blue line is instead relative to the test carried out at a temperature above the LCST. The black line indicates the approximative point where the gold substrate starts to interact with the tip and considered as the 0 distance from the surface. The magenta dotted line represents the approximative volume occupied by the swelled brushes, while the dark blue dotted line the approximative volume occupied by coiled polymer chains.

For a better determination of the polymer film thickness in the dry state, samples were characterized by means of an ellipsometer. A gold-coated wafer, cleaned in piranha, was used to determine the optical constants of the bare gold substrate. A SAM modified with the halogen initiator of ATRP was used to determine the monolayer thickness. The optical characteristics of the surfaces have been simulated using two different methods: an oscillator model and a Sellmeier dispersion curve. The two methods produced a good fit with similar extrapolated results that furnished a mean SAM thickness of 1,7 nm. The obtained value is consistent with the literature data reported for analogues surfaces[8,9]. Finally, to determine the PNIPAM thickness, the surface has been fitted to a two-layer model with the polymer and a substrate composed by gold and the SAM. A total thickness of 27,5 ± 2,0 nm has been calculated for the PNIPAM-grafted samples obtained by a reaction time of 0,5 hours.

Biological *in vitro* experiments have been used to demonstrate the smart properties of PNIPAM coating as regard cell sheet engineering applications.

As stated before, cell sheet detachment is induced by the transition of the PNIPAM brushes from a collapsed to a swelled state[10,11,12]. To trigger cells adhesion it is then sufficient to control the temperature of the culture medium. At 37 °C (usual culture temperature) cells can adhere and proliferate on samples surface but, when temperature is decreased below the LCST, an active and passive process of cell detachment starts[13,14]. In the present study, cell culture tests have been carried out using osteoblast-like cells.

To verify initial cells adhesion, the culture on three samples has been stopped after one day from the seeding. The results displayed a good initial response with a physiological spreading and a typical morphology for MG63 cells (Figure 3.2.11). The cells number has been determined as previously specified and gave the results of 286 cells/mm^2.

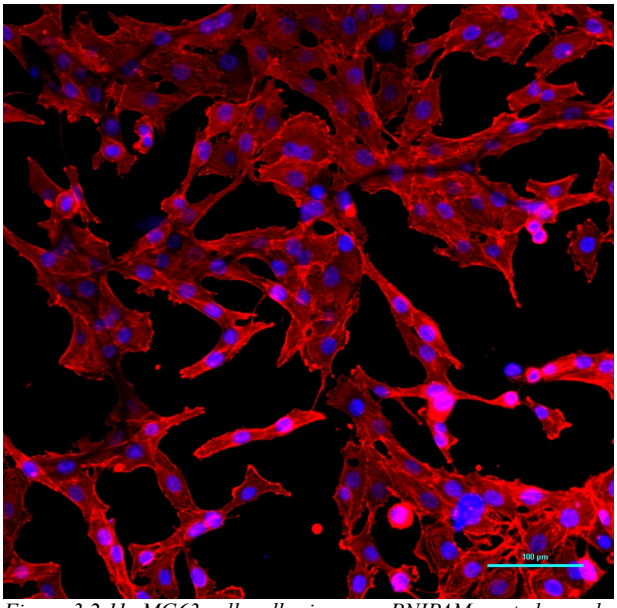

Figure 3.2.11: MG63 cells adhering on a PNIPAM-coated sample after 24 hours from the seeding. Cell nuclei are marked in blue, while the cytoskeleton in red.

Cells were capable to reach confluence after 3 days from the seeding and consequently cell detachment was verified. Samples were transferred under a laminar hood and, after culture medium reached room temperature, a sheet of cells has been observed to slowly detach from the PNIAPM coated surfaces (Figure 3.2.12). During the detachment, it has been observed a cell shape change from a spread to a rounded state. Subsequently, cells started to detach in from of a sheet that tended to contract.

In the control wells nothing has been noted.

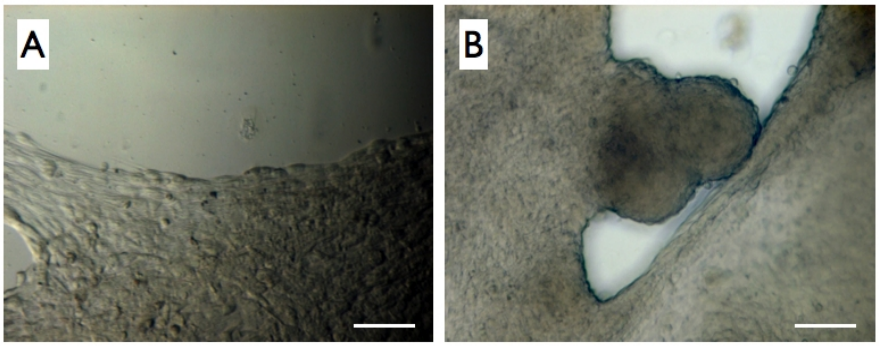

Figure 3.2.12: images of two different regions of a MG63 cell sheet contracting during the detachment from a PNIPAM-coated sample.

After the complete detachment, some cell laminae have been gently collected and stained with FDA-PI to assess the viability.

As Figure 3.2.13 attests, except a negligible minority, cells survived to the detachment indicating the capability for the PNIPAM-coated samples to induce detachment without damaging cells.

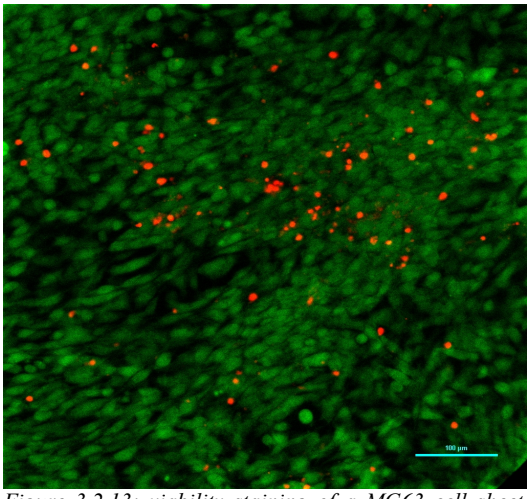

Figure 3.2.13: viability staining of a MG63 cell sheet detached from a PNIPAM-coated sample. Alive cells (green) and dead cells (red).

Similarly, cell morphology was observed staining cell sheets with rhodamine phalloidin and DAPI (Figure 3.2.14). Unfortunately, this image is not so clear since the collapse of the cytoskeleton filaments limits the recognition of cell shape. However, as it will better elucidate in the discussion part, this is commonly observed.

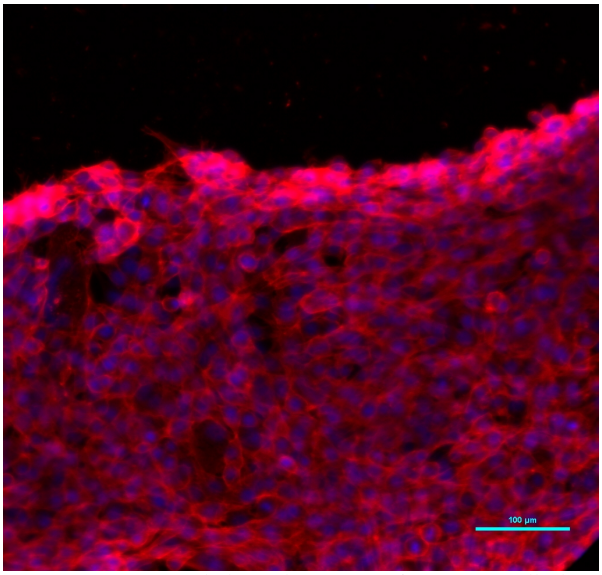

Figure 3.2.14: morphological staining of a MG63 cell sheet after the detachment from a PNIPAM-coated sample. Cell nuclei (blue) and cytoskeleton (red).

As described in material and methods, detached cell sheets have been placed in a new culture well to test its re-adhesion capability. Within few hours from the "re-seeding", cells have been observed to tightly adhere to the bottom of the well and start to proliferate. After 48 hours, the cell sheet culture has been stopped and the results observed by confocal microscopy. Again cells exhibited a good viability (Figure 3.2.15). In this case an increase in dead cells (red spots in Figure 3.2.15) is the consequence of cell sheet folding due to a difficult handling of the lamina during the placement in the culture well. The overlapping of cells, in fact, caused a decrease in passive diffusion that impeded a correct delivery of nutrients and removal of metabolic wastes for the cells adhering to the polystyrene substrate. Therefore, cell apoptosis

has been observed.

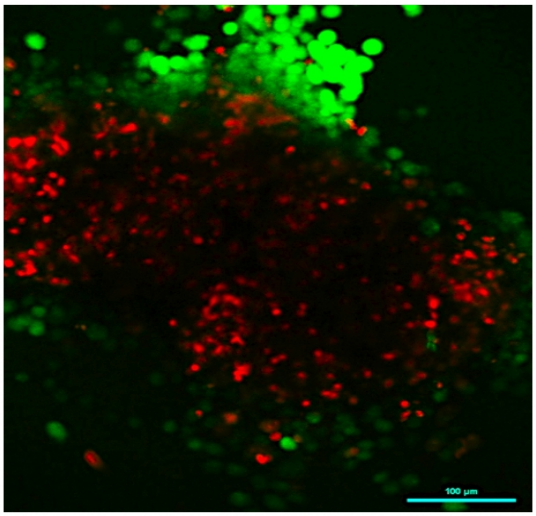

Figure 3.2.15: MG63 cell sheet, harvested from a PNIPAM-coated substrate, re-seeded in a culture well. The image has been taken 48 hours after the cell layer re-adhesion. Alive cells are marked in green while red spots represent dead cells.

Once a positive result as regard cell sheet engineering has been assessed, it has been investigated the smart behaviour of PNIPAM in the outermost surface.

To accomplish the task the Wilhelmy plate technique has been used. This permitted to observe the wettability evolution during the phase transition and, furthermore, to establish the final characteristics of PNIPAM-coated surfaces at the end of the process. As stated earlier, this is crucial in order to study the interaction between cells and the smart substrate during the culture period.

In particular, surface dynamics have been investigated modifying temperature but also immersion speed to highlight the kinetic contribution to the transition process. The results of advancing contact angle are summarized in Figures 16-19: the first two graphs are relative to the first immersion cycle (Figure 3.2.16: data plotted as function of temperature; Figure 3.2.17 as function of immersion speed), while the latter two graphs are relative to the second

immersion cycle (Figure 3.2.18: as function of temperature; Figure 3.2.19 as function of immersion speed, below).

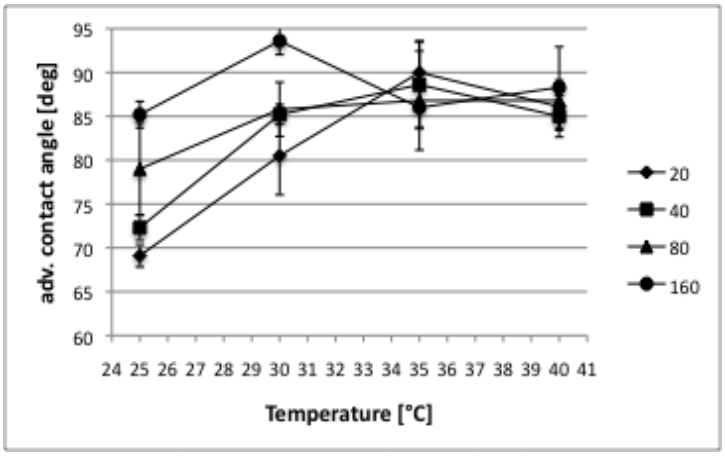

Figure 3.2.16: advancing contact angle on tethered PNIPAM (synthesis reaction time 0,5 hr) at different immersion speeds (20, 40, 80 and 160 μm/sec). First immersion cycle, plotted as function of temperature.

At low speed (especially at 20 μm/sec) it has been possible to notice that, as expected, the contact angle of PNIPAM tended to increase with increasing temperature (Figure 3.2.16). The transition was not sharp and close to the LCST, but it has been more gradual and extends over a wider temperature range. It is also evident that above 35 °C a plateau has been reached with contact angles values ranging from 85° to 90°. Observing the graph, it is important to emphasize that a faster immersion speed led to a reduced responsiveness toward temperature, until the limit case of the highest tested speed (160 μm/sec), where no evident variation in the contact angles occured while changing the temperature. At this speed the surface has been equally hydrophobic regardless of the temperature of water in which samples are dipped.

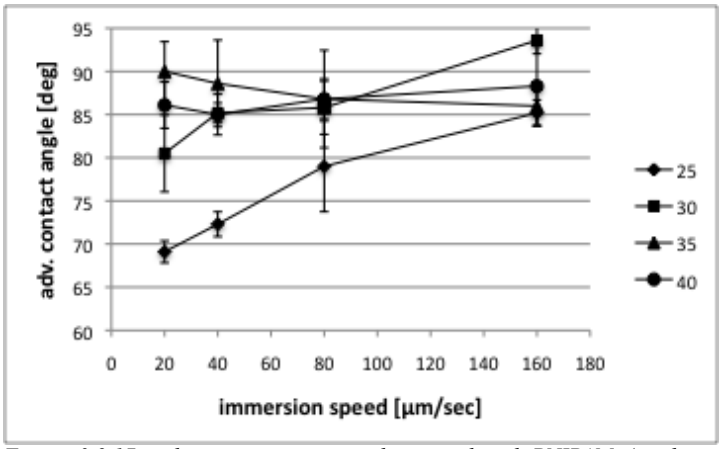

Figure 3.2.17: advancing contact angle on tethered PNIPAM (synthesis reaction time 0,5 hr) at different temperature (25, 30, 35 and 40 °C). First immersion cycle, plotted as function of immersion speed.

This trend, typically kinetic, is well evidenced by the graph that reports the advancing contact angle as function of the immersion speed (Figure 3.2.17). The curve at 25 °C is a monotonically increasing function of immersion speed, while for higher temperatures (35 °C and 40 °C) this trend is virtually inexistent; on the contrary, these curves are levelled around the maximum recorded values for advancing contact angles. Even in the intermediate case of 30 °C the trend is not so evident, nevertheless, it is possible to see a decreasing trend in wettability with increasing speed.

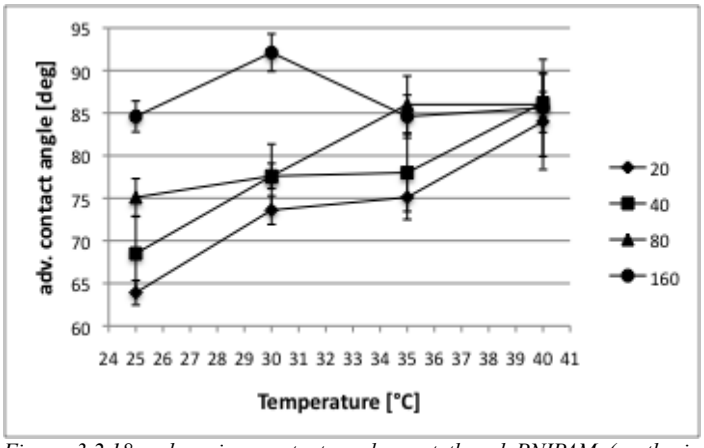

Figure 3.2.18: advancing contact angle on tethered PNIPAM (synthesis reaction time 0,5 hr) at different immersion speeds (20, 40, 80 and 160 µm/sec). Second immersion cycle, plotted as function of temperature.

Observing the advancing contact angle of the second cycle of immersion (Figure 3.2.18 and Figure 3.2.19), it can be seen a general shift of the curves toward lower hydrophobic values. This fact indicates that there is a tendency for the polymer to retain some water after the first cycle. It is also observed that the increase in advancing contact angle, with increasing temperature, extends now over a wider temperature range. In particular, no plateau are detectable even at high temperature, while only at the highest tested speed there is a flat response in the contact angle values. Contrary to the first cycle then, the surface is evidently more sensitive to temperature. This is also clear from the graph displaying curves as functions of immersion speed (Figure 3.2.19): only at 40 °C the curve is essentially flat while, at lower temperature, the dependence on the immersion speed is more evident.

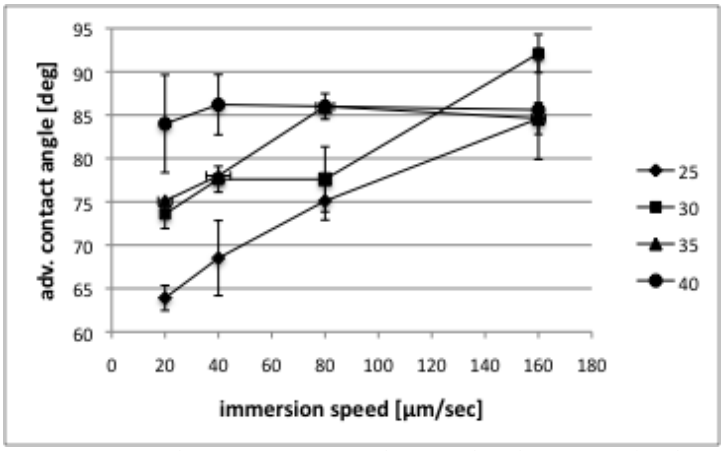

Figure 3.2.19: advancing contact angle on tethered PNIPAM (synthesis reaction time 0,5 hr) at different temperature (25, 30, 35 and 40 °C). Second immersion cycle, plotted as function of immersion speed.

Receding contact angles are substantially indistinguishable between the first and the second cycle (Figure 3.2.20 and Figure 3.2.21). No appreciable dependence on temperature or speed is noticeable; the surfaces exhibited little sensitiveness to variations in temperature or speed, even when the polymer chains have been supposed to be in a "wet" state (after the first immersion cycle). The only exception is remarkably seen in tests at 25 °C. At this temperature the receding contact angle values resulted constantly higher if compared to all the other cases.

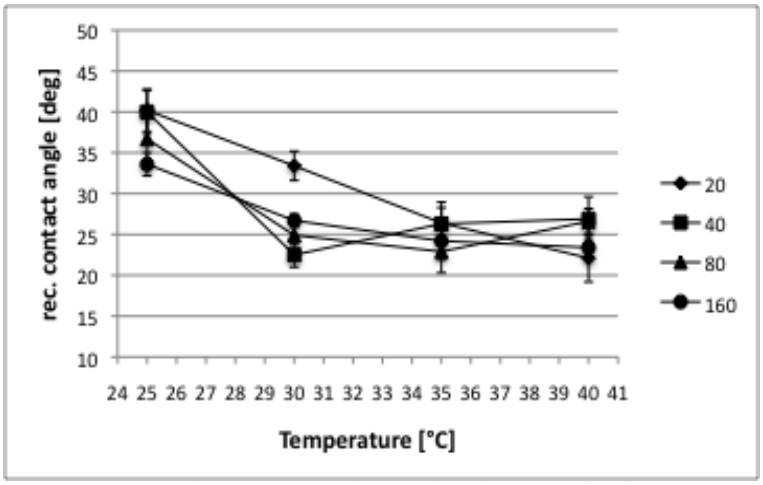

Figure 3.2.20: receding contact angle on tethered PNIPAM (synthesis reaction time 0,5 hr) at different immersion speeds (20, 40, 80 and 160 µm/sec). First and second immersion cycle, plotted as function of temperature.

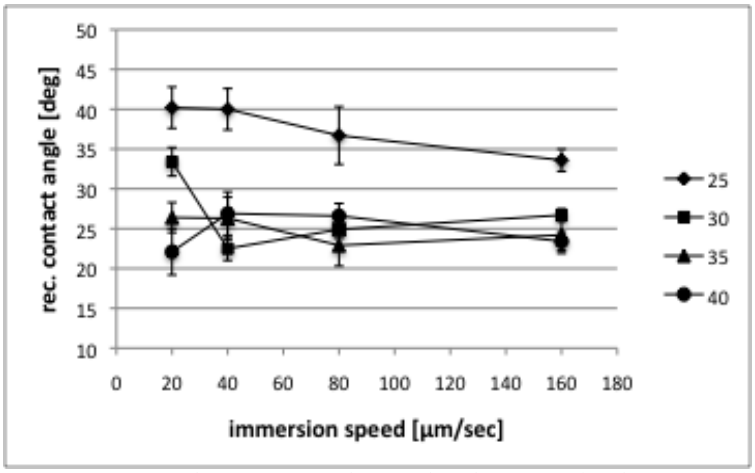

Figure 3.2.21: receding contact angle on tethered PNIPAM (synthesis reaction time 0,5 hr) at different temperature (25, 30, 35 and 40 °C). First and second immersion cycle, plotted as function of immersion speed.

As it is possible to notice in Figure 3.2.21 also the plot as function of immersion speed doesn't suggest any remarkable reactivity of the surface when conditions change. This actually denotes a distinctive difference of advancing form receding contact angles. The latter display generally little variations with almost identical values, in agreement with reported literature data for PNIPAM brushes[7,15,16]. However, it is more evident from this plot that the results at 25 °C differ considerably from the others obtained at higher temperatures. The values in this case are always clearly higher and seem to have a slight tendency to decrease with increasing speed.

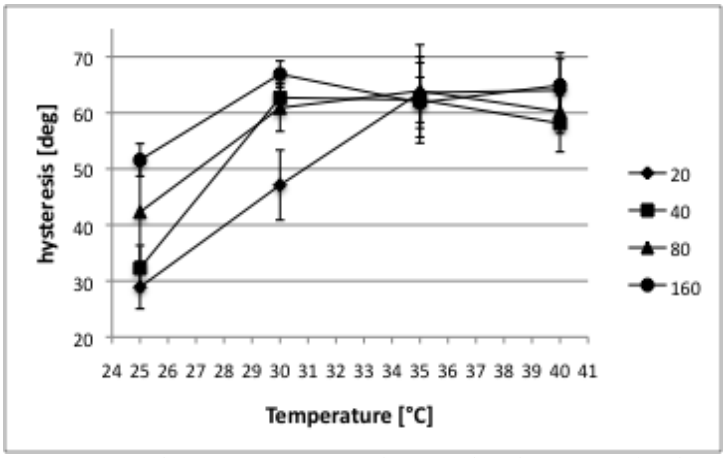

Figure 3.2.22: hysteresis contact angle on tethered PNIPAM (synthesis reaction time 0,5 hr) at different immersion speeds (20, 40, 80 and 160 μm/sec). First immersion cycle, plotted as function of temperature.

The data on hysteresis (defined as the difference between advancing and receding contact angle, Figures 22-25) reflect the trend of advancing contact angles, since receding contact angles are almost constant. Obviously the cases obtained at temperatures of 25 °C present some differences. Due to the fact that receding angles are higher at this temperature, hysteresis results markedly inferior, as it is more readily observable in the graphs as function of the immersion speed (Figure 3.2.23 and Figure 3.2.25).

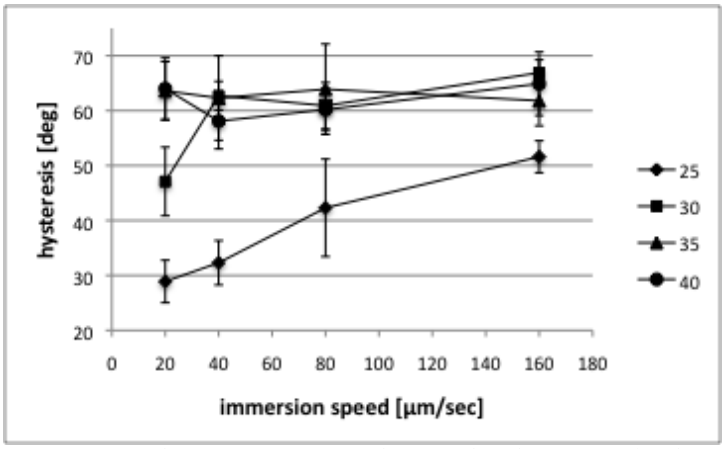

Figure 3.2.23: hysteresis contact angle on tethered PNIPAM (synthesis reaction time 0,5 hr) at different temperature (25, 30, 35 and 40 °C). First immersion cycle, plotted as function of immersion speed.

Hysteresis values are, in general, quite high and tend to converge to a common value when both temperature and immersion speed increase. This fact indicates that the surface is far from a thermodynamic equilibrium state with superficial dynamics doubtless affecting the measured advancing and receding contact angles.

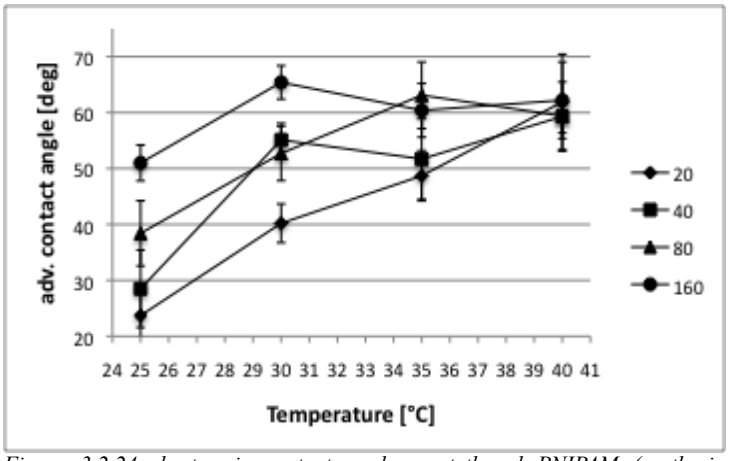

Figure 3.2.24: hysteresis contact angle on tethered PNIPAM (synthesis reaction time 0,5 hr) at different immersion speeds (20, 40, 80 and 160 µm/sec). Second immersion cycle, plotted as function of temperature.

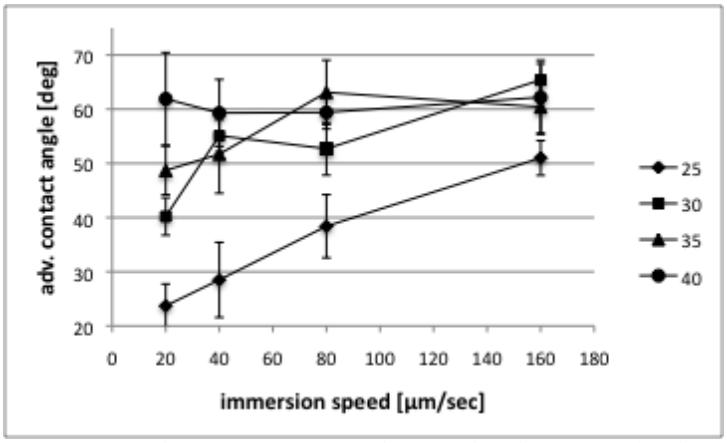

Figure 3.2.25: hysteresis contact angle on tethered PNIPAM (synthesis reaction time 0,5 hr) at different temperature (25, 30, 35 and 40 °C). Second immersion cycle, plotted as function of immersion speed.

Further useful information can be drawn observing the curves recorded by the Wilhelmy microbalance. In the graph obtained at 20 µm/sec and 25 °C a sharp jump is observed in the "mass" axis when the sample comes into contact with water and the meniscus forms (Figure 3.2.26, A). The shape of this first part is particularly interesting. At low speeds and temperatures, in fact, the curves systematically displayed a rounded shape (highlighted by the red circles in figure 25 °C) immediately after the ZDOI (zero depth of immersion). This behaviour was especially evident in the second immersion cycle. This indicates that the meniscus did not reach an immediate equilibrium with the surface but tended to expand for a short distance along the surface coated with PNIPAM. Consequently, the instrument recorded a gradual increase on the "mass" axis thus producing the bow shape. Once the meniscus reached a thermodynamic stable state, the curve assumed the common and smooth downward trend. Even if such behaviour could be associated with an irregular geometry of the sample, this possibility has been rejected due to the precise cut of silicon wafer and the disappearance of the phenomenon at higher temperatures and speeds.

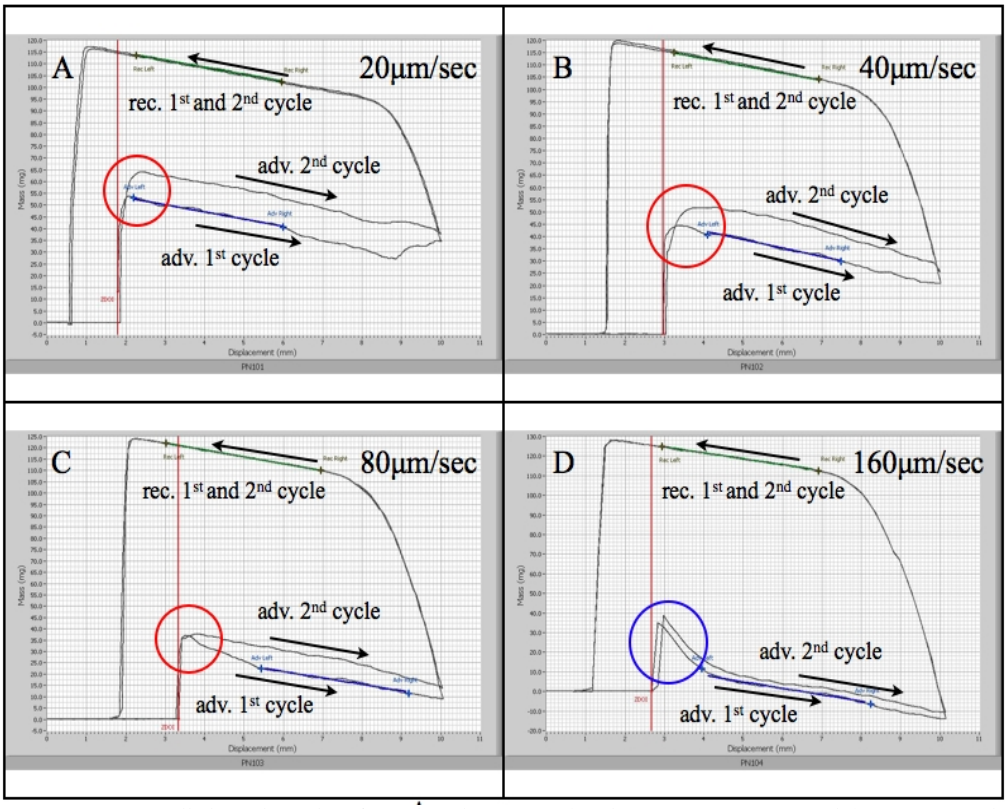

Figure 3.2.26: Wilhelmy plate plots for tethered PNIPAM (synthesis reaction time 0,5 hr) at 25 °C and different immersion speed (A: 20 µm/sec, B: 40 µm/sec, C: 80 µm/sec, D: 160 µm/sec).

Observing in fact the other plots at 25 °C (Figure 3.2.26, C-D), it is possible to note that this phenomenon tended to disappear until, in the limit case at 160 µm/sec and 25 °C, a pronounced wedge shape appeared immediately after the ZDOI instead of the bow profile (blue circle in Figure 3.2.26 D). This phenomenon has been attributed to an initial contact of the probing liquid with the edge of the silicon wafer. This side surface remained in fact uncoated and thus it exhibited a higher wettability. After this initial jump, however, when the meniscus rapidly came in contact with the polymer-coated surface, it quickly reached a new equilibrium thereby attesting on more hydrophobic values.

Another interesting fact, already analyzed observing the figures relative to advancing contact angles, is the decrease in difference of wettability between first and second cycle as

consequence of immersion speed increase. This event is even more evident from the plots at 30 °C (Figure 3.2.27, A-D), such as the bow-to-wedge profile shift in the initial contact with water.

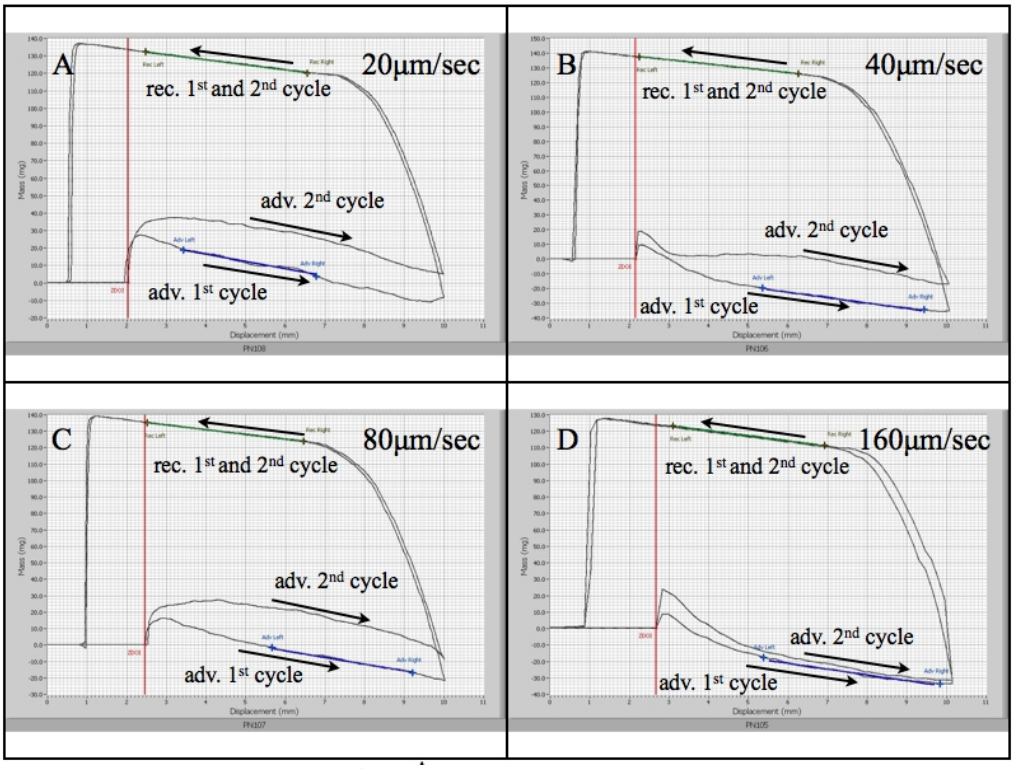

Figure 3.2.27: Wilhelmy plate plots for tethered PNIPAM (synthesis reaction time 0,5 hr) at 30 °C and different immersion speed (A: 20 µm/sec, B: 40 µm/sec, C: 80 µm/sec, D: 160 µm/sec).

Really remarkable is the phenomenon observed at temperatures above 30 °C (Figure 3.2.29, A-D, and Figure 3.2.30, A-D).

In these cases, regardless of contact angles values, it has been observed the emergence of a stick/slip behaviour that caused the sawtooth plot recorded by the instrument. This clearly

indicates a change in the nature of the surface when temperature exceeds the LCST.

As schematically described in Figure 3.2.28, the sawtooth profile (evidenced in the image box) is caused by a slow increase in contact angle (blue arrows) followed by an abrupt "jump" (red arrows) toward more hydrophilic values. After this hydrophilic shift the phenomenon starts again with the typical loops of stick/slip processes.

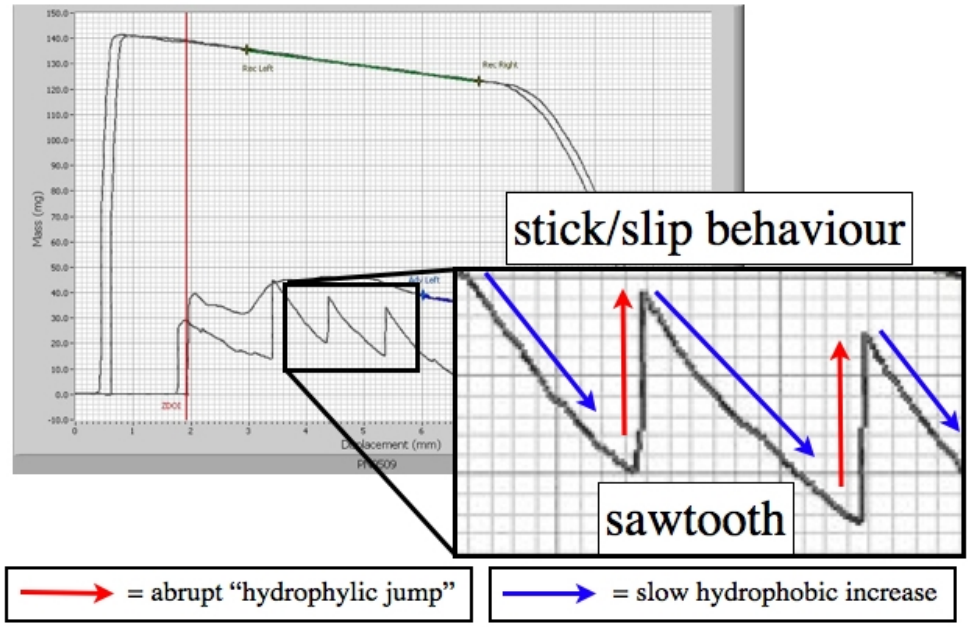

Figure 3.2.28: schematic description of the stick/slip phenomenon. The sawtooth profile (evidenced in the box) is caused by a slow increase in contact angle (blue arrows) followed by an abrupt "jump" (red arrows) toward more hydrophilic values.

Interestingly, an increase in velocity and temperature induced a sawtooth profile with ever-shorter intervals and a parallel decrease in the magnitude of the "hydrophilic jumps".

In particular, it has been noted that at 35 °C and low speed (Figure 3.2.29, A-B), the stick/slip phenomenon disappeared during the second immersion cycle with an associated shift of the contact angles toward more hydrophilic values. This symptom testifies that the brushes

remained hydrated after the first cycle, hence inducing the end of the sawtooth profile. However, at higher immersion speed (80 μm/sec), stick/slip profile never disappeared although fewer "jumps" have been recorded in the second cycle (Figure 3.2.29, C). Finally, at the highest speed, the sawtooth frequency of the first and second cycle was rather similar (Figure 3.2.29, D).

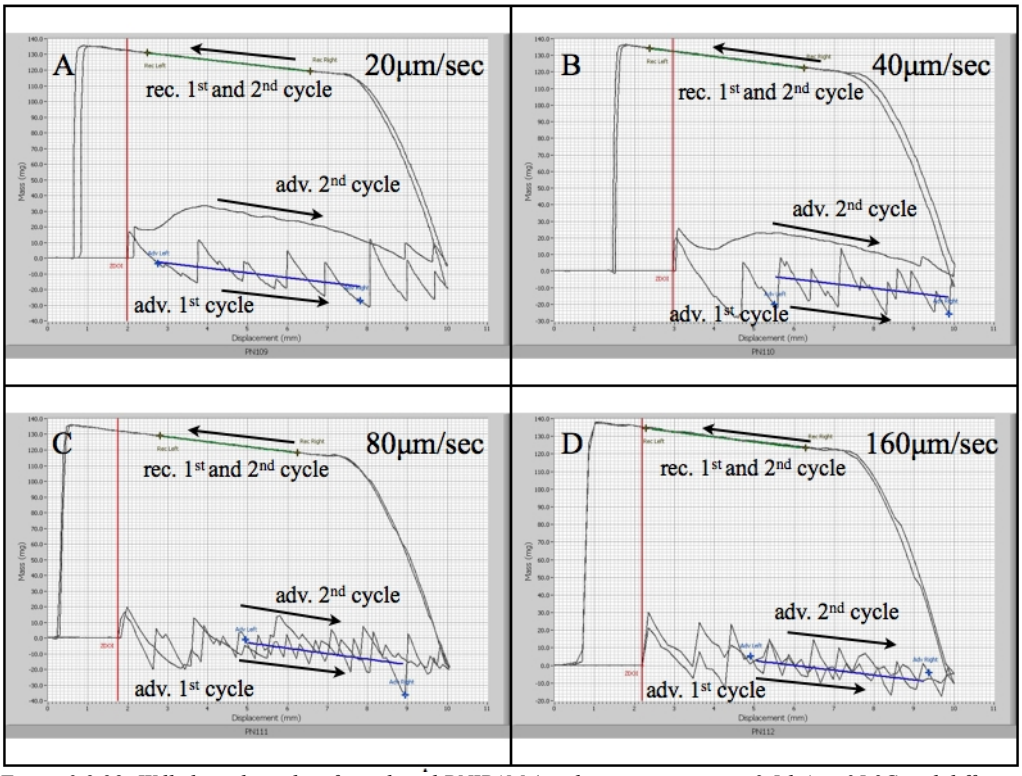

Figure 3.2.29: Wilhelmy plate plots for tethered PNIPAM (synthesis reaction time 0,5 hr) at 35 °C and different immersion speed (A: 20 μm/sec, B: 40 μm/sec, C: 80 μm/sec, D: 160 μm/sec).

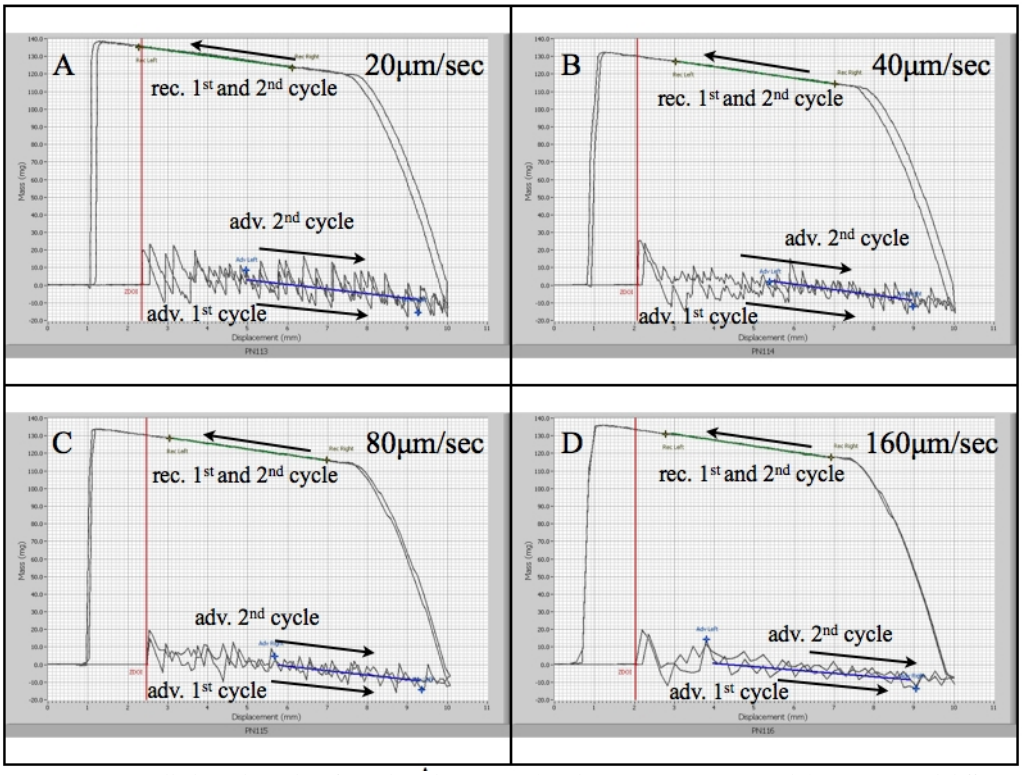

Figure 3.2.30: Wilhelmy plate plots for tethered PNIPAM (synthesis reaction time 0,5 hr) at 40 °C and different immersion speed (A: 20 µm/sec, B: 40 µm/sec, C: 80 µm/sec, D: 160 µm/sec).

At 40 °C the stick/slip phenomenon didn't disappear, regardless of the immersion cycle or immersion speed (Figure 3.2.30, A-D), and more "jumps" have been observed in comparison to the cases at 35 °C. An interesting phenomenon is noticeable at high immersion speed (160 µm/sec) (Figure 3.2.30, D), the stick/slip behaviour becomes more irregular and less marked, probably as consequence of a high kinetics that prevents a fluid development of the phenomena.

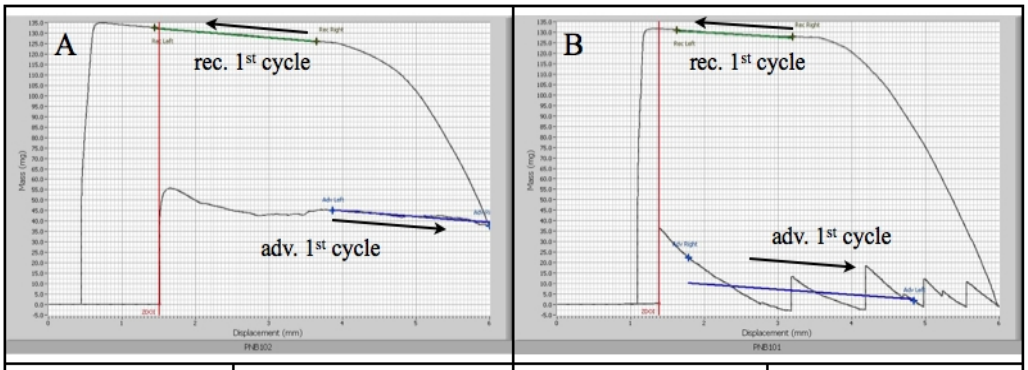

T = 25 °C	imm. speed = 2 µm/sec	T = 40 °C	imm. speed = 2 µm/sec
adv. contact angle	70,0°	adv. contact angle	83,6°
rec. contact angle	28,9°	rec. contact angle	26,2°

Figure 3.2.31: Wilhelmy plate plots and relative advancing and receding contact angles for tethered PNIPAM (synthesis reaction time 0,5 hr) at 25 °C (A) and 40 °C (B). Immersion speed = 2 µm/sec.

The observation of this typically kinetic process persuaded the authors to test the PNIPAM-coated surface also at very slow immersion speed.

It is in fact known that kinetic phenomena, occurring during the wetting process, tend to disappear if speed is relatively higher or slower compared with the evolution of the phenomenon. This is exactly what has been noticed: maintaining unchanged the temperature, but decreasing the velocity to the minimum allowed by the equipment (2 µm/sec), the instrument recorded fewer "jumps" (Figure 3.2.31, A). Despite the diminished "sawtooth number", the advancing contact angle remained at a value similar to the case obtained at 20 µm/sec and 40 °C.

Similarly, the surface wettability, tested at 25 °C, produced the same advancing contact angle values at 2 µm/sec (Figure 3.2.31, B) such as at 20 µm/sec.

However, as will be clear from the next part of this chapter, increasing the film thickness led to some modification in the surface behaviour and, in those cases, an immersion speed of 2 µm/sec resulted sufficient to induce a complete disappearance of the stick/slip phenomenon.

Discussion

- PNIPAM synthesis and chemical/physical characterization

The properties of PNIPAM has been investigated starting from the synthesis of non-grafted polymer and its subsequent analysis to verify chemical and smart characteristics.

From ATR-FTIR spectrum, all the typical fingerprints of this polymer were clearly recognizable and the synthesized PNIPAM peaks perfectly match with the plot obtained for the commercial product (Figure 3.2.2). This testifies the success in the polymer synthesis and the possibility to purify it, to a high degree, from the reaction mixture.

A further proof has come from NMR data (Figure 3.2.3). Peak interpretation well fited with the molecular structure of the polymer and no additional signals, deriving from impurities contaminations, have been recorded.

The responsiveness toward temperature variation was checked with the cloud point test. Heating the perfectly transparent solution (Figure 3.2.4, A), no apparent variation has been noticed until, abruptly, the phase separation occurred at the LCST. The aqueous solution tuned then to a cloudy state (Figure 3.2.4, B) as consequence of the light scattering caused by PNIAPM agglomeration. The LCST, for the commercial polymer, lay at approximately 34 °C, while, in the case of the non-grafted PNIPAM, the transition temperature has been observed at 34,5 °C. The difference in LCST between the two polymers can be probably explained by a slightly lower molecular weight of the synthesized polymer compared to the commercial product (20000-25000 M_n). It has, in fact, already mentioned that the LCST in bulk solution occurs in a range of temperatures extending from approximately 30 to 35 °C and that one of the most influencing parameter is PNIPAM chain length[17].

After these positive tests on the non-grafted PNIPAM, it has been proceeded with the study of the polymer tethered on a surface.

A hydroxyl terminated SAM was modified into the polymerization initiator (Figure 3.2.5) followed by the proper synthesis of the polymer with a similar procedure to that adopted for

non-grafted PNIPAM.

Also in this case, FTIR analysis assessed the effective synthesis of the smart polymer with a spectrum exhibiting all the characteristics peaks for this compound (Figure 3.2.6). The difference in relative intensity of the amide I and II peaks, compared to the spectrum obtained from the non-grafted polymer (Figure 3.2.2 and Figure 3.2.6 respectively), is usually considered not significant and a possible consequence of the grazing angle configuration[18]. Another source of uncertainty with this FTIR configuration is the relatively low signal-to-noise ratio above the 2700 cm^{-1}. However, also in this region of the spectrum the PNIPAM fingerprints are recognizable.

AFM measurements gave the first feedback of smart PNIPAM properties. A different volume occupied by the brushes have been observed above and below the LCST testifying the transition from a coiled to a swelled state (Figure 3.2.10). Moreover, the surface displayed a lower elastic modulus when the AFM tip approached it at a temperature below the LCST, emphasizing the hydration of PNIPAM brushes.

Ellipsometric measurements have been, instead, used to verify the thickness of the dry PNIPAM film. A direct comparison of the obtained values with the literature data is quite difficult since no standard ATRP procedure exists for PNIPAM and the variation of just one parameter can alter the results. However, the obtained values for the dry film thickness appear consistent with the range of data commonly reported in the literature for similar reaction process[7,19,20].

- biological characterization and cell sheet detachment

After the general chemical/physical characterization, it has been tested the effective capability for the obtained PNIPAM-coated surfaces to trigger cell adhesion.

Mg63 ostroblast-like cells, seeded on samples coated with PNIPAM, responded positively adhering to the coiled brushes and proliferating up to confluence.

Physiologic cells response within few hours from the seeding is an important parameter to attest the interaction of the culture substrate with cells. In particular, observing their spreading

and morphology it is possible to estimate the biocompatibility of the surface.

In this case, it has been possible to note how the majority of cells well adhered to the substrate with a typical morphology for MG63[21] (Figure 3.2.11). Despite some cells maintained a rounded shape, sign of a loose adhesion, a general good cellular spreading has been observed with many filopodia protruding from cell borders, hence, assessing a positive biological response toward the material.

Comparing the obtained value of 286 cells per square millimetre to the initially seeded cells (circa 300/mm^2), it is possible to affirm that the surface induced a good cells viability. After the critical phase of adhesion, in fact, the cell population was 95% of the starting cells, confirming the impression of a good cell-substrate interaction when the PNIPAM is in a coiled state.

After cells reached confluence, culture medium temperature has been decreased to verify cell detachment.

As expected, cells started to detach in the form of a sheet. The process underwent the typical phases described in the literature[13,14] with cells starting to get a round shape and, at the same time, losing the adherence to the substrate. After several minutes, cells have been observed to definitely detach and contract in a floating mass (Figure 3.2.12).

The detached layer was stained and observed by confocal microscope to assess cells viability. Practically all cells survived to the detachment process confirming the smart characteristics of the coating and the possibility to obtain a cell sheet with undamaged cell-cell junction (Figure 3.2.13).

This has been also confirmed from the cell lamina stained with rhodamine phalloidin and DAPI, that mark, respectively, the cytoskeleton and the nucleus of cells (Figure 3.2.14). As mentioned before, the image definition may appear as poor, but this phenomenon is commonly observed[22,23] and is the result of the collapse of the cytoskeleton filaments that form an indistinct mass. However, the clear preservation of the cell thick texture is evident. It proves, once again, that this technique allows for a non-destructive harvest of cell sheets.

Chapter 3

- outermost behaviour of PNIPAM brushes studied by Wilhelmy plate tests

Contact angle measurements performed on PNIPAM coated samples suggested a complex dynamics of the outermost surface.

In order to better understand this phenomenon, it is necessary to consider the interesting works presented in the literature about the behaviour of PNIAPM brushes tethered on a surface.

Different research groups[24,25,26,27] developed theoretical models for these systems and experimental results[28,4,29,30] largely confirmed the conclusions extrapolated by the former studies. These works assessed that, unlike PNIPAM in bulk solution, grafted chains exhibited a gradual transition with phase separation extending on a broader range.

In particular, as Zhang and others[29] reported, the phase separation occurs through a series of complex phenomena that are the results of close packaged chains and substrate interactions.

However, there is no complete agreement on this process. In the literature, for example, the contact angle data reported by some authors[16,28,31,32] showed a sharp trend similar to that of the polymer in solution, while other authors[33,19,34,35] reported a behaviour displaying a smoother transition. Finally, in one case responsiveness has been found to be inexistent for advancing contact angle, but a smooth increase in the receding contact angle has been observed when temperature was increased[36].

In the present work, to study PNIPAM surface dynamics, contact angles were measured by means of a Wilhelmy microbalance. This apparatus, relatively economical but reliable, allows for a precise and accurate characterization of the surface dynamics by controlling, over several cycles, the immersion speed during the wetting and de-wetting process. The collected data are extremely reliable on advancing and receding (and therefore hysteresis) contact angle thanks to the fact that a relatively large surface is probed[37]. Moreover, this technique permits to observe particular phenomena, such as the stick/slip here reported, that are otherwise not so easily investigated by means of a simple goniometer. The latter instrument, in fact, suffers much more from the experience and subjectivity of the investigator[38] and it is not designed to estimate the contact angle with the same precision available for a sensitive microbalance.

The theory on wettability is based on the assumption that an ideal surface-liquid pair should

not exhibit contact angle hysteresis thanks to the fact that the system is in a true thermodynamic equilibrium and, consequently, only one contact angle can met this state[39]. Obviously, real surfaces and probing liquids present some deviations from the ideal state and a certain degree of hysteresis is commonly observed.

It is reputed that two different types of hysteresis exist: a true thermodynamic and a kinetic hysteresis. The former is time or frequency independent and the contact angle discrepancy are the consequence of non-equilibrium transitions. The latter, which depends on time and/or frequency, is the result of a slow equilibrium time[39].

The two factors that most contribute to the first type of hysteresis are generally attributed to surface roughness and heterogeneity. Time-independent hysteresis will not be discussed in detail since the effects related to heterogeneity has been supposed to give minor consequences to the measurements. At the same time, a surface can be considered as smooth when roughness is less than 0.1-0.5μm. Due to the low substrate roughness (less than 8 nm by AFM measurements) and the dry state brushes thickness (less than 30 nm), it is possible to assume that PNIPAM-coated surfaces can be considered as smooth for this kind of test.

Then, hysteresis in this case will depend more on the time-dependent factors. The latter are mostly attributable to three factors: i) surface deformation, ii) penetration of the liquid-test into the surface and iii) molecular reorientation of polymer chains.

As will be explained, the third phenomenon greatly influenced the contact angle dynamics, but, possibly, also the others may have had tangible effects.

As evidenced in the results section, at low immersion speed, the PNIPAM-coated surfaces showed an increase in the advancing contact angle as result of a rise in the probing liquid temperature (Figure 3.2.16 and Figure 3.2.17). The change in wettability has been the known consequence of the swelled-to-coiled transition of PNIPAM, nevertheless, when immersion speed increased, the phenomenon started to disappear. It has been supposed that the variation in sensitiveness toward temperature change was related to kinetics effects. It is in fact reasonable to think that samples dried under nitrogen expose the more hydrophobic groups of the polymer chains toward air to minimize surface energy. Then, once the samples are immersed in water at a temperature below the LCST, polymer undergoes a rearrangement with hydrophilic groups coordinated by water while the hydration of the polymer chains takes

place. Since the swelling process is typically kinetic, when immersion speed is increased, the mechanism of rearrangement and hydration is substantially "frozen". The hydration time of the polymer chains becomes too long compared to the immersion velocity and the surface appears as hydrophobic. This can, in particular, explain the reason why the "bow shape", in the plot registered by the instrument, disappears replaced by a sharp profile. This phenomenon requires a slow hydration of brushes and a consequent slow-moving water front advance along the surface, while it disappears when immersion speed is relatively fast.

With increasing temperature, water progressively becomes a poor solvent for PNIPAM and, thereby, hydrophobic interactions dominate with water progressively expelled from the polymer. Consequently, the tests carried out at temperature above the LCST display an attenuated dependence on speed immersion. In the second cycle, instead, the polymer is partially wet and the phenomenon of hydration/dehydration is more pronounced during temperature change (Figure 3.2.18 and Figure 3.2.19). Only at the highest tested speeds the temperature does not affect the polymer behaviour. This, interestingly, is congruent with the data reported by Zhang[29,30]. He observed from quartz crystal microbalance analysis that PNIPAM needed a longer time to dehydrate, manifesting a hysteresis during the swelling/coiling process.

No significant change in receding contact angles has been noticed varying temperature or immersion speed (Figure 3.2.20 and Figure 3.2.21). Once fully wet, the surface is therefore in a stable equilibrium state. The obtained values are comparable with the data reported in the literature[7,15]. Nevertheless, at 25°C, higher contact angles have been recorded, indicating a divergent behaviour compared to the other measurements. This fact is quite unusual since water, at these temperatures, is a good solvent for PNIPAM, hence, a value similar, or even lower, to the other cases would have expected. One possible hypothesis is that the surface responded similarly to a swollen hydrogel as result of a considerable hydration of brushes at 25°C. A high water uptake means an extremely soft, and thus highly deformable, surface (Figure 3.2.32, A). In this state the film could be unstable and contact angle measurements could lead to atypical results.

The phenomenon of surface deformation is a controversial matter in contact angle experiments. An example reported by Andrade[39] relates to a study on poly(vinylpyrrolidone)-

coated surfaces showing effects potentially ascribable to localized surface deformation (Figure 3.2.32, B). A highly confined ripple has been hypothesized to cause a localized change in the meniscus shape with consequent contact angle changes. Andrade reported a sharp increase in the receding contact angle that, in some cases, exceeded the advancing contact angle.

It could be hypothesized that a similar behaviour occurred also for PNIPAM brushes. However, the phenomenon is not as evident as in the case reported by Andrade and, at the moment, doubts remain about this explanation. Further investigations may clarify this behaviour.

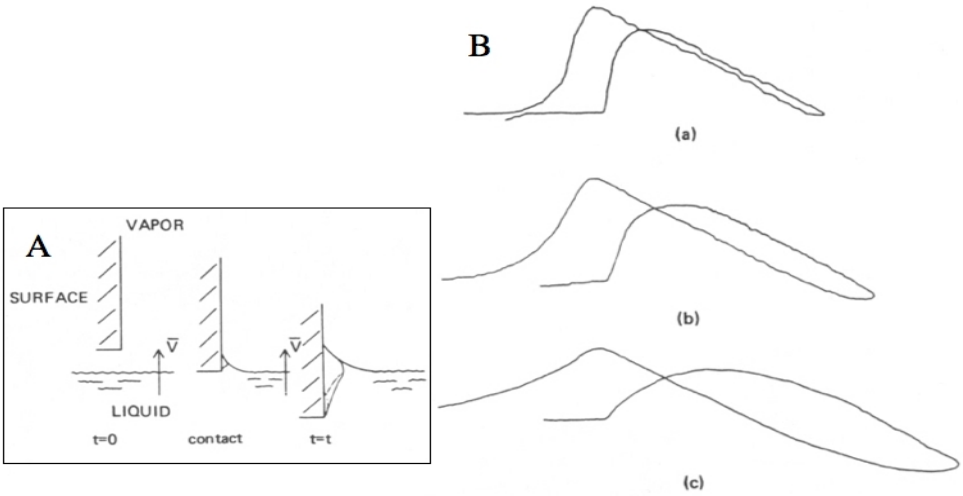

Figure 3.2.32: A: contact angle-induced surface deformation superimposed on a moving liquid line, leading to a deformation ripple which relaxes after the liquid front passes. B: Wilhelmy plate plot of a fully hydrated poly(vinyl pyrrolidone) coating on glass. Note that the advancing angle is lower than the receding angle, producing a negative hysteresis. After examining all the possible explanations for this effect, the only thing remaining is contact angle-induced deformation coupled with the velocity of the liquid front. Note that the hysteresis appears to increase (in absolute value) as one goes to faster speed: velocity (a) < velocity (b) < velocity (c) [39].

Another interesting phenomenon, observed during the Wilhelmy plate tests, has been the appearance of a stick/slip behaviour.

Sawtooth plots have already been reported in the literature and explained by different

mechanisms[40,41,42].

In a paper focusing precisely on PNIPAM, this behaviour was observed by means of a methodology resembling the axisymmetric drop shape analysis[40]. In this particular case, the stick/slip was recorded both in advancing and in receding contact angles and explained as a redistribution of the material on the surface. The meniscus motion, in fact, induced the onset of transport phenomena that affected also contact angle measurements. In that case, however, the polymer wasn't grafted onto the surface and was therefore free to move.

For brushes grafted onto surfaces, like those here studied, the explanation proposed by Morra seems more logical[41,42]. In these articles the author demonstrated that samples coated with poly(2-hydroxyethylmethacrylate) (PHEMA) brushes exhibited a stick/slip behaviour as a result of superficial reorientation of polymer chains.

In particular, the stick/slip phenomenon has been found to be greatly connected to the molecular architecture of the polymer and the test conditions. The author reached this conclusion comparing his results to similar experiments conducted by Andrade and others[43,44,45]. Morra supposed that the absence of stick/slip phenomena in Andrade's investigation was related to a more rigid polymer as consequence of crosslinking. Citing Yasuda[46], Morra remarkably asserted that the presence or absence of crosslinking is "a key-feature in determining the dynamic behaviour of polymer surface".

In the case here reported, PNIPAM brushed are not crosslinked and certainly able to reorient at temperatures below the LCST. However, polymer chains rearrangements are not so obvious when temperature rise. It is plausible to expect that at temperature between 30°C and 35°C the polymer start to form strong intra/inter-molecular interactions among amide groups, leading to an energy barrier that must be overcome during the hypothetical reorientation process.

By means of a Wilhemly plate measurement and varying the immersion speed, Morra was able to demonstrate that the sawtooth phenomenon was, in fact, a reorientation process[41]. When the advancing front of the probing liquid was sufficiently slow, compared to the rearrangement process, the three-phase boundary reached an equilibrium state and the sawtooth profile disappeared.

This is also in accordance with Andrade. He observed that, due to their kinetic nature, such phenomena are transitory and their effects disappear "if the interaction between solution and

the solid phase is either very fast or extremely slow in comparison with the time of measurement"[39].

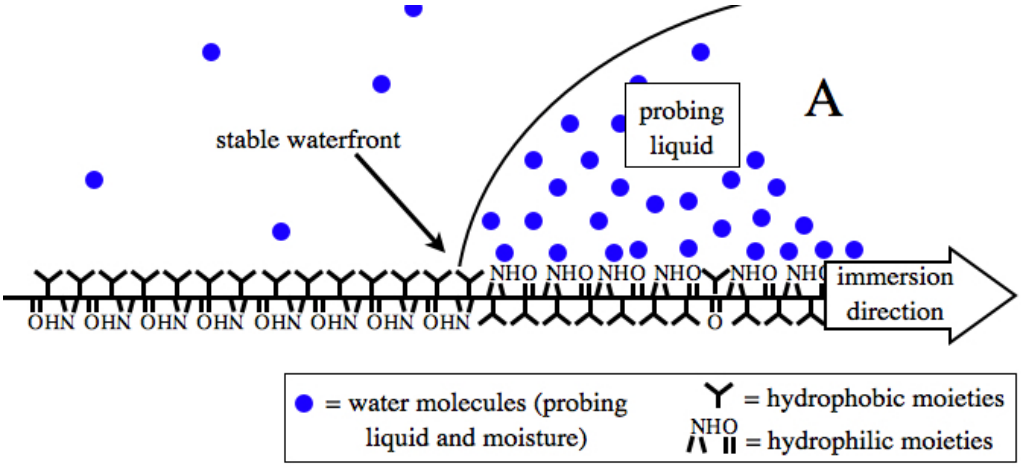

Figure 3.2.33: scheme of stick/slip phenomenon development, part A: the waterfront is in a stable equilibrium with the PNIPAM surface.

In this work, it has been decided to proceed in a similar manner. Decreasing immersion speed the sawtooth frequency diminished but it was not possible to obtain a plot without perturbations due to equipment limits. However, as it will be explained in the next section of this chapter, for thicker PNIPAM coating the immersion velocity was sufficiently slow to record a plot without perturbations and, at the same time, to observe a decrease in the advancing contact angle values. As predicted by theory, in this condition the kinetics of reorientation is relatively fast compared to the advance of the liquid front and, thus, the stick/slip phenomenon disappears.

These results led to the assumption that, also in the case here reported, the sawtooth profile is the macroscopic manifestation of a reorientation process that takes place on the surface when it is wetted by the probing liquid.

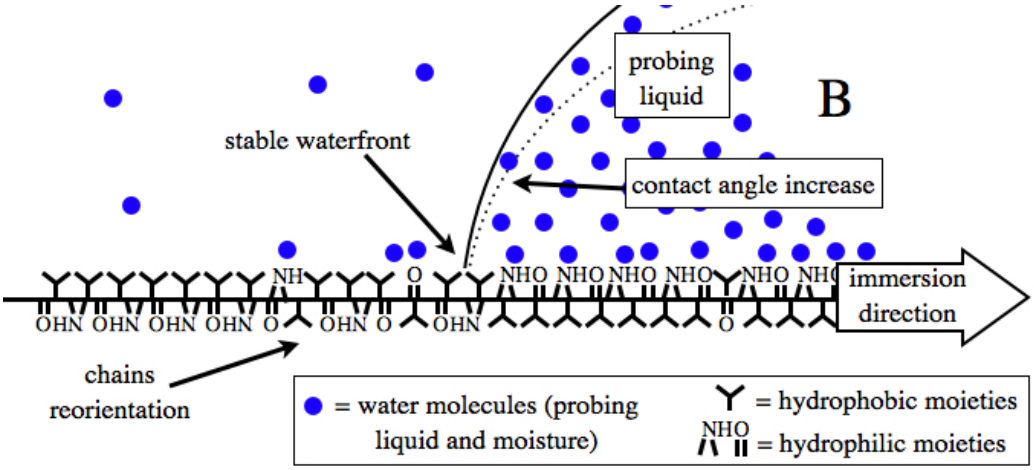

Figure 3.2.34: scheme of stick/slip phenomenon development, part B: the waterfront is still stable while sample is immersed in the probing liquid, thus leading to the increase in contact angle. however, at the same time, the reorientation process takes place at the three-phase boundary but, thanks to moisture, also on non-wetted surface.

In particular, it has been supposed that the mechanism starts when the meniscus reaches a thermodynamic equilibrium with the coated surface and the waterfront advance is "blocked" by the hydrophobic moieties that PNIPAM chains initially expose toward water (Figure 3.2.33). While the sample is pushed more deeply into the liquid, the meniscus remains stable and, consequently, a slow but continuous increase in the contact angle is observed (Figure 3.2.34). However, during this process, the brushes reorientation takes place at the three-phase boundary. This leads to the instability (Figure 3.2.35) of the waterfront that, consequently, breaks the equilibrium state and the liquid advances along the surface until a new stable front is formed (Figure 3.2.36). When a new equilibrium is reached, the process starts again and thus the typical recorded sawtooth loop.

Moreover, it appears from the collected data that this behaviour depends both on kinetic and thermodynamic factors. An increase in temperature and immersion speed induces, in fact, a thickening of the sawtooth frequency.

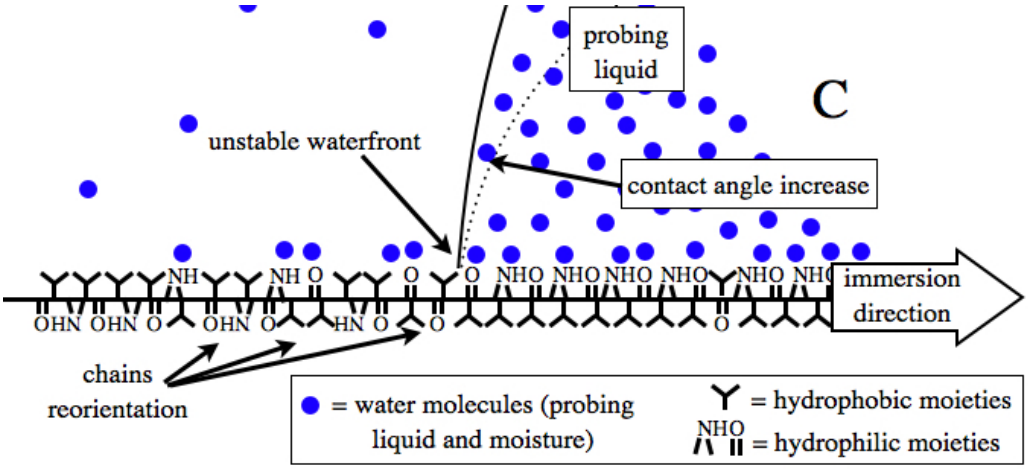

Figure 3.2.35: scheme of stick/slip phenomenon development, part C: the immersion of the sample in the probing liquid and contact angle increase continue but due to the reorientation process the waterfront becomes unstable.

The reason why stick/slip "jumps" vary in number and magnitude, as consequence of temperature and immersion speed changes, is susceptible to speculation; at the moment no scientific evidences have been found to overcome the problem. However, it has been supposed that this mechanism is related to an interaction between moisture and the polymer that takes place before the waterfront directly reaches it (Figure 3.2.34 and Figure 3.2.35). This hypothesis could explain the mechanism by which a new thermodynamic equilibrium is reached.

Once the state of equilibrium is "broken", the meniscus proceeds along the surface and the extent of this advancement is influenced by the hydration state of the brushes. The more "wet" the brushes are, the more the waterfront advances along the surface, before a new equilibrium is established between the meniscus and the probing liquid. This means that a lower speed gives more time for moisture to interact with PNIPAM and thus the stick/slip phenomenon occurs with a diminished frequency.

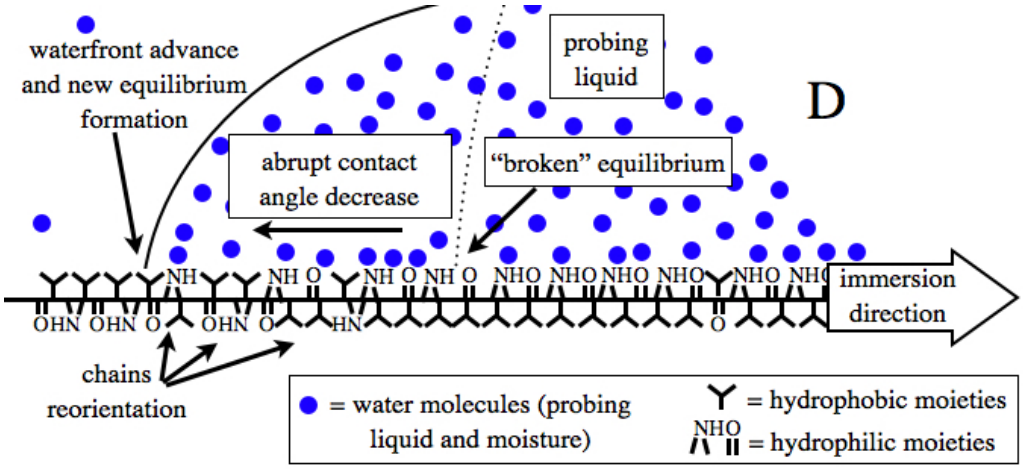

Figure 3.2.36: scheme of stick/slip phenomenon development, part D: the instability of the waterfront leads to the rupture of the three-phase boundary and the consequent water advance along the surface until a new stable state is reached and the process starts again.

Instead, the dependence on temperature can be explained with an increase in the number of intra-molecular bonds among PNIPAM chains[47], as result of a temperature rise.

The more the bonds, the slower the process of reorientation, with concomitant increase in sawtooth frequency due to a lower extent of surface covered by the advancing waterfront during each "jump".

As seen, the sawtooth profile tends to disappear decreasing the immersion speed but, due to its kinetic nature, the same process should also occur proceeding in the opposite direction.

Increasing the immersion speed should, in fact, lead to a parallel disappearing of the sawtooth phenomenon. Due to equipment speed limit, this has not been verified, however, at 160 μm/sec and 40 °C (Figure 3.2.30) the stick/slip behaviour appeared increasingly unstable. The sawtooth profile was, in fact, less defined and regular, moreover, the magnitude of each "jump" was markedly decreased.

Also the shape of the sawtooth profile was particularly interesting. Contrary to all the other cases, the "jump" toward hydrophilic values was not so sharp, resembling more an isosceles

triangle. This means that the waterfront advanced along the surface with a velocity comparable to the immersion speed.

In the end, when the latter velocity would be higher than the former, the stick/slip behaviour should, again, come to an end, as theory predicts. Contrary to the case al low immersion speed, however, in this condition the rearrangement process is negligible compared to the waterfront advance with the result that the advancing contact angle should attest on the higher reported values.

3.3 Experimental section.

Influence of Brush Thickness on PNIPAM behaviour

Introduction

In the third part of this chapter, the influence of the PNIPAM film thickness on the polymer smart behaviour will be presented. It has already been mentioned in the background section of this chapter that, in the literature, PNIPAM-grafted chains are reported to have a behaviour dependent upon molecular weight[1,2, 3]. Moreover, it seems that the modification induced by this parameter on PNIPAM phase separation could affect the mechanism of cell detachment, despite this argument is still disputed[4,5,6].

Consequently, it has been decided to modify the reaction time to obtain different coating thickness and subsequently verify the influence that this induced on both the polymer interaction with cells and the wettability behaviour.

To investigate the properties of samples with different brush lengths, it has been firstly proceeded to correlate the reaction times to the dry PNIPAM thickness. Then, the influence of the smart polymer thickness toward protein adsorption has been evaluated to emphasize possible difference of interaction with the biological system. As done in the previous part of the chapter, cell culture tests has been carried out to understand the cell response toward the smart material in the coiled and swollen state. This permitted to notice that, while cell sheet detachment has been successfully attained regardless of PNIPAM thickness, the brush length influenced both the initial cell adhesion and the subsequent cell detachment. However, the employment of two different cell lines highlighted the fact that an even greater influence on the cell sheet detachment is ascribable to cell characteristics. Similarly to the previous section,

the smart characteristics of PNIPAM has been studied also by means of the Wilhelmy microbalance technique. Also in these cases, it has been noticed the phenomena described in the first experimental section, but a correlation with polymer thickness has also been noticed and a possible explanation furnished.

Materials and Methods

Materials, ellipsometric measurements and Wilhelmy plate tests have been carried out with the same procedures adopted in Chapter 3.2. *Surface-initiated polymerization* has been performed with the same conditions reported in the previous part but in this case the reaction has been stopped after 4 different time: 0,5 – 1 – 2 – 3 hours.

Protein adsorption. Four samples (10x7,5 mm) for each reaction time have been tested: two were incubated in the culture medium for 25 minutes at 37 °C, while the other two at room temperature for the same incubation time. No pre-wetting treatments have been performed on samples. After incubation, medium has been stored and samples have been gently washed with deionized water to remove the physisorbed proteins and subsequently placed into a clean test chamber wells.
1 ml of eluting medium (sodium dodecyl sulphate 0,1%wt (SDS)) has been added on sample surfaces for 20 min at room temperature, under static conditions. Then, the supernatants have been carefully removed, aliquoted and frozen at –80 °C.
For 1D-electrophoresis the desorbed protein samples have been freeze-dried and resuspended in 20 ml of "sample buffer" (NuPAGE® LDS Sample Buffer, Invitrogen). 6 μl of each resuspended sample were then loaded on acrylamide SDS-PAGE gels. NuPAGE® Novex 3-8% (Tris-Acetate) gels were used for the detection of high molecular weight proteins (40-500 kDa). Each gel was loaded with a molecular weight protein standard (HiMarkTM, Invitrogen or Protein Marker, Broad Range, BioLabs) and culture medium as control sample (1:20 in "sample buffer"). SDS-PAGE was performed in a XCell SureLockTM Mini-Cell (Invitrogen). The 3-8% gels were run at 150 V, constant voltage. Following electrophoresis, the acrylamide gels were stained using the Imperial Protein Stain (Pierce), and, in order to increase the bands

profile intensity, it has been successively stained with ProteoSilver Silver Stain Kit (Sigma). Finally the stained gels were digitalized by a GEL LOGIC 200 (Kodak) imaging system and the data were elaborated by means of the Kodak 1D Image Analysis Software.

Cell culture. Before cell culture, all samples have been disinfected by immersion in ethanol 70% followed by washing with sterile phosphate buffer solution (PBS), then placed in a 24-wells plates. Two different cell lines have been tested: human embryonic rabdomyosarcoma cells (RD) and rabbit cornea cells (SIRC). In the first case 1 ml of RD cell suspension (passage 37, obtained from Istituto Zooprofilattico di Brescia) was seeded in each well at a concentration of $0{,}5x10^5$ cells/ml (~300 cells/mm^2). Eagle's minimum essential medium in Hanks' balanced salt solution (Hanks' MEM, Invitrogen) supplemented with 10% Fetal Bovine Serum (FBS), sodium piruvate (1mM, Euroclone), L-glutamine (4mM, Euroclone), 2% vitamins, 2% non essential aminoacids, 1% Penicillin was used as culture medium.
In the second case, 1 ml of SIRC cell suspension (passage 404, obtained from Istituto Zooprofilattico di Brescia) was seeded in each well at a concentration of $0{,}5x10^5$ cells/ml (~300 cells/mm^2). Eagle's minimum essential medium in Earle's balanced salt solution (Earl's MEM, Invitrogen) supplemented with 10% Fetal Bovine Serum (FBS), sodium piruvate (1mM, Euroclone), sodium bicarbonate (1mM, Euroclone), L-glutamine (4mM, Euroclone), 1% vitamins, 1% non essential aminoacids, 1% Penicillin was used as culture medium.
In both cases, the respective cells have been also seeded in an empty well as control test. Cells were incubated at 37ºC in a 5% CO_2 atmosphere incubator, changing the medium one day after the seeding and subsequently every two days.
Initial cell adhesion (after 24 hours), cell viability and morphology after detachment, cell re-adhesion and cell viability after 24 hours from the re-adhesion have been performed with the same procedures adopted in the previous part.

Results

As mentioned in the introduction of this third part, different reaction times have been used to obtain a variation in thickness coating and subsequently study the influence that this change produced on the PNIPAM behaviour. The synthesis reaction time lasted for respectively 0,5 – 1 – 2 – 3 hours and produced the film thickness of Table 1 where PNIPAM coated surfaces are abbreviated as PN05, PN1, PN2, PN3. PN is the acronym of the polymer name while the number is the reaction time in hours.

	PN05	PN1	PN2	PN3
PNIPAM dry thickness (nm)	27,5 (±2,0)	34,4 (±3,7)	40,4 (±2,4)	48,9 (±4,4)

Table 1: ellipsometric measurement of the dry PNIPAM brush thickness

Plotting the film thickness versus time reaction (Figure 1), it is possible to notice that the values lay on a straight line as the theory of controlled/living radical polymerization indicates for polymer chain growth[7].

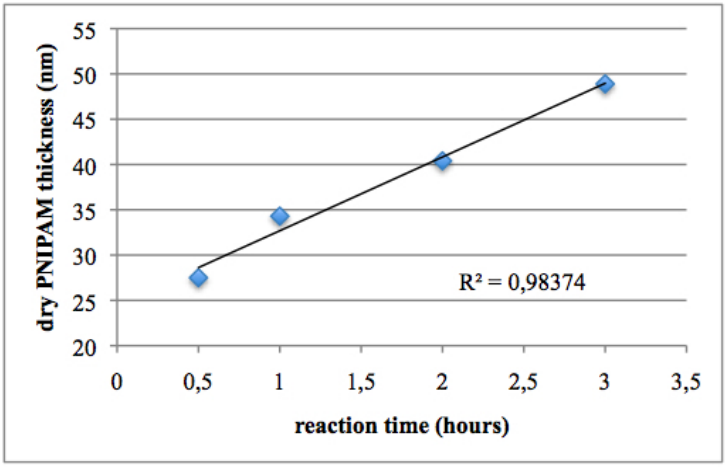

Figure 1: PNIPAM brushes growth versus reaction time

Protein adsorption tests have been carried out at two temperatures: below the LCST, at 20 °C, and, above the LCST, at 37 °C (the standard cell culture temperature). The tests demonstrated that PNIPAM brushes adsorbed more proteins when coiled while the amount of polypeptides decreased for the polymer chains being in the hydrated state (Figure 2). From the bands of adsorption, it is possible to conclude that a lower amount of proteins binded to the PNIPAM brushes as consequence of a coating thickness increase.

In general, a strong band of adsorption appeared at a value of approximately 60 kDa, corresponding to albumin, while the other bands were markedly less intense.

Interestingly, the same bands were distinguishable in all samples, the only variable being the profile intensity when temperature or film thickness varied. This is important since it means that, regardless of temperature and PNIPAM thickness, the surfaces don't present a peculiar affinity toward some specific protein.

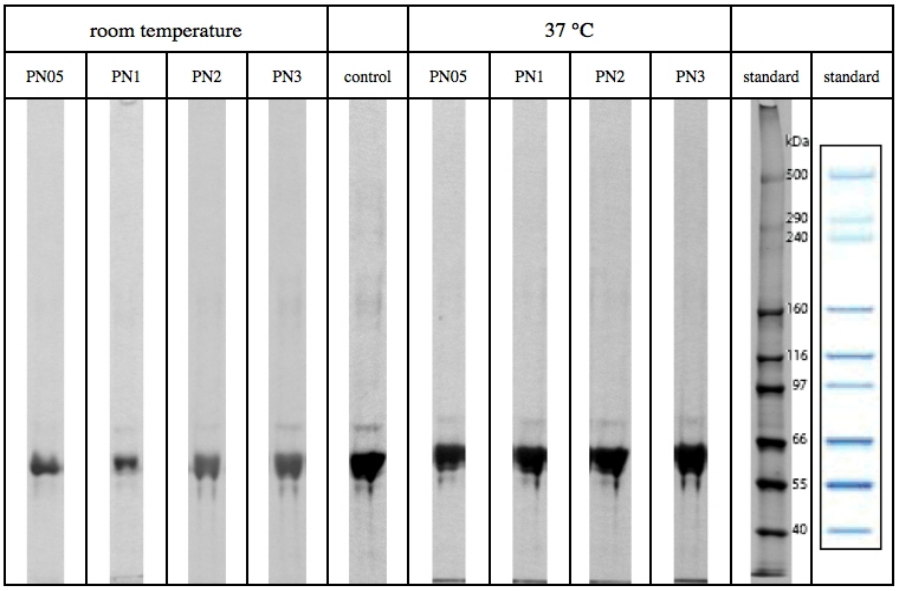

Figure 2: NuPAGE test for protein adhesion at different temperature on PNIPAM-coated surfaces. Cell culture medium has been used as proteins source while an empty cell culture well has been used as control.

PN1 exhibited the least amount of proteins adsorbed at room temperature (Figure 2, columns on the left side), when the polymer was in the hydrate state. But, when PNIPAM was in the coiled state, the same surface responded similarly to the other cases (Figure 2, columns on the right side). PN2 and PN3 gave comparable results, with fewer adsorbed proteins at room temperature compared to the amount at 37 °C, but in these cases the difference was more limited. PN05 result laid at values similar to PN1 but shifted toward a higher amount of proteins in the hydrated state.

In general, when the polymer was coiled comparable results have been obtained from al the surfaces and the control as well. On the contrary, the protein amount adsorbed at room temperature presented some differences with PN1 and PN05 attesting on lower values.

Biological i*n vitro* experiments have been conducted on two different cell lines, RD and SIRC. Similarly to the experiment carried out for MG63 cells, the cell adhesion has been verified after 24 hours from the seeding. Samples have been stained as described in the material and methods section. The cytoskeletons and the cell nuclei have been so marked and

then observed by the confocal microscope.

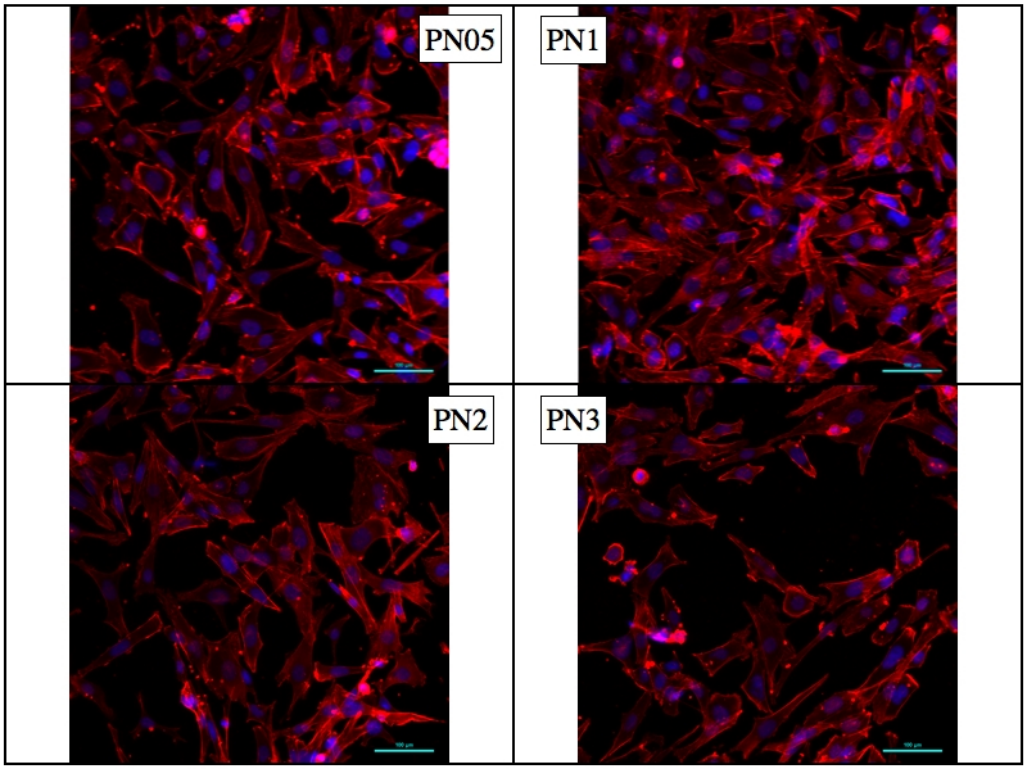

Figure 3: RD cells adhesion on the different PNIPAM-coated surfaces after 24 hours from the seeding. Cell nuclei (blue spots) cell cytoskeletons (red) are clearly distinguishable.

RD cells well adhered on all samples (Figure 3) but as shown in Figure 4 the polymer substrates induced a different cell response. Cell spreading and morphology appeared as positive, regardless of thickness. However, the number of adhering cells testified that a thinner smart polymer layer was more biocompatible for RD cell. In particular, PN1 displayed the best results with a 22% increase in cell number if compared to the initially seeded cells. This value is 1,5 times higher than the data obtained for PN3, the surface that manifested the worst results. Nevertheless, it is not possible to assess that the response displayed by the latter surface was negative since the number of cells adhering on that surface after 24 hours still represented the 83% of the starting value.

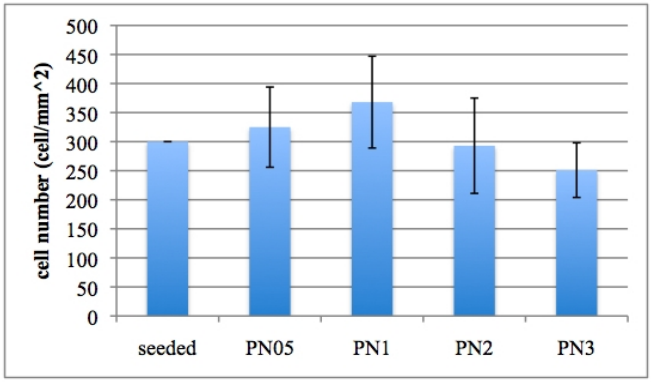

Figure 4: RD cell number per square millimetre 24 hours from the seeding. The initially seeded RD cells are represented by the first column

The cell morphology (Figure 3) appeared as consistent with other images found in the literature as regard this cell line[8]. No particular morphologic differences have been noticed among the tested surfaces. The cell nuclei was visibly large and particularly evident such as a well defined and a robust cytoskeleton, typical of the smooth muscle cells. The cell shape was oblong with the exception of some cells that maintained a more compact and faceted form and a minority of cells still in a spheroid state. No particular organization or orientation has been observed.

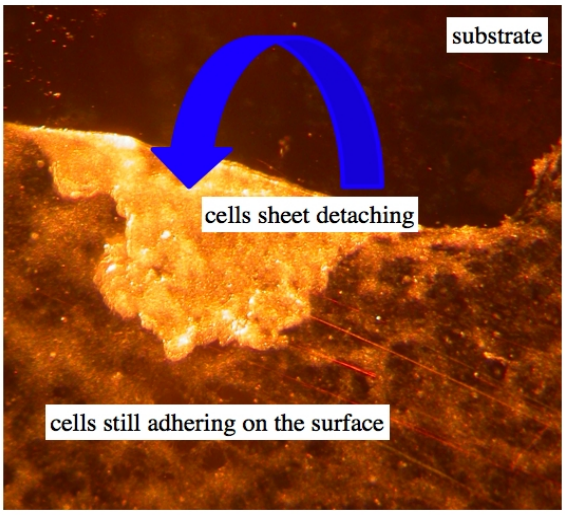

Figure 5: RD cell sheet during the detachment process observed by optical microscope

After 5 days from the seeding, cell confluence has been observed on all samples and the cell sheet detachments have been carried out. The same procedure adopted for MG63 detachment has been used and, similarly, cells have been observed to lift off from the surface in the form of a sheet (Figure 5). Viability staining confirmed that, for all the tested samples, cells perfectly survived to the detachment process (Figure 6).

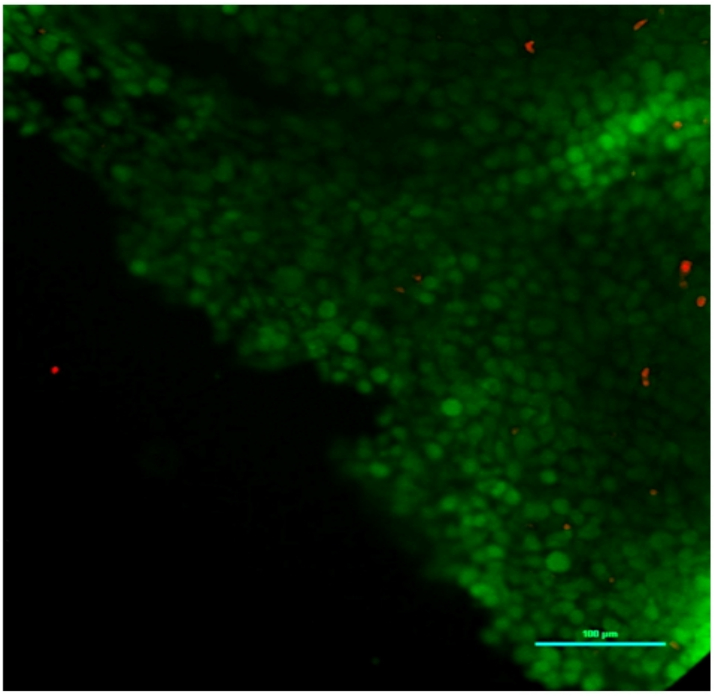

Figure 6: RD cell sheet stained to mark cell viability after detachment. Green spots represent alive cells while dead cells are red.

Only one image has been reported here since no dissimilarities have been noticed among the cell sheets detached from the different PNIPAM-coated surfaces.

Rhodamine phalloidin and DAPI staining evidenced parallel results. Actually, no apparent differences have been observed from case to case observing the cytoskeletons and cell nuclei after the lift-off (Figure 7). However, from this image, it was evident the preservation of cell-cell junctions, so important for the success of cell sheet engineering techniques.

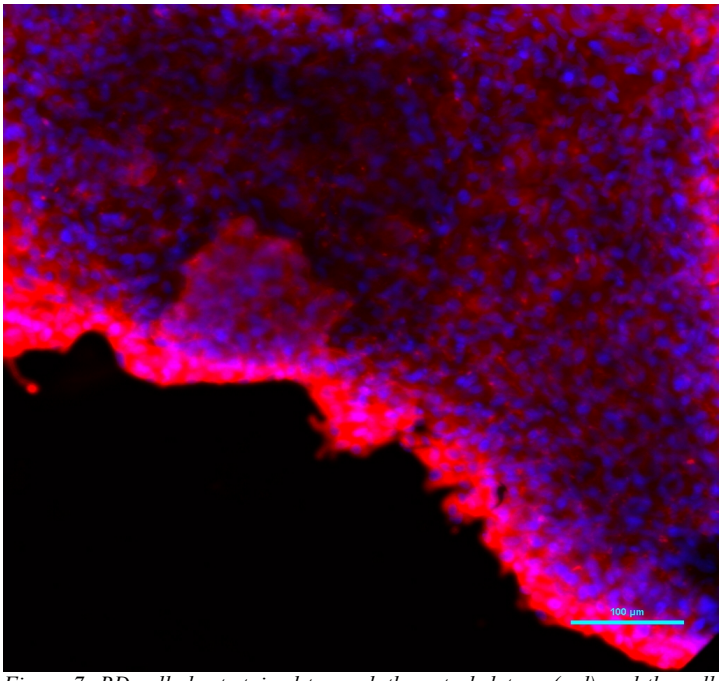

Figure 7: RD cell sheet stained to mark the cytoskeletons (red) and the cell nuclei (blue) after detachment.

Although uniform results have been achieved with the cell sheets detached from the various samples, some differences have been noticed in the lift-off duration. It seemed that cell lift-off, lasted for a shorter period on thinner PNIPAM coating. In the mean, the time necessary for the completion of the process lasted for 45-75 minutes for PN05 and PN1 samples, while for PN2 and PN3 it needed approximately 15 minutes more.

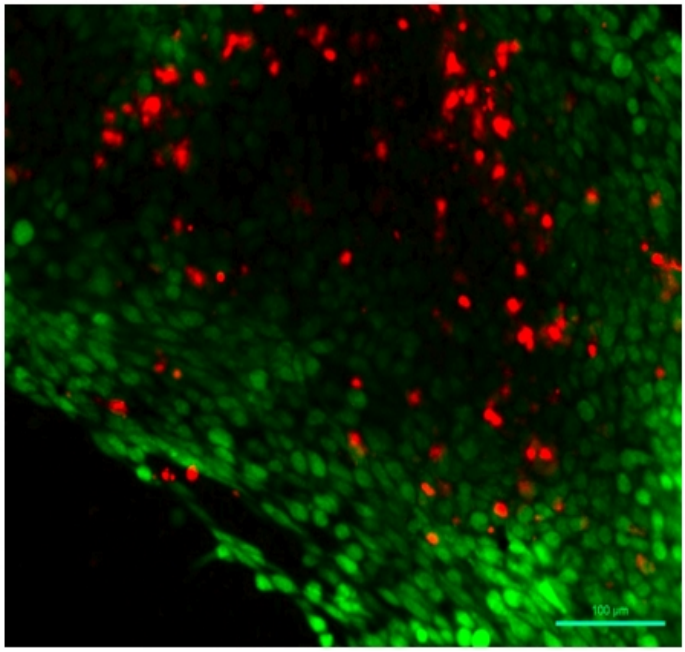

Figure 8: RD cell sheet, harvested from a PNIPAM-coated substrate, re-seeded in a culture well. The image has been taken 24 hours after the cell layer re-adhesion. Alive cells are marked in green while red spots represent dead cells.

As for MG63 cells, it has been tested the capability for the detached cell sheets to re-adhere on a new surface. A cell lamina has been placed in a new culture well with the necessary amount of culture medium. After one day cells have been stained and observed. Also in this case the images confirmed a positive result (Figure 8).

An equal series of experiments have been performed with SIRC cells. 24 hours after the seeding, a more uniform response of cells has been noticed such as a comparatively similar cell number throughout the different samples (Figure 9).

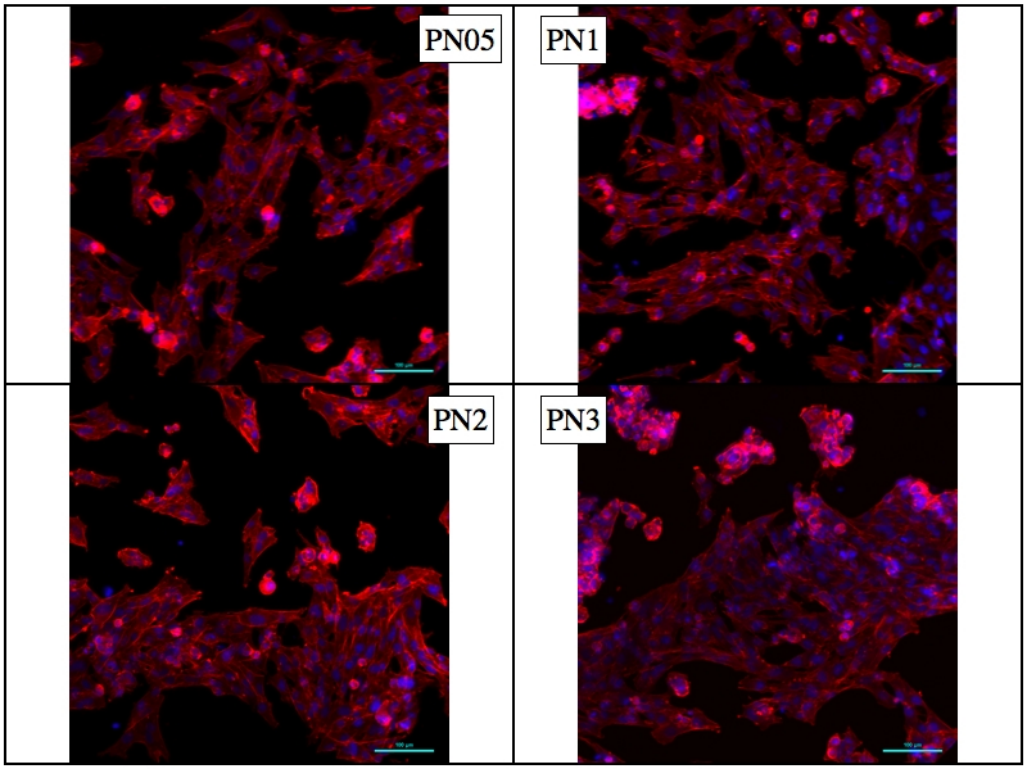

Figure 9: SIRC cells adhesion on the different PNIPAM-coated surfaces after 24 hours from the seeding. in the figures cell nuclei (blue) and cytoskeletons (red) are marked.

The better biocompatibility of PN05 and PN1 was confirmed but, in this case, the variation was not so remarkable (less than 20%) and even the difference with the initial cell number was limited (Figure 10). The cell morphology was completely different from the previous case: cells were smaller in size and with a less marked cytoskeleton. The shape was fibroblast-like and elongated with some filopodia protruding from the shorter sides. Cells have been observed to adhere on the surface preferably in grouped, and partially organized, islands.

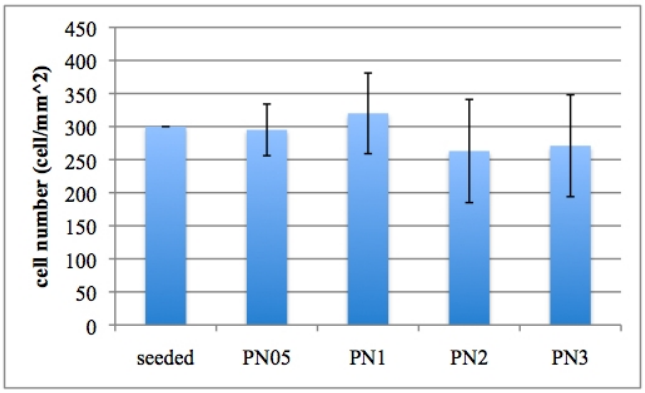

Figure 10: SIRC cell number per square millimetre 24 hours from the seeding. The initially seeded SIRC cells are represented by the first column

SIRC cells needed less time to reach full confluence (4 days) but the detachment process was similar to the previous case. Also the time needed for the detachment has been comparable and, as reported earlier, a bit shorter for the samples coated with a thinner layer of smart polymer. The viability staining of detached cell laminae gave, once again, a positive result (Figure 11) such as the staining used to mark nuclei and cytoskeleton (Figure 12).

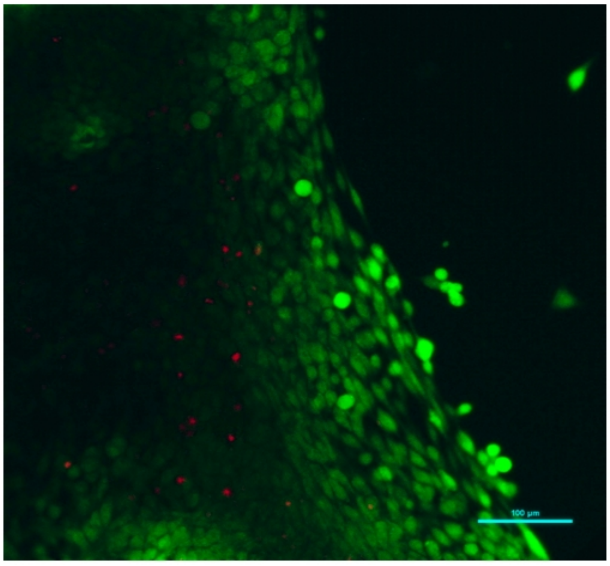

Figure 11: SIRC cell sheet stained to mark cell viability after detachment. Green spots represent alive cells while dead cells are red.

The cell layer appeared, in fact, as a compact mass with cells well adhering the one to the others; nevertheless, an even less defined and more corrugated surface has been highlighted from this image if compared with the previous cases.

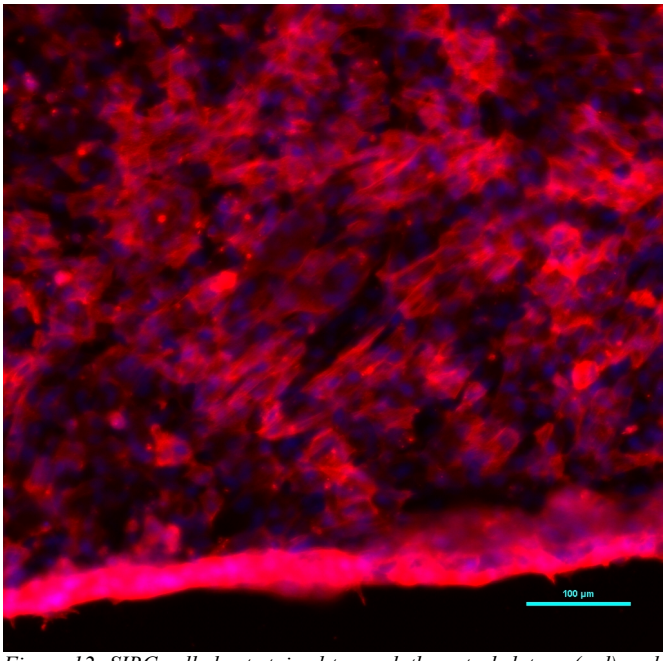

Figure 12: SIRC cell sheet stained to mark the cytoskeletons (red) and the cell nuclei (blue) after detachment.

Finally, it has been investigated the cell sheet behaviour once it was placed in a new culture well. As in the former tests, the cell lamina adhered and displayed a good response after 24 hours (Figure 13).

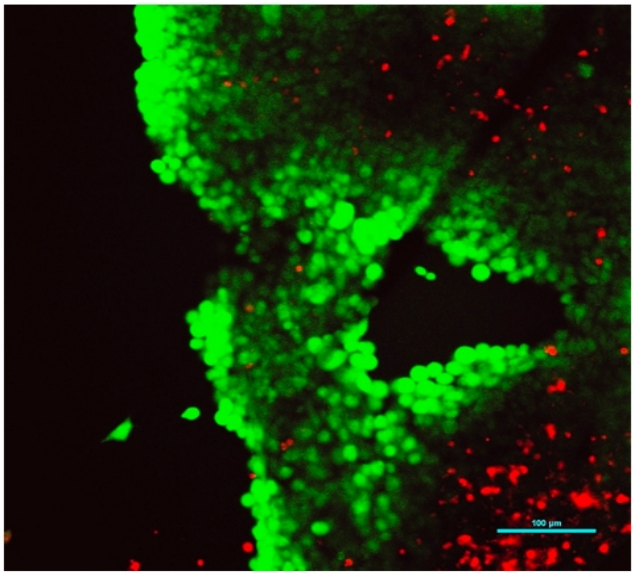

Figure 13: SIRC cell sheet, harvested from a PNIPAM-coated substrate, re-seeded in a culture well. The image has been taken 24 hours after the cell layer re-adhesion. Alive cells are marked in green while red spots represent dead cells.

Advancing contact angles measurements have been summarized in Figure 14 and Figure 15. Analyzing the plot as function of temperature (Figure 14), it is possible to notice that, increasing thickness, the responsiveness of the brushes seems to decrease. In particular, at low immersion speed and low temperature, the advancing contact angles are similar for all the tested samples. Instead, the contact angles recorded at 40 °C are higher for shorter polymer chains. Moreover, when immersion speed has been raised, the surface became less responsive with contact angles rather constant. The behaviour then corresponds to the case described in the Chapter 3.2. In this case, however, the samples with longer brushes displayed lower contact angle values.

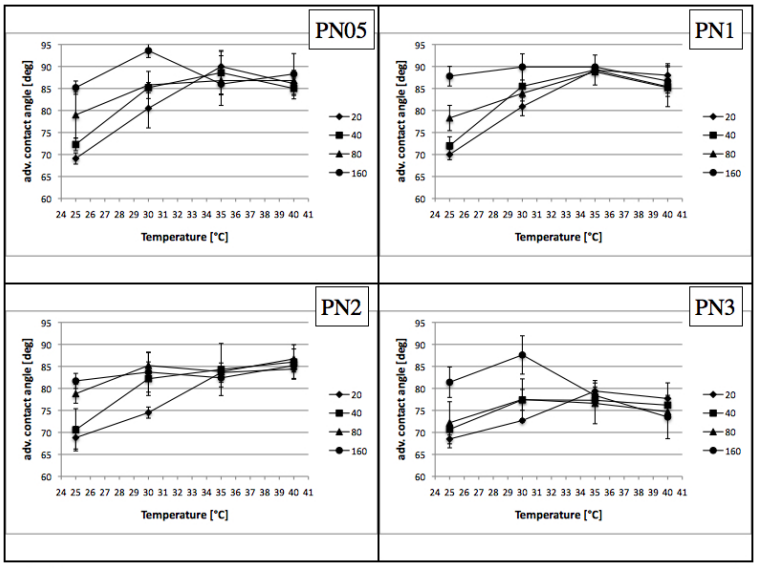

Figure 14: advancing contact angle on tethered PNIPAM with different dry polymer thickness. First immersion cycle at different immersion speeds, plotted as function of temperature.

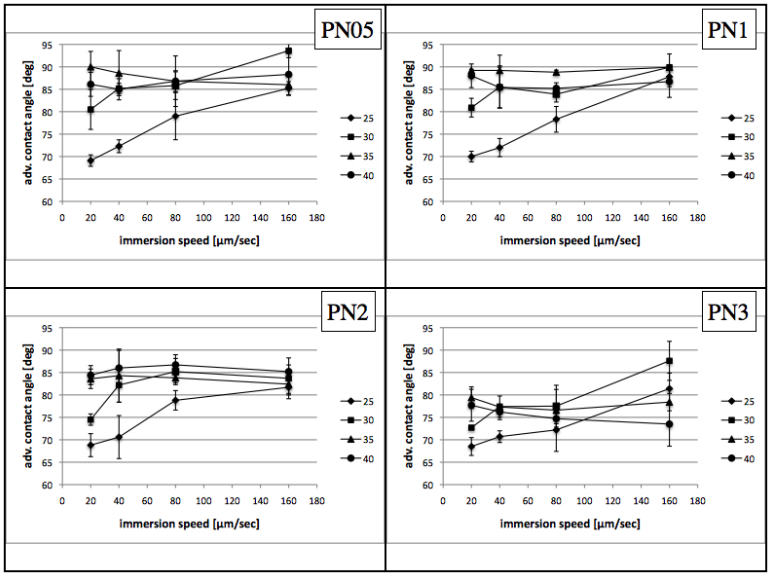

Figure 15: advancing contact angle on tethered PNIPAM with different dry polymer thickness. First immersion cycle at different temperature, plotted as function of immersion speed.

As regard the second immersion cycle (Figure 16 and Figure 17), the considerations that had been outlined in the previous part of this chapter are still valid.

Furthermore, for thicker brushes, a general decrease in the contact angle variation has been noticed between the swelled and the coiled state. At the same time, these surfaces displayed a higher wettability in comparison to samples with longer PNIPAM chains.

The last phenomenon has been particularly evident from the graphs as function of immersion speed. While for PN05 and PN1 the highest contact angles are around or above 85°, the values exhibited by PN3 are constantly below 80° (with the only exception of one datum).

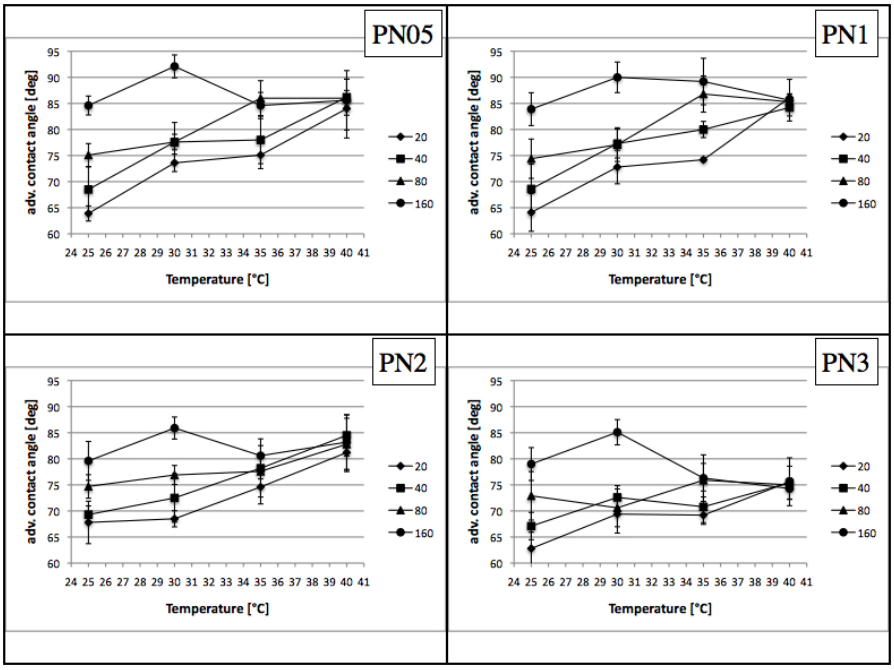

Figure 16: advancing contact angle on tethered PNIPAM with different dry polymer thickness. Second immersion cycle at different immersion speeds, plotted as function of temperature.

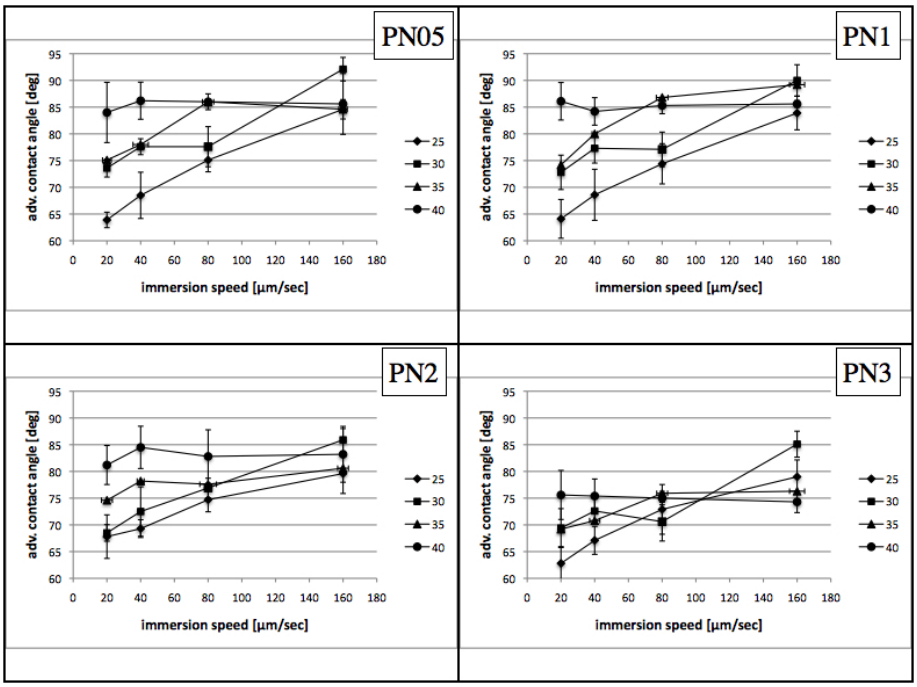

Figure 17: advancing contact angle on tethered PNIPAM with different dry polymer thickness. Second immersion cycle at different temperature, plotted as function of immersion speed.

The hydrophilic shift of surfaces with a longer reaction time was evident also from receding contact angles (Figure 18 and Figure 19). Once again, the phenomenon has been more evident at higher temperature.

As for the case described in the previous part, the receding contact angles didn't change between the first and second immersion cycle.

Interestingly the strange phenomenon observed at 25 °C has been observed in all the tested samples. At this temperature the surface appeared as more hydrophobic despite, in this condition, the PNIPAM brushes should be highly hydrate. A possible interpretation of these data has already been proposed in the discussion part of Chapter 3.2 but certainly this behaviour merits a deeper investigation.

Furthermore, PN2 data displayed a rather different trend: apart from a higher contact angle value at 25 °C, a decrease in wettability has been observed in correspondence of the highest tested temperature. This fact is of difficult interpretation and has not been observed for the other samples.

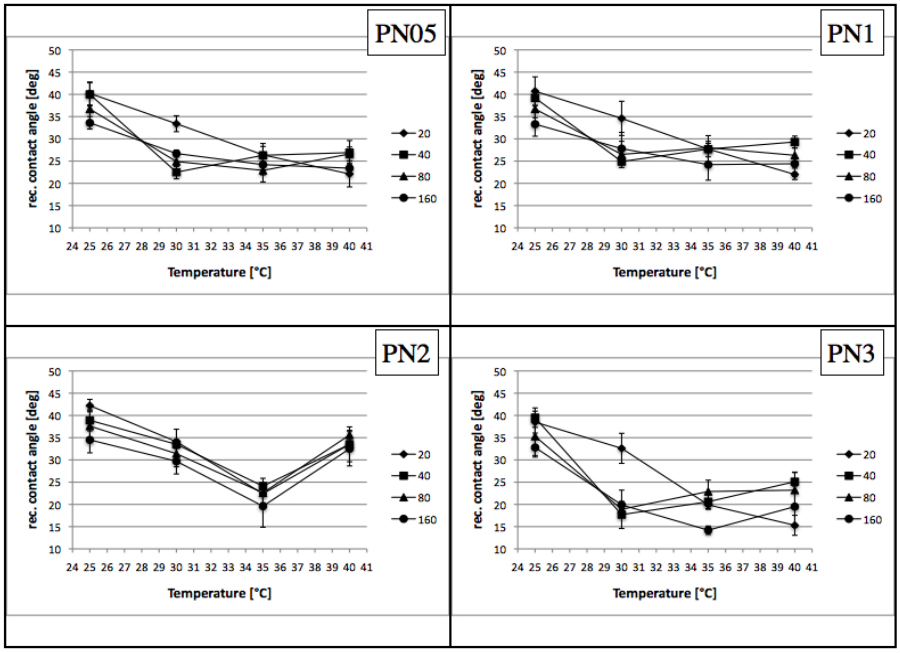

Figure 18: receding contact angle on tethered PNIPAM with different dry polymer thickness. First and second immersion cycle at different immersion speeds, plotted as function of temperature.

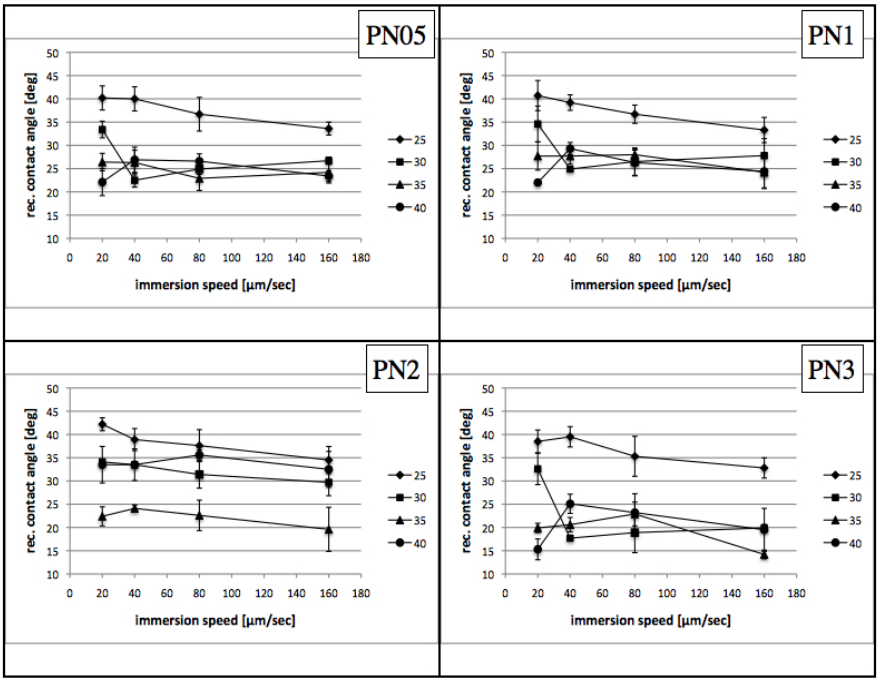

Figure 19: receding contact angle on tethered PNIPAM with different dry polymer thickness. First and second immersion cycle at different temperature, plotted as function of immersion speed.

Contact angle hysteresis (Figures 20-23) appeared as relatively constant throughout the different samples with no remarkable differences. Moreover, between the first and the second cycle, only a modest shift toward lower values has been recorded. Thus, the considerations drawn in Chapter 3.2 can be also extended here.

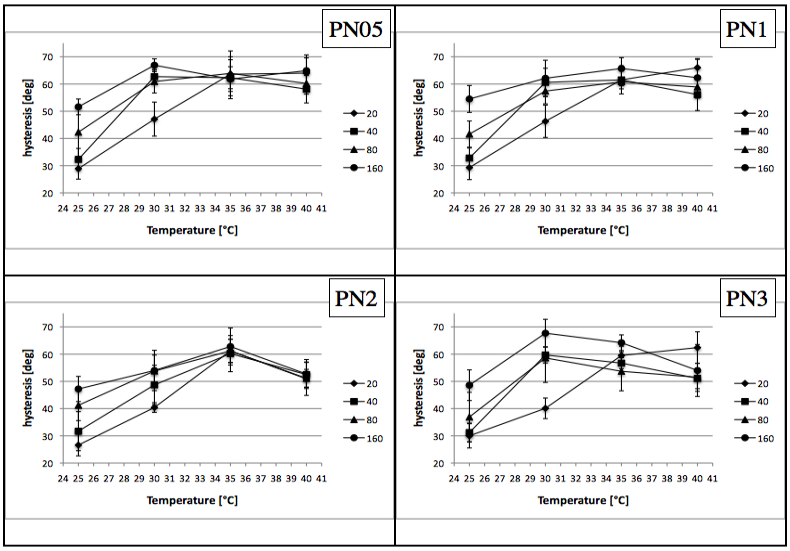

Figure 20: hysteresis contact angle on tethered PNIPAM with different dry polymer thickness. First immersion cycle at different immersion speeds, plotted as function of temperature.

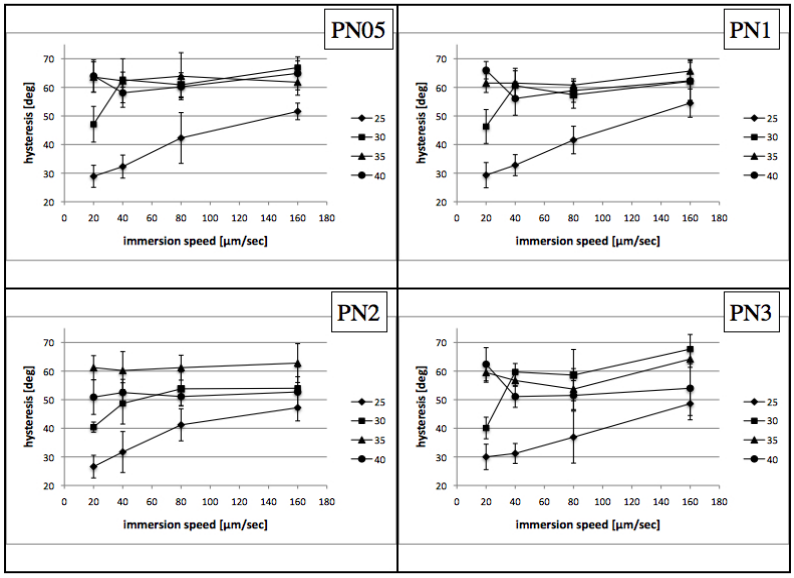

Figure 21: hysteresis contact angle on tethered PNIPAM with different dry polymer thickness. First immersion cycle at different temperature, plotted as function of immersion speed.

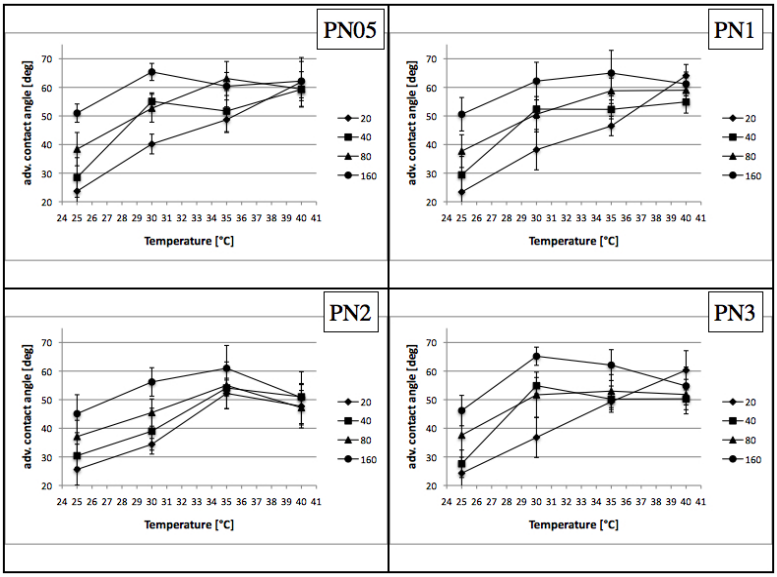

Figure 22: hysteresis contact angle on tethered PNIPAM with different dry polymer thickness. Second immersion cycle at different immersion speeds, plotted as function of temperature.

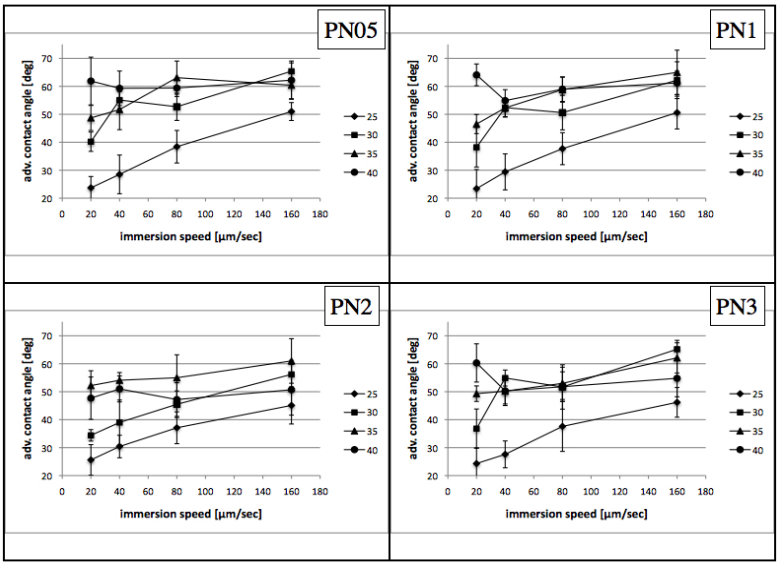

Figure 23: hysteresis contact angle on tethered PNIPAM with different dry thickness. Second immersion cycle at different temperature, plotted as function of immersion speed.

As regard the plots recorded by the Wilhelmy microbalace, it will be presented here just few and most significant graphs for each of the PN1, PN2 and PN3 samples (Figures 24-26).
(the authors kindly refer the reader to the previous part of this chapter for PN05 plots).
Some differences have been recognizable among the samples coated with a varying PNIPAM thickness, but the general observations made for PN05 are still perfectly relevant.
The "bow-shape", immediately after the ZOID, was present in all cases (red circles in Figures 24-26, A) such as its disappearance at higher velocity in favour of the wedge profile (blue circles in Figures 24-26, C).
Above the LCST, the plots are again characterized by the sawtooth profile during the wetting process (Figures 24-26, B and D). Similarly to PN05, at 35 °C and low immersion speeds the stick/slip phenomenon disappeared in the second cycle (plots not shown).
The dependence of sawtooth frequency from temperature and immersion speed has been confirmed also for PN1, PN2 and PN3, such as the irregularity of the phenomenon at the highest temperature and immersion speed (Figures 24-26, D).

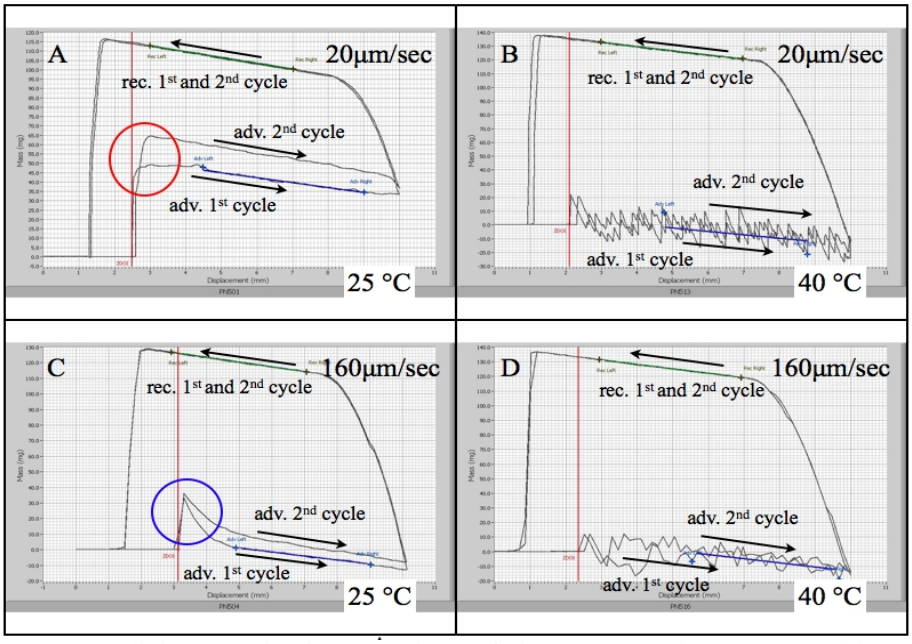

Figure 24: Wilhelmy plate plots for PN1 at the specified temperature and immersion speed (A: 20 µm/sec and 25 °C, B: 20 µm/sec and 40 °C, C: 160 µm/sec and 25 °C, D: 160 µm/sec and 40 °C).

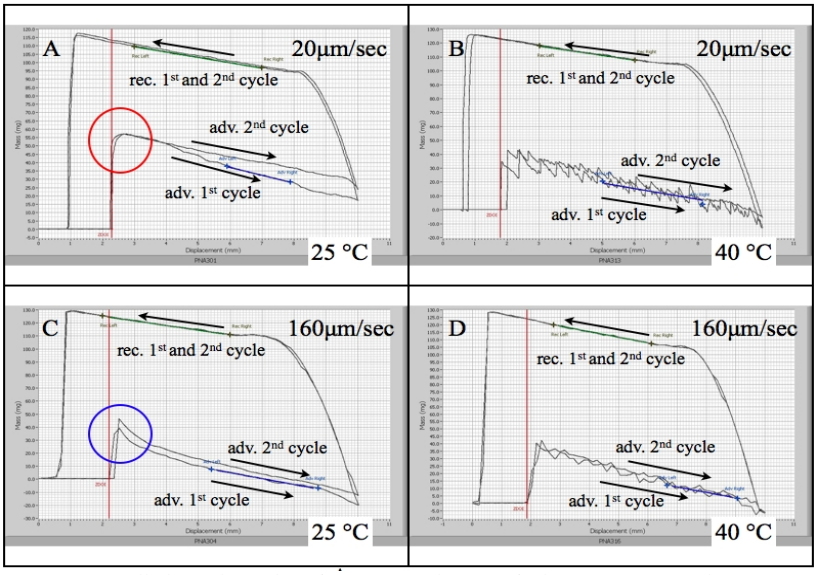

Figure 25: Wilhelmy plate plots for PN2 at the specified temperature and immersion speed (A: 20 µm/sec and 25 °C, B: 20 µm/sec and 40 °C, C: 160 µm/sec and 25 °C, D: 160 µm/sec and 40 °C).

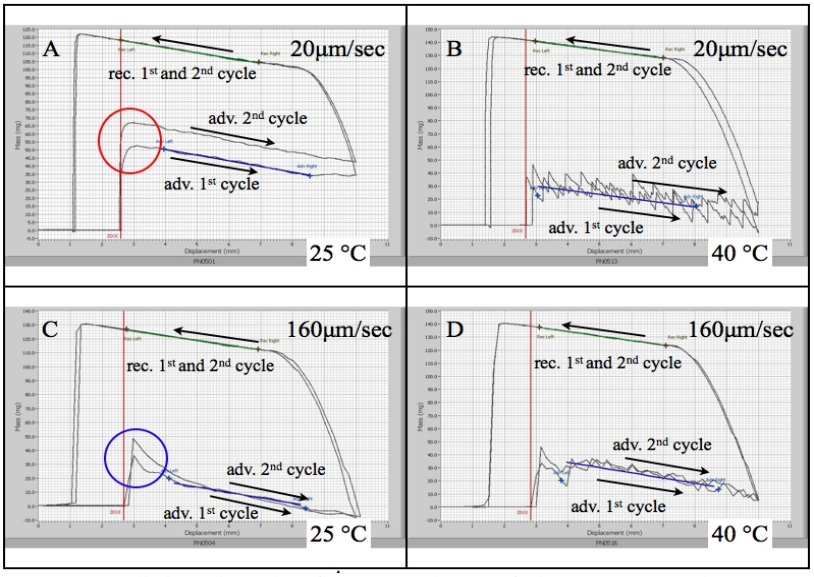

Figure 26: Wilhelmy plate plots for PN3 at the specified temperature and immersion speed (A: 20 µm/sec and 25 °C, B: 20 µm/sec and 40 °C, C: 160 µm/sec and 25 °C, D: 160 µm/sec and 40 °C).

As previously mentioned, the tests carried out at particularly slow immersion speed (5-2 μm/sec) emphasized the kinetic contribution to the sawtooth phenomenon. The attenuation of the stick/slip occurrence has been in fact evident from these tests, particularly for thicker PNIPAM coating.

To emphasize the decrease in the sawtooth frequency, firstly a sample (PN3) has been tested at 5 μm/sec and 40 °C (Figure 27). Comparably to what has been seen for PN05 (at 2 μm/sec, Figure 3.2.31), the sawtooth profiles have become more rare than the case at 20 μm/sec. However, the advancing contact angle didn't undergo a significant decrease.

However, a further decrease in the immersion speed (2 μm/sec) caused the complete disappearance of sawtooth. Furthermore, a more consistent decrease in advancing contact angle has been observed (Figure 28, A). Interestingly, the value was now comparable to the test carried out at the same velocity but at 25 °C (Figure 28, B). Analogous behaviour has been observed also for the samples with an intermediate PNIPAM thickness (Figure 29 and Figure 30, respectively for PN1 and PN2).

Contrarily to PN05, then, the lowest immersion speed allowed by the instrument (2 μm/sec) has been sufficient to obtain plots without perturbations.

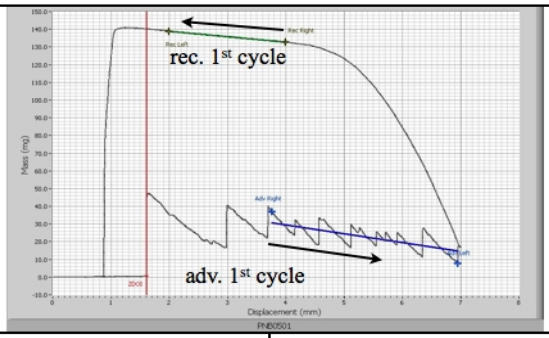

T = 40 °C	imm. speed = 5 µm/sec
adv. contact angle	76,6°
rec. contact angle	20,2°

Figure 27: Wilhelmy plate plots and relative advancing and receding contact angles for PN3 at 40 °C and 5 µm/sec.

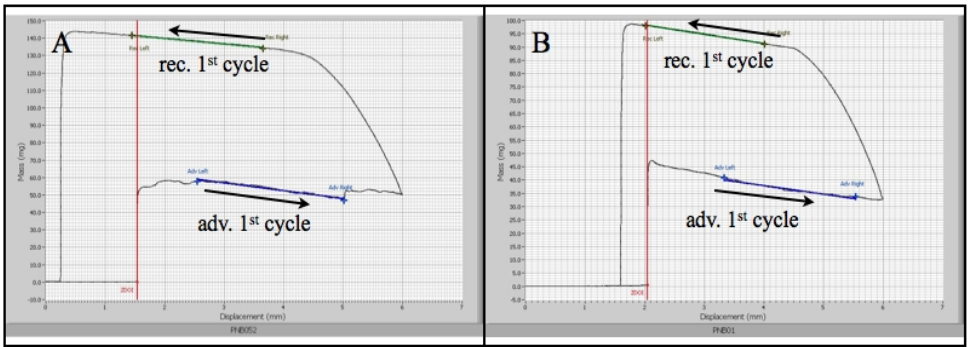

T = 25 °C	imm. speed = 2 µm/sec	T = 40 °C	imm. speed = 2 µm/sec
adv. contact angle	67,1°	adv. contact angle	72,4°
rec. contact angle	20,6°	rec. contact angle	37,8°

Figure 28: Wilhelmy plate plots and relative advancing and receding contact angles for PN3 at 25 °C (A) and 40 °C (B). Immersion speed = 2 µm/sec.

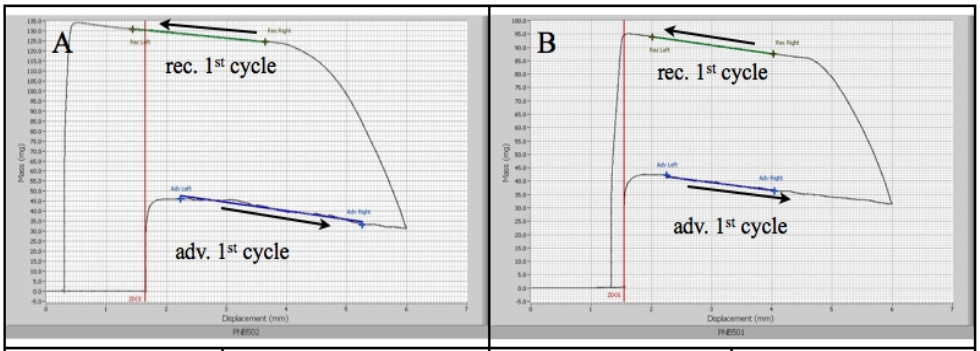

T = 25 °C	imm. speed = 2 µm/sec	T = 40 °C	imm. speed = 2 µm/sec
adv. contact angle	70,6°	adv. contact angle	72,6°
rec. contact angle	30,3°	rec. contact angle	46,2°

Figure 29: Wilhelmy plate plots and relative advancing and receding contact angles for PN1 at 25 °C (A) and 40 °C (B). Immersion speed = 2 µm/sec.

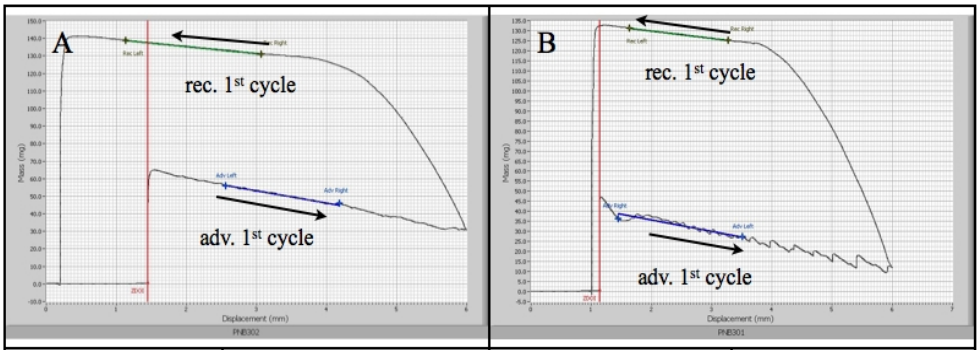

T = 25 °C	imm. speed = 2 µm/sec	T = 40 °C	imm. speed = 2 µm/sec
adv. contact angle	68,0°	adv. contact angle	70,9°
rec. contact angle	24,4°	rec. contact angle	24,6°

Figure 30: Wilhelmy plate plots and relative advancing and receding contact angles for PN2 at 25 °C (A) and 40 °C (B). Immersion speed = 2 µm/sec.

Discussion

As it is possible to notice from the plot of dry film thickness versus reaction time (Figure 1), the polymer chain growth versus the reaction time well fit with a linear function, as it is predicted for a controlled/living radical polymerization[7]. However, it is important to underline that theory refers to the molecular weight. Then, for the reported data, this is true only hypothesizing a homogenous chain compaction in the day state. The hypothesis seems, nevertheless, consistent since ellipsometric measurements are sensitive also to polymer density and the obtained data appeared indistinguishable from this point of view. Another aspect attesting film homogeneity is a comparatively low standard deviation that, again, confirms the controlled chain growth.

As mentioned before, the comparison of the obtained data with the literature is a relatively demanding task since changing the reaction mixture, to adapt to the specific necessities, lead to different reaction conditions and consequently to varying molecular weight and polydispersity index. However, the comparison with available data[9,10,11] demonstrates that the results are reasonable and compatible with standard outcomes for the technique.

Protein adsorption tests represent a remarkable solution to study cell-material interaction. Mammalian cell adhesion on a surface is in fact always mediated by a polypeptide layer that enables cells to perceive and interact with the surrounding environment.

Then, establishing the type and the amount of protein adhering on a surface provides useful information about the possible interaction of cells with the material and, thus, giving an insight of the degree of biocompatibility.

From the present results, it can be observed that, as expected, the polymer in the coiled state absorbs a higher amount of proteins allowing for a good cells adhesion and proliferation (Figure 2). On the contrary, a minor amount of protein is adsorbed by the PNIPAM-coated surfaces at room temperature due to a highly hydrate surface and low mechanical properties that hinder the proteins adsorption and cell adhesion.

This fact is especially evident for the thinner polymeric layer (PN1 and PN05) and the result

has an interesting parallel with cell culture tests since a more rapid detachment from these surfaces has been observed.

A comparison with the literature data, as regard cell detachment behaviour as function of PNIPAM thickness, is somewhat problematic.

It has been observed[4], in fact, that the polymer structure probably influences the smart response. This conclusion has been drawn observing the differences in cell adhesion and detachment from surfaces coated with brushes or crosslinked PNIPAM.

For crosslinked PNIPAM, in fact, the authors[5] concluded that cell adhesion and proliferation at 37 °C was possible only for ultrathin coating (<20 nm).

Different results have been observed for PNIAPM brushes grown via ATRP[6,12]. In one case, Okano et al.[12] noticed that cells could adhere also on thick PNIPAM layer (dry film thickness > 60 nm), despite a marked decrease in cell adhesion has been reported in comparison with thinner coatings. However, this result is in disagreement with the observation reported by another author. Xu et al.[6] noticed an increase in cell adhesion as consequence of film thickness increase. Despite different cells (Okano used endothelial cells, while Xu fibroblasts) and a different PNIPAM thickness range (from 1,8 to 64,7 nm for Okano, from 3 to 31 nm for Xu) have been used by the authors, the dissimilarity in the results are difficult to explain. Similar incongruities have been also pointed out by Cole[4] in his recent review on the argument.

In the present work, it has been noticed that RD cells manifested a higher sensitivity toward PNIPAM thickness, preferring the thinner polymer coating (Figure 4). However, the variation in RD cells adhesion was not marked as in the mentioned works.

SIRC cells showed, once again, higher adhesions on PN1 and PN05 but the differences among the surfaces are, in this case, less evident (Figure 10).

The different behaviour between RD and SIRC emphasizes the fact that results are influenced not simply by surface characteristics but also from cells behaviour. This can partially explain the disagreement on the data reported in the literature. Thus, a direct comparison of the outcomes appears problematic due to the large number of variables involved.

As regard advancing contact angles, it can be observed that all surfaces manifested the same behaviours already described in Chapter 3.2. However, it is important to stress that the

magnitude with which these occurred varied as function of the brush thickness (Figure 14 and Figure 16).

In general, at low immersion speed, it has been possible to notice a decrease in sensitiveness for PNIPAM coating with longer polymer chains. In particular, at 25 °C, the advancing contact angles remained rather constant regardless of brush length but, above the LCST, for thicker coating layers the wettability increased.

In the literature, contrasting results are once more reported about PNIPAM brushes (grown via ATRP) with different thicknesses.

When coating thickness increased, Plunkett[9] noticed a concomitant increase of advancing contact angles at temperature above and below the LCST. On the contrary, Okano[12] reported the opposite behaviour. Finally, Braun[13] observed rather constant contact angles regardless of thickness.

Another curious fact is the variability in wettability for PNIPAM brushes when in a coiled state. While, in fact, the contact angle data for the swollen polymer are comparable, the results reported for the polymer at temperature above the LCST are rather differents. Okano observed advancing contact angle values ranging from 53° to 36°, while Braun reported values around 60°. On the contrary, Plunkett obtained more hydrophobic surfaces with advancing contact angle that started from 72°, for the thinner coatings, to 88°, for the thicker films. These values reveal the general disagreement on the contact angle values reported in the literature that has been the argument of recent review[4]. The differences has not been yet clarified and, despite possible causes have been proposed, Cole et al. concluded that only a better characterization of the polymer architecture and physical/chemical features may resolve the problem.

The results obtained during this thesis work, in absolute values, resemble more the data obtained by Plunkett but, as stated, he noticed an increase in contact angle as consequence of longer polymer chains while the trend here reported is the opposite. A real comparison of the obtained values is however impossible at the moment due to the problematics mentioned by Cole et al.. Further characterizations are then needed for a full understanding of the variability in the reported results.

The Wilhelmy plots (Figures 24-26) clarify that PN1, PN2 and PN3 underwent the same stick/slip process described in Chapter 3.2.

For PN1, PN2 and PN3, however, it has been possible to observe the complete disappearance of the stick/slip phenomenon decreasing the immersion speed (figures 28-30).
From the analysis of the phenomenon proposed in the previous part, it can be hypothesized that longer polymer chains possess a less organized inter/intra molecular bonds and thus retain a higher amount of water molecules. This explanation takes in account the decrease in advancing contact angle observed at temperature above the LCST for samples with a thicker coating. At the same time, this could explain why an increase in PNIPAM thickness induced an acceleration of the superficial reorientation process. In fact, compared to the immersion speed (2 μm/sec), the rearrangement becomes sufficiently quick to reorient the hydrophilic moieties toward water while the waterfront advances.

General Conclusions

PNIPAM is probably the most studied and used smart polymer.
Among the wide range of applications for this polymer, one is of especial importance for tissue engineering. As Okano demonstrated[14, 15, 16, 17], PNIPAM, thanks to its capability to undergo coiled-to-swelled transition, can in fact be utilized to trigger cells adhesion. This behaviour has been employed to harvest cell laminae that has been successfully used to heal damaged tissues.
Despite this technique has been in use since the beginning of nineties and a large number of papers has been published on the topic, the phase separation process of tethered PNIPAM is still today argument of discussion.
The subject of this chapter has been the study of the behaviour of tethered PNIPAM during the phase transition. In particular, the investigation focused the attention on the outermost part of the polymer brushes since this is the region that is directly in contact with the biological environment.
Initially it has been verified the effective synthesis of the polymer via ATRP, both for non-grafted and grafted PNIPAM. The chemical/physical characterization of the obtained samples has been then carried out by means of several techniques. In particular, it has been assessed that the dry film thickness growth followed a linear trend as predicted by controlled/living

radical polymerization.

AFM measurements demonstrated that the PNIPAM coating underwent the swelled to coiled transition as consequence of a temperature increase, while cell culture tests assessed that this has been effective in triggering cell adhesion.

Different cell lines have been successfully tested. At 37 °C, cells adhered to the PNIPAM-coated surfaces with a positive biocompatibility observed for all cell lines. In few days cells were able to reach confluence. Then, decreasing temperature below the LCST, cell sheet detachment has been successfully accomplished and the examination of the cell laminae confirmed that cells survived to the lift-off process maintaining good cell-cell junctions. A final positive test was carried out placing the cell sheets in a new culture well to observe cells re-adhesion.

Once the smart properties of PNIPAM have been assessed, the behaviour of the outermost polymer chains region has been investigated during the coil-to-globe transition by means of Wilhelmy plate technique.

While the collected data on advancing contact angle confirmed the qualitative theoretical modelling reported in the literature for tethered PNIPAM, an interesting phenomenon, never described before, has been observed. Above the LCST, when the polymer chains formed inter/intra-molecular bonds and gradually collapsed on the substrate, a sawtooth profile made its appearance in the plot recorded by the instrument.

This stick/slip phenomenon has been explained with a reorientation mechanism of the polymer chains. Temperature and immersion speed has been varied to reveal the kinetic dependence of this behaviour.

It has been noticed that, at 35 °C, the surface tended to retain some water and became more temperature sensitive after the first immersion cycle leading to the end of the sawtooth profile. On the contrary, at higher temperature, the phenomenon appeared more stable regardless of immersion cycle, probably as consequence of more inter/intra molecular bonds.

However, varying the immersion speed, it has been possible to emphasize the kinetics nature of the phenomenon. When the immersion speed was so high that the reorientation process became negligible, the stick/slip behaviour appeared unstable.

On the contrary, decreasing the advancing waterfront velocity, the rearrangement process was

sufficiently fast that no perturbation has been recorded in the plot and, at the same time, a decrease in the advancing contact angle has been observed.

In the last part of the chapter, the focus of the research turned to the study of possible correlation between this phenomenon and the brushes length.

It has been noticed that longer polymer chain induced a decrease in the advancing contact angle above the LCST, probably as consequence of more mobile superficial brushes. However, an increase in coating thickness produced a decrease in temperature sensitivity in the second cycle.

On the basis of these results, it is possible to assess that on the outermost region of the brushes, when PNIPAM came in contact with water, the hydrophobic moieties are exposed toward the liquid to minimize surface energy. This conclusion is particularly important to comprehend the interaction of this polymer with cells and confirm the view drawn by Cole in his recent review on the subject. He remarkably stated that it is misleading to believe that the cell detachment mechanism is based on a simple hydrophobic/hydrophilic interaction. On the contrary, “it is physically more meaningful to view the change in the bio-adhesiveness of PNIPAM as a consequence of considerable changes in the *hydration* and consequent *mechanical properties* of the polymer as it passes through the LCST”.

4 SELF-ASSEMBLED MONOLAYERS:

Chapter 4

4.1 Background

As it has been pointed out in Chapter 2.1, SAMs have been long considered a good surface model in the mechanistic studies of cell migration.

Tailoring at molecular level the surface properties by means of SAMs, enabled scientists to better comprehend cells functionalities and their communication with the surrounding environment (love). A further step in this field has been undertaken adding specific moieties that could actively interact with the living systems. In particular, in Chapter 2.2 it has been briefly mentioned the concepts at the base of some of these switching systems controlled by electrochemical and electrical stimuli.

Some "active" molecules have been widely studied to modify the surface characteristics of electrodes[1,2,3,4,5] thanks to molecular structural modification induced by electrochemical reactions. Among this class of smart polymers, it has been already mentioned the particular behaviour of the hydroquinone moiety and its capability to undergo a reduction/oxidation process as consequence of an electrical field variation.

Mrksich has been the first that understood the potentiality of this process for biological studies and he set up some "dynamic" systems that were able to actively interact with cells[6,7,8]. In particular, he developed a mixed surface composed of an antifouling background, which has been used to prevent nonspecific attachment of cells to the monolayer, and the active species. The latter molecules are constituted by an O-silyl hydroquinone ether in which a side hydroxyl proton is substituted by an RGD sequence used to mediate the adhesion of cells (Figure 4.1.1 A).

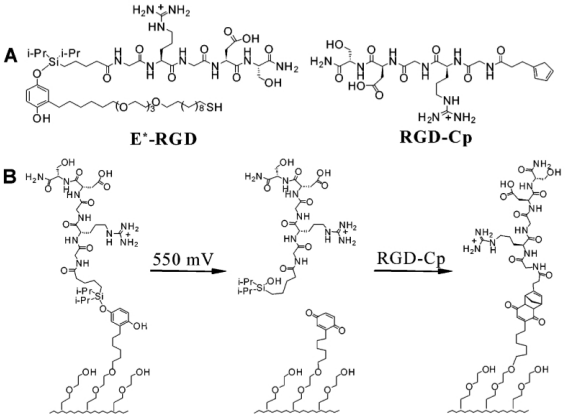

Figure 4.1.1: (A) Structures for the functionalized alkanethiol used to prepare dynamic substrates (E-RGD) and the cyclopentadiene moiety (RGD-Cp) used to selectively immobilize ligand. (B) A monolayer presenting the O-silyl hydroquinone undergoes electrochemical oxidation to give a benzoquinone, with hydrolysis of the silyl ether and selective release of the RGD ligand. The resulting benzoquinone reacts with RGD-Cp by way of a Diels-Alder reaction, which selectively immobilizes the second ligand. The RGD peptide mediates the adhesion of cells[8].*

As stated, the O-silyl hydroquinone ether is electroactive and provided for the selective release of the peptide from the substrate by means of a known red/ox mechanism: when an electrical potential has been applied to the substrate, the oxidation of the hydroquinone to the corresponding benzoquinone caused the hydrolysis of the silyl ether and the release of the RGD.

But the complex system set up by Mriksich could subsequently immobilize a second ligand thanks to a further reaction. The benzoquinone group, in fact, could undergo a selective immobilization of a diene-tagged peptide (Figure 4.1.1 B) by way of a Diels-Alder reaction and, therefore, provides the basis for a second dynamic activity. At the same time, however, this last reaction could be electrochemically inhibited reducing the benzoquinone to hydroquinone thus permitting the modulation of the process.

The culture tests revealed the possibility to trigger cell adhesion and migration as consequence of RDG sequences release. Mrksich noticed that the ability to effect multiple

changes in the bioactivity of his substrates could be especially useful in the study of heterotypic cell-cell interactions and for the mechanistic comprehension of cell migration.

The interesting results obtained by Mrksich induced the authors to study this solution. A commercially available molecule similar to the O-silyl hydroquinone ether has been found (QEG, Figure 4.1.2). Interestingly, the producer, ProChimia Surfaces Sp. z o.o., asserted that it possessed similar properties to the molecule used by Mrksich and it has been decided to test it.

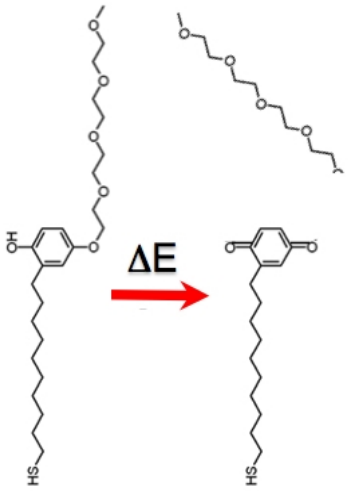

Figure 4.1.2: chemical structure and reaction scheme of the molecule (QEG) furnished by ProChimia Surfaces Sp. z o.o.

4.2 Experimental section. Electroactive SAM

Materials and Methods

Substrate. Silicon gold coated substrates, used for PNIPAM grafting, were obtained from FBK (Fondazione Bruno Kessler, Italy). The samples were prepared starting from a Si (100) wafer on which 20 nm of chromium were deposited to improve the adhesion of the final polycrystalline gold (99.9999% pure) layer approximately 150 nm tick. Silicon thickness ranged from 0,3 mm to 1 mm depending on tests methods.

Self assembled monolayer (SAM) preparation. Samples obtained by FBK have been immersed for 10min in piranha solution (70:30 H2SO4/H2O2) for a first cleaning treatment. The substrates have been then rinsed with Milli-Q water, subsequently with ethanol and finally dried under nitrogen. A final treatment in RF plasma (15 sec in a low vacuum glow discharge plasma at 200 W with 40 mL/min oxygen flux) has been performed to obtain a clean surface. Immediately after these treatments the samples have been soaked in a 2 mM ethanol solution of HS-(CH2)11-quinone-EG4OMe (95%, QEG) (Figure 4.1.2) for 48 h. Once removed from solution, the samples have been rinsed with ethanol in order to remove the physisorbed thiols and subsequently dried under nitrogen. As control surface for cyclic voltammetry and for electrochemically-induced cell sheet detachment, an amino terminated SAM has been used (11-amino-1-undecanethiol hydrochloride, 95%, NH2). This surface have been prepared with the same procedure used for QEG. Both QEG and NH2 have been purchased by ProChimia Surfaces Sp. z o.o..

Infrared reflection absorption spectroscopy. Attenuated total reflectance Fourier transform infrared reflection absorption spectroscopy (ATR-FTIR) QEG thiol and on the same molecule self-assembled on the gold substrate have been carried out with a Spectrum One (PerkinElmer) coupled with a VeeMax II Accessory (PIKE) for grazing angle (GA) measurements. Light was p-polarized and spectra were collected at 65° in grazing angle reflection mode. For each sample 128 scans were collected with a 4 cm-1 resolution.

Cyclic voltammetry. Cyclic voltammetry on QEG SAMs was performed with a Keithley 6517A electrometer controlled by a custom-made NI Labview program. PBS has been used as the electrolyte at pH 7.4. The voltammetric scan ranged from –800 mV to +800 mV at 100 mV/s. All experiments has been carried out in a custom-designed electrochemical cell with the SAM as the working electrode, a gold-coated wafer as the counter electrode, and an Ag/AgCl reference electrode. NH2 SAMs have been used as control suraface.

Static contact angle. Static contact angle on SAM have been performed by means of a custom made goniometer using a 3 µl drop of milli-Q water as probing liquid. For each sample, at least three measurements from different surface locations were averaged.

X-ray photoelectron spectroscopy (XPS). The XPS measurements were carried out using an ESCA200 instrument (Scienta-Gammadata ESCA 200 Uppsala Sweden). Wide scans were acquired with a tilt angle of 165° in the BE energy range 1200 – 0 eV using a 500 eV pass energy while high resolution core line spectra were performed setting the analyzer pass energy at 150 eV and the energy step at 0.05 eV. Because the samples are conductive, they do not require charge compensation, leading to an energy resolution of 0.3 eV measured on the Ag Fermi edge.

Cell culture. Before cell culture, all samples have been disinfected by immersion in ethanol 70% followed by washing with sterile phosphate buffer solution (PBS), then placed in a 24-wells plates. Two different cell lines have been tested: human embryonic rabdomyosarcoma cells (RD) and human osteosarcoma cells (MG63).

In the first case 1 ml of RD cell suspension (passage 37, obtained from Istituto Zooprofilattico di Brescia) has been seeded in each well at a concentration of $1x10^5$ cells/ml. Eagle's minimum essential medium in Hanks' balanced salt solution (Hanks' MEM, Invitrogen) supplemented with 10% Fetal Bovine Serum (FBS), sodium piruvate (1mM, Euroclone), L-glutamine (4mM, Euroclone), 2% vitamins, 2% non essential aminoacids, 1% Penicillin has been used as culture medium.
In the second case, 1 ml of cell suspension of human osteosarcoma cells (MG63, passage 112, obtained from Istituto Zooprofilattico di Brescia) has been seeded in each well at a concentration of $1x10^5$ cells/ml. Minimum essential medium (MEM, Invitrogen) supplemented with 10% heat inactivated Fetal Bovine Serum (FBS), sodium piruvate (1mM, Euroclone), L-glutamine (4mM, Euroclone), 1% vitamins, 1% non essential aminoacids, 1% Penicillin has been used as culture medium.
In both cases, the respective cells have been also seeded in an empty well as control test. Cells were incubated at 37ºC in a 5% CO_2 atmosphere incubator, changing the medium one day after the seeding and subsequently every two days.

Electrochemically induced cell sheet detachment. RD cells reached confluence 4 days after seeding on both QEG and NH2. The electrochemically-induced cell sheet detachment has been performed similarly to the cyclic voltammetry test but, in this case, samples have been treated with a continuous electrical potential of 600 mV for 5 minutes, to induce the hydrolysis of the side chains, followed by a potential of -300 mV for 30 seconds to induce the reduction of the molecule to the hydroquinone conformation. NH2 SAMs have been used as control surface.

"Spontaneous" cell sheet detachment. MG63 cells reached confluence 3 days after seeding on QEG samples. Cell sheet detachment has then been achieved in the following ways.
Two different methods were tested: the use of plastic tips tweezers and the use of a forced medium flux produced by a pipette. As control test the same procedure has been carried out on cells seeded in a Petri culture well.

Detached cell sheet analysis. Morphological observations of MG63 cell sheets after detachment have been performed by scanning electron microscopy (SEM) (Cambrige Stereoscan 200 – operating mode: high vacuum, secondary electron SE detector). Cell laminae, prior to imaging, have been fixed using a glutaraldehyde solution (25% glutaraldehyde in cacodylic buffer solution 0.1 M, pH=7.2), and then dehydrated by dipping in aqueous ethanol solutions at increasing alcohol concentrations. For SEM imaging, samples have been gold-sputterd (SEM Coating Unit PS3, Assing S.p.A., Rome, Italy).
For histological analysis, a MG63 cell sheet, fixed in a formaldehyde solution (4% in PBS), has been sent to S. Chiara Hospital (Trento, Italy). Here it has been opportunely treated and embedded in paraffin. Subsequently the cell sheet embedded in paraffin has been cut in slides, stained and observed by optical microscope.

Results and Discussion

Self-assembling result of QEG has been verified by ATR-FTIR in grazing angle (Figure 4.2.1). Despite a lower quality in the spectrum signal, the curve of the QEG SAM (Figure 4.2.1, above) is comparable to the spectrum obtained for the thiol (Figure 4.2.1, below).

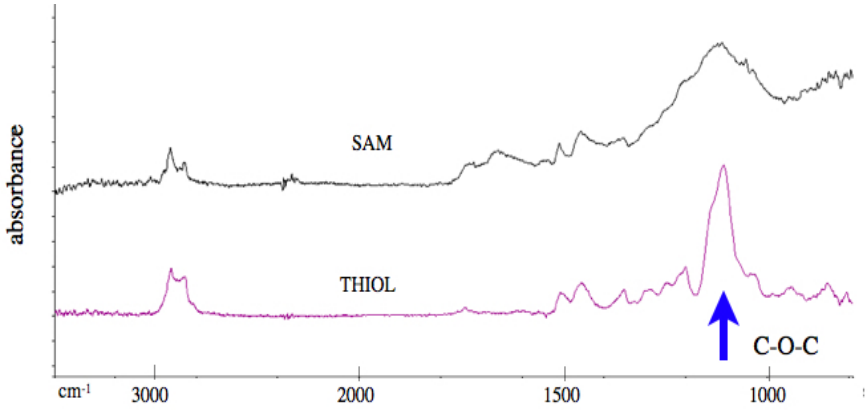

Figure 4.2.1: ATR-FTIR spectra collected in grazing angle modality of QEG thiol (below) and the same molecule self-assembled on gold (above. The arrow indicates the wavelength corresponding to the ether signal of the PEG side chain present in the molecule.

In particular, the characteristic signal of the ether group, presents in the side-chain of hydroquinone moieties, is recognizable in both the spectra at approximately 1120 cm-1.
To gain evidence of the electrochemical oxidation of immobilized QEG into the benzoquinone group and the subsequent side chain cleavage, a cyclic voltammetry test has been used. The test results (Figure 4.2.2) exhibited a trend commonly observed for similar process[1,2,3].

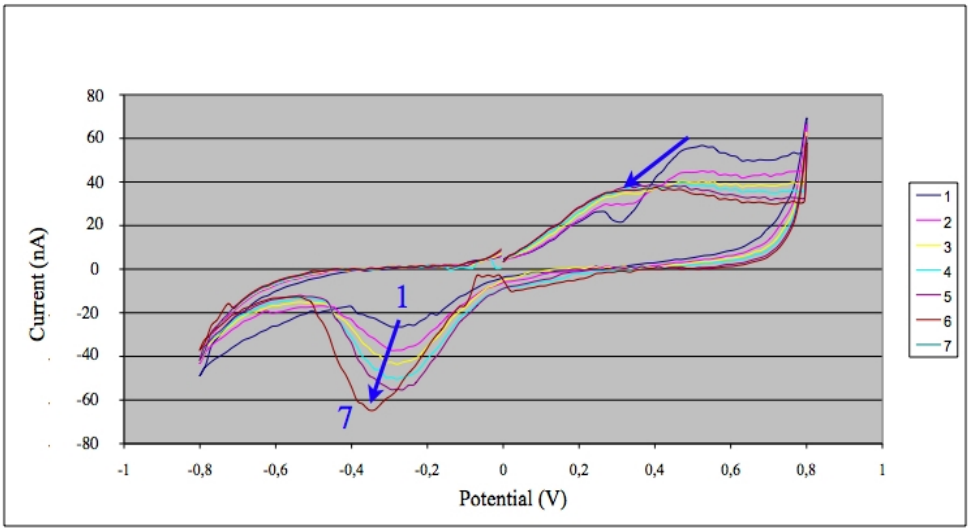

Figure 4.2.2: cyclic voltammograms of QEG. The numbers in the box indicate the cycle number, while the blue arrows highlight the modification in the peak shape from the first cycle to the seventh.

In the first cycle, during the oxidation reaction, it has been possible to distinguish two peaks. The peak in correspondence of the lower voltage can probably be ascribed to the deprotonation of the hydroxyl side-group that became the carbonyl group present in the oxidized benzoquinone. The peak at higher voltage has been instead related to the cleavage of the short poly(ethylene glycol) (PEG) side-chain on the hydroquinone moiety. After few cycles the second peak disappeared, substituted by a larger peak at approximately 400 mV. Observing the plots at negative voltage, the scans showed a wave for reduction connected to benzoquinone, which continued to increase in intensity, reaching a maximum current after some cycles.

Similar studies found in the literature[3] assessed that the peak positions, observed in the cyclic voltammogram, are related to the number of methylene units in the alkyl chain spacer that divides the hydroquinone moiety from the gold substrate. In particular, the absolute voltage difference between the two waves tends to increase augmenting the methylene units[3].

For an alkyl chain spacer composed of 11 carbon atoms, such as the molecule here used, it has been found a sufficient agreement of the data with the literature values.

The same cyclic voltammetry performed on NH2 (Figure 4.2.3) showed the no peaks, indirectly confirming that the waves noticed for QEG are related to the molecule characteristics.

Confronting the literature data[6,7,9] and the obtained cyclic voltammetry, it has been also possible to conclude that no significant desorption of thiols from gold surface occurs at the voltage and for the time length selected for the electrochemically-induced cell sheet detachment (5 minutes at +600 mV and 30 seconds at -300 mV). This is a crucial aspect since it has to be excluded any cell release due to side-reactions.

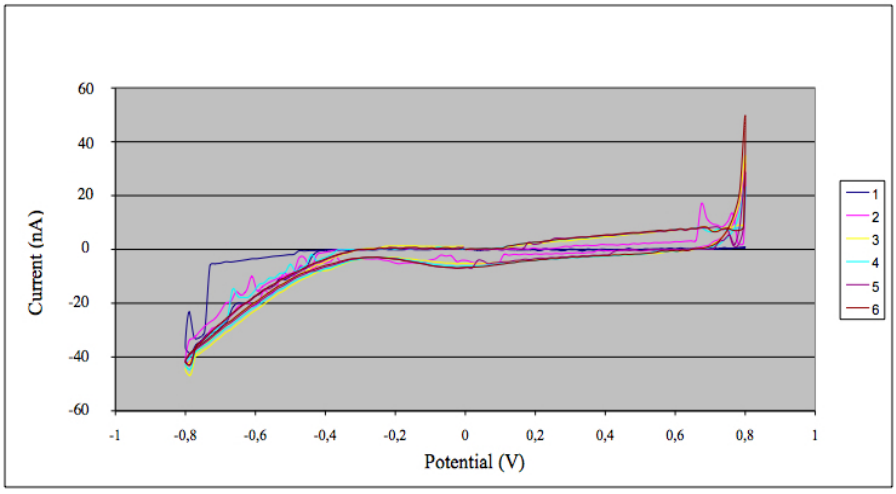

Figure 4.2.3: cyclic voltammograms of NH2. The numbers in the box indicate the cycle number

A chemical/physical characterization of the surfaces, before and after the cyclic voltammetry, has been carried out by means of static contact angle and XPS analysis.

As regard contact angle (Figure 4.2.4), it has been possible to notice that the surface, despite the PEG side-chains, was not particularly hydrophilic. In the literature[10] the contact angle value reported for PEG terminated SAM is 40°, while QEG surface was somewhat more hydrophobic. This fact could be related to the steric volume of the hydroquinone moiety that caused two effects: an increase in SAM defects and a low PEG density that induced a partial exposure of the quinone aromatic ring.

After the cyclic voltammetry, a decrease in the wettability has been observed as could be expected by the release of the PEG chains.

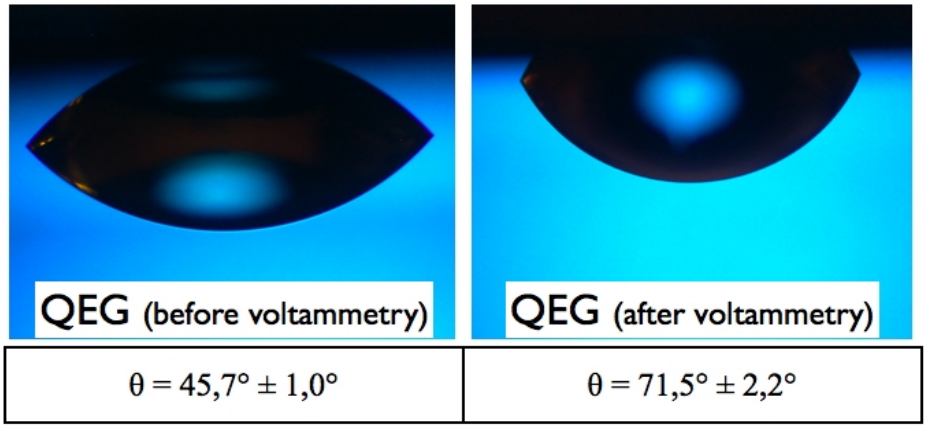

Figure 4.2.4: static contact angle on QEG before (left) and after (right) cyclic voltammetry

However, XPS analysis (Figure 4.2.5) showed that the surface presented a O/C ratio higher than the theoretical value and, more importantly, it increased after the treatment.

This is in contradiction with the expected chemistry of the QEG surface after the electrochemical side-chain cleavage.

XPS	O/C	S/C	C=O/C
QEG	0,171	0,007	0,012
QEG (theoretical)	0,24	0,04	0
QEG after voltammetry	0,252	0,019	0,037
QEG after voltammetry (theoretical)	0,125	0,062	0,125

Figure 4.2.5: theoretical and experimental (XPS analysis) O/C, S/C and C=O/C ratios for QEG before and after voltammetry

Despite the analytical results didn't confirmed the occurrence of the expected process, it has been decided to test QEG and NH2 SAMs by cell culture and, subsequently, electrochemically-induced cell detchment.

On NH2, RD cells well proliferated but no difference in cell adhesion has been noticed after voltammetry.

Cells adhered and proliferated efficiently also on QEG surface (Figure 4.2.6, left), but, even in this case, no significant cell detachment have been noticed after the electrochemical treatment (Figure 4.2.6, right).

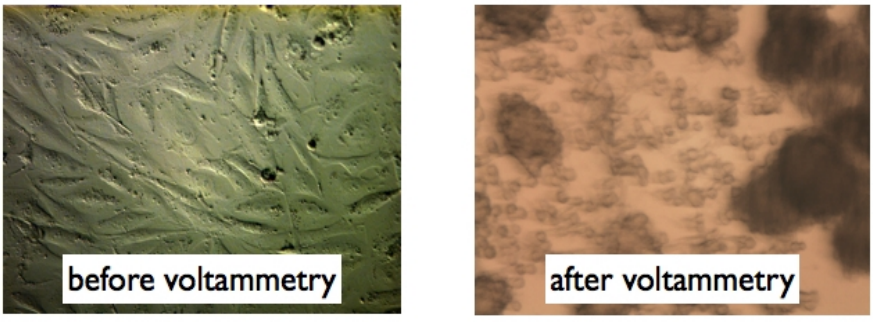

Figure 4.2.6: RD cells, adhering on QEG, observed by optical microscope before (left) and after (right) electrochemically-induced cell detachment

Therefore, a second culture test has been carried out with MG63 cell line to verify if the negative results were the consequence of cells peculiarities or a surface failure.
The experiment revealed, however, unexpected results.
It has in fact been noticed that this kind of cells could rapidly proliferate on QEG surface (Figure 4.2.7, left) but they loosely adhered on it. The interesting consequence of this behaviour was that, once confluence has been reached, it was possible to induce a "spontaneous" cell lift-off with cells detaching in the form of a sheet. A gentle pressure with plastic tweezers or a forced medium flux, produced by a pipette, was sufficient to start the lift-off (Figure 4.2.7, right). The final outcome was a cell sheet with comparable characteristics to the cell sheets obtained by PNIPAM-coated samples but, in this case, no active stimuli have been necessary.

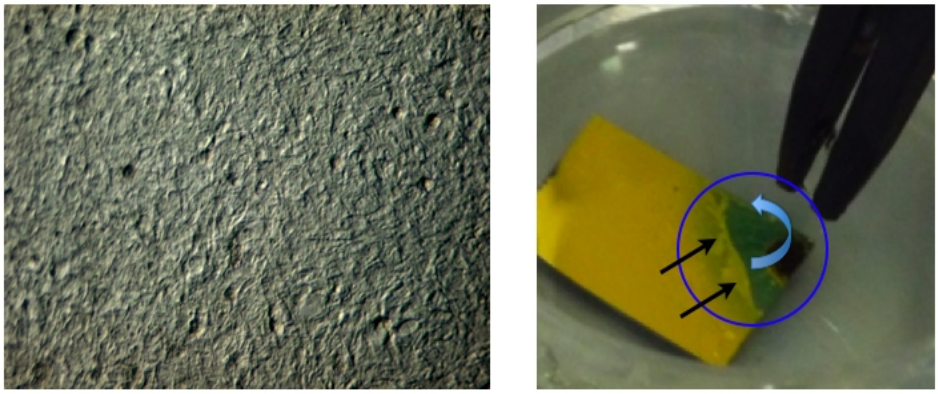

Figure 4.2.7: MG63 cells, adhering on QEG, observed by optical microscope (left). On the right a picture of MG63 cells while "spontaneously" detaching from QEG (blue circle). The partially detached, floating cell sheet is highlighted by the black arrows. The bright corner on the right of the sample is the "uncovered" QEG surface, while the opaque region represents cells still adhering on the substrate.

Despite the attractive result, it is worth to emphasize that this unusual behaviour is strongly cell-line dependent, in fact, no cell sheet detachment has been observed for RD cells cultured in the same conditions.
The characterization of the cell sheet by SEM analysis revealed no significant damages as result of the detachment process (Figure 4.2.8, A-B).

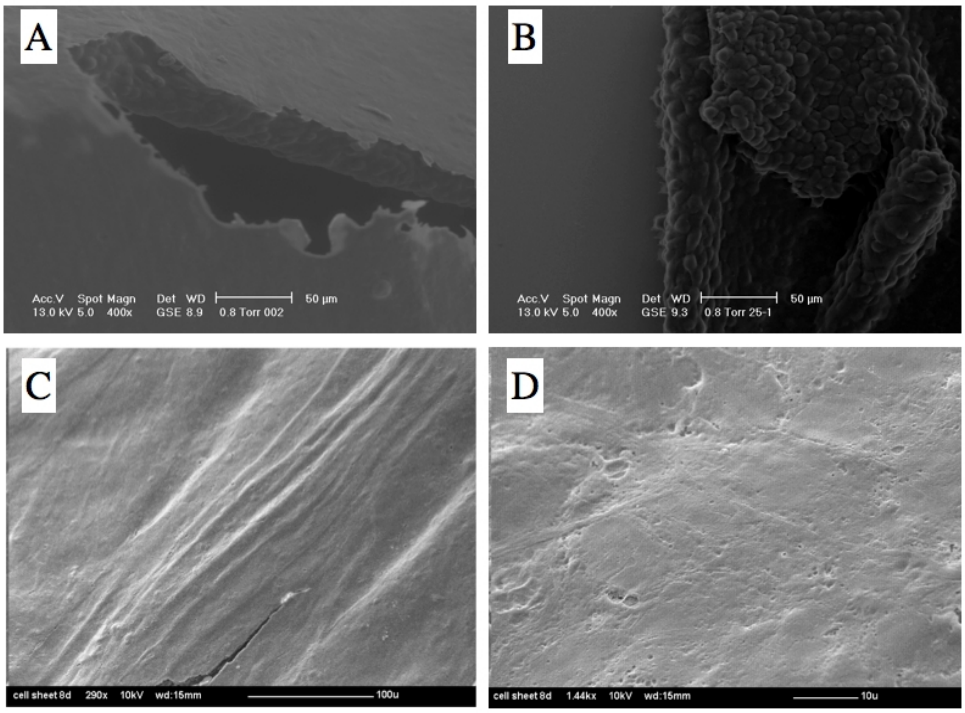

Figure 4.2.8: SEM images of MG63 cell sheets "spontaneously" detached from QEG. A) the "bottom" side of the lamina, B) the "top" side of the cell sheet. C,D) two different details of a lamina before the detachment.

The SEM analysis before the detachment (Figure 4.2.8, C-D) revealed the presence of many filaments of the cytoskeleton with cells that overlap in what appeared like a multilayered lamina .

Histological images (Figure 4.2.9) confirmed that, after detachment, a tight cell-cell junction was maintained to such an extent that it has been virtually impossible to distinguish the shape of a single cell. If, in fact, cell nuclei (darker spots) were easily recognizable, the cytoskeletons appeared like an amalgamated mass. The holes inside the sheet, in this case, were not the consequence of a failure in detachment but the consequence of technical limits. These holes, in fact, have to be attributed to the technical impossibility of fixing the cell lamina inside the embedding wax in a perfectly flat position. Obviously then, when slides has

been cut from the fixed wax mass, it has not possible to obtain a perfect sheet and some parts of the cell layer have been “cut away”.

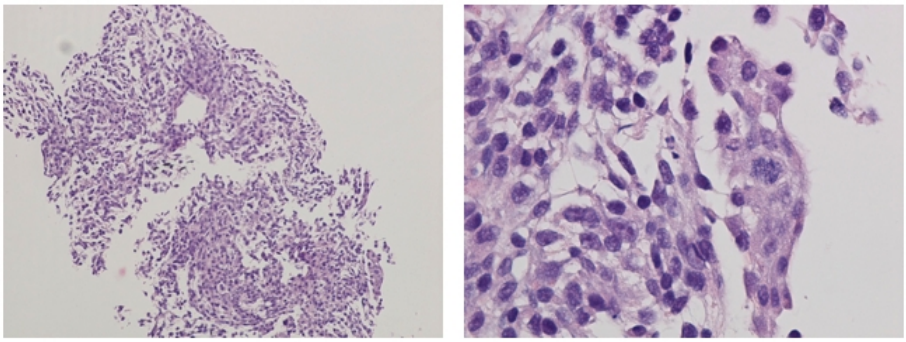

Figure 4.2.9: histological analysis of MG63 cell sheet "spontaneously" detached from QEG. The pictures represent two region (at different magnitude) of the same histological slide.

4.3 Experimental section. Mixed SAMs

Introduction

Due to the negative results obtained by electrochemically-induced cell sheet detachment on QEG, it has been decided to temporary abandon this research field until a new molecule could be available.

At the same time, however, since a "spontaneous" detachment from SAMs has never been observed, it has been decided to further investigate the phenomenon.

Despite, as mentioned before, detachment occured only for MG63 cells, the result is, nevertheless, interesting since osteoblast-like cell sheet can be used in various tissue-engineering studies.

This field of research is remarkably important since bone defect regeneration represents one of the main issues in biotechnology. Currently, autologous bone is one of the preferred surgical solutions but this technique is severely limited by the reduced number and dimension of the donor sites[11].

An alternative approach, discussed in the introductive chapter, is to employ scaffold loaded with cells that facilitate bone regeneration. The solution has been extensively studied and different solution as been proposed[12,13]. More recently, some authors proposed a further development to overcome the limits of this technique and, thus, enhance the success rate[11,14,15]. It consists in the combination of the scaffolds with osteoblast cell sheet instead of single isolated cells. This approach is supposed to be more efficient for a rapid defect healing since this solution permits the preservation of the extracellular matrix and cell-cell junctions that enhance scaffold cellularization and cell viability.

The methodologies reported in the literature to produce osteoblast cells sheets are generally two: the mechanical detachment of cells, utilizing a cell scraper, or the use of PNIPAM-coated cell culture dish.

The former technique is the more rudimental form of cell sheet detachment adopted for this kind of studies. The latter has been discussed in Chapter 3 and, despite it has been specifically developed for other purposes[16], more recently, some authors investigated the possibility to use PNIPAM grafted Petri dish also in bone tissue engineering[11,17].

In light of this fact, the possibility to use an alternative substrate to produce sheets of osteoblast-like cells is remarkably interesting. Despit the use of osteoblast-like cell is limited to laboratory studies, this cells are particularly important and represents one of the mainly used cell model for *in vitro* tests[13].

As a first hypothesis to explain the "spontaneous" cell sheet detachment, it has been supposed that cells loosely adhered on QEG surface due to the PEG side chains.

The antifouling properties of this polymer have been the argument of various studies[18,19,20]. Chain density and length are the known key features that enable the surface to resist the attachment of cells.

Then, despite cell attachment are usually considered as an on/off mechanism, it has been supposed that the low PEG density on QEG could be the optimal compromise between fouling and proteins repulsion that leads to the low MG63 cell adhesion.

The hypothesis was verified producing mixed SAMs composed of two thiols: one with a PEG terminal functionality (P4EG), the other, shorter, terminated with a methyl group (CH3). The former has been used as the antifouling molecule, while the second substituted the steric volume of the hydroquinone moiety (Figure 4.3.1).

SAMs with different ratios of the two thiols have been obtained, under the hypothesis that no significant segregation occurred between the two molecules[10,21,22].

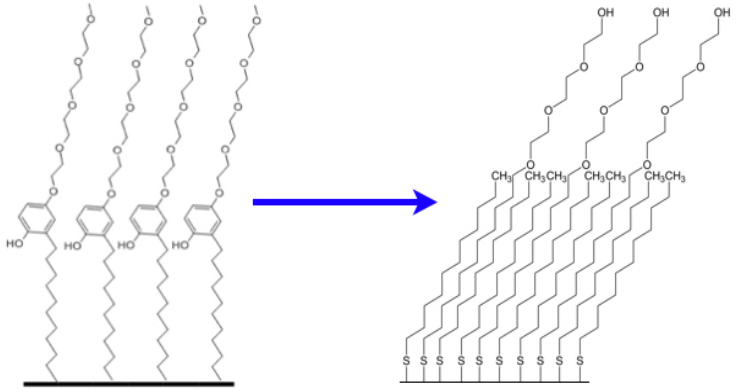

Figure 4.3.1: structures of the QEG (left) and mixed P4EG/CH3 SAM (right). The second has been used to verify if MG63 low adhesion on QEG was due to a low PEG density on QEG surface.

Materials and Methods

Substrate and self-assembling procedure are the same used in the previous part of the chapter. In particular, the thiol solution, in this case, has been composed of (1-mercaptoundec-11-yl)tetra(ethylene glycol) (95%, P4EG) and 1-undecanethiol (98%, CH3) mixed in the proper ratio. Both molecules have been obtained from Sigma. The final molarity has been, again, 2 mM.

ATR-FTIR in grazing angle, static contact angle, culture tests, and the relative SEM images, have been carried out with the same procedure described in the previous part.

Result and Discussion

ATR-FTIR spectra, collected in grazing angle, showed a gradual increase of the peak relative to the ether signal of the PEG chains (highlighted by the vertical line in the spectra of Figure 4.3.2) when the CH3 thiols concentration decreased in favour of P4EG.

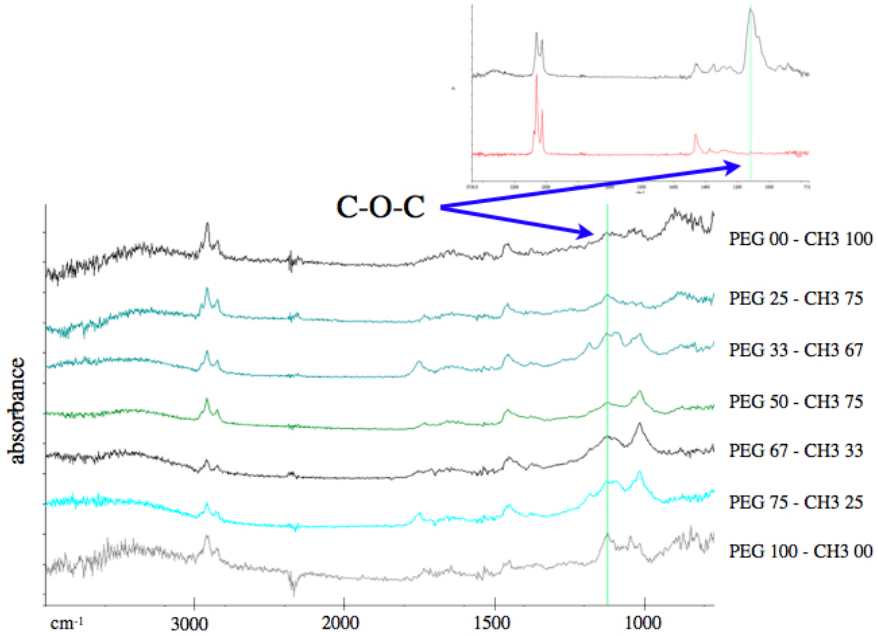

Figure 4.3.2: ATR-FTIR spectra of mixed SAM collected in grazing angle. The vertical line highlights the wavelength that corresponds to the ether signal of P4EG. The absorbance increases at the increase of P4EG concentration in the SAM (from top to bottom).In the up-right corner are reported spectra of the two thiols: P4EG (above) and CH3 (below).

Static contact angle measurements confirmed the progressive change in wettability from the hydrophobic 100% methyl terminated SAM to the hydrophilic 100% PEG terminated SAM (Table 4.3.1).

As reported in the literature[22], the contact angle variation for this kind of SAM is almost a linear function of the CH3/P4EG concentration (Figure 4.3.3).

PEG - CH3 (%mol)	Static contact angle
0 - 100	101,8° ± 0,8°
25 - 75	80,3° ± 1,9°
33 - 67	71,4° ± 4,7°
50 - 50	56,9° ± 6,7°
67 - 33	46,1° ± 4,1°
75 - 25	35,9° ± 3,2°
100 - 0	27,6° ± 1,3°

Table 4.3.1: static contact angles of P4EG/CH3 mixed SAM

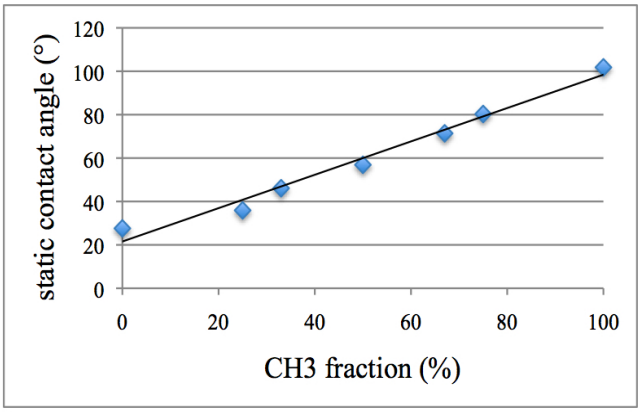

Figure 4.3.3: Static contact angle variation as function of the composition of mixed SAMs

The various mixed SAM surfaces presented, after 24 hours from the seeding, different cell viability (data not shown), with a higher cell number on SAM presenting intermediate wettability[23] and fewer cells on surfaces extremely hydrophobic. Unexpectedly, however, MG63 cells have been found to adhere also on surfaces composed of P4EG only and, after few days from the seeding, they were able to reach confluence.

Even more interestingly, by means of plastic tweezers it was possible to detach a cell sheet from all the tested surfaces, regardless of wettability or chemical composition.

Again, no similar behaviour has been noticed for the control, where MG63 cells tightly adhered on the bottom of the culture well.

The observation, by SEM, of the detached lamina demonstrated that undamaged cell layer could be obtained from 100% CH3, 100% P4EG or SAMs composed by the mixing of the two molecules (Figure 4.3.4).

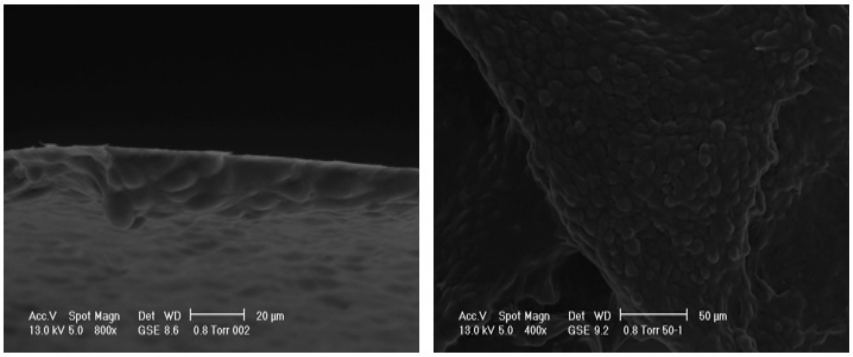

Figure 4.3.4: SEM images of MG63 cell sheets "spontaneously" detached from mixed SAM. Cell sheet side view (left), and top view (right).

This led to the conclusion that the initial hypothesis was wrong. The low MG63 cell adhesion couldn't depend on a particular PEG chain density since cell sheet detachment has also been obtained form SAM surfaces without P4EG. Then, to investigate the possible causes that induce the low MG63 adhesion on SAMs, more information about the phenomenon were needed and the next step has been to test thiols with different terminal groups.

4.4 Experimental section. Different Terminating Groups

Introduction

As stated before, in this section it has been analysed possible difference in MG63 cell adhesion/detachment as consequence of different chemical terminating groups of SAMs. This has been accomplished to highlight a possible correlation between MG63 cell low adhesion the the SAM substrates and the chemical/physical surface features.

Interesting studies on interaction of proteins and cells with SAMs of different nature[1,2,3,4,5] have already been reported in the literature.

However no "spontaneous" detachment has ever been observed from this kind of surfaces.

In this part of the chapter, then, this peculiar behaviour has been examined observing proteins and MG63 cell response toward the different SAMs.

Materials and Methods

Substrate and self-assembling procedure are the same used in the first part of the chapter. for the experiments relative to this part eight different thiol have been tested: 11-mecapto-1-undecanol (97%, denominated as: OH), 11-mercapto-undecanoic acid (95%, COOH), (1-mercaptoundec-11-yl)tetra(ethylene glycol) (95%, P4EG), 1-undecanethiol (98%, CH3), 1H,1H,2H,2H-perfluorodecanethiol (97%, F) (purchased from Sigma Aldrich), 11-amino-1-undecanethiol hydrochloride (95%, NH2), 29-amino-(1-mercaptoundec-11-yl)hexa(ethylene glycol) hydrochloride (95%, EGNH2), (E)-11-(4-(phenyldiazenyl)phenoxy)undecane-1-thiol

(95%, dAzBe) (obtained from ProChimia Sp. z o.o., Poland).

Wilhelmy plate experiments. Dynamic contact angle have been measured using a Cahn 322 microbalance. For this test, silicon wafer coated with gold on both sides have been used. Samples dimension where 10x15 mm with a thickness of 300 μm to have negligible surfaces not covered with SAM. The contact angle of the culture Petri dish has been measured testing a similarly sized piece of a culture well-plate. Two subsequent immersion cycles have been carried out at room temperature and with an immersion speed of 20 μm/s. Milli-Q water as been used as the test liquid. Advancing and receding contact angle values have been calculated as the average of three independent runs.

Atomic force microscopy (AFM) measurements. The AFM system used in this study was a NT-MDT scanning prob microscopy solver P47H equipped with a S7 scanner (scanning by sample). The measurements were performed in the contact mode with samples immersed in milli-Q water at room temperature. A Si cantilever with a spring constant of 0.03 N/m and a tip radius of 10 nm was used (scanning rate 0.6-1 Hz). All images (512 _ 512 pixels) were collected over a 4x4 μm scan area in the “height mode”, which kept the force constant. The roughness value is the average calculated on at least three different regions for each sample.

Protein adsorption. Samples were incubated in MG63 culture medium for 25 min at 37 °C. Two samples (10x7.5 mm) for each tested molecule were used and no pre-wetting treatments have been performed on samples. After incubation, medium has been stored and samples have been gently washed with deionized water and placed into clean test chamber wells.

For a qualitative measurement of protein binding strength, samples were subjected to protein elution procedure according to an experimental protocol based on the sequential washing of the sample surfaces by media with different chemical strengths. Specimens have been washed three times with water, and then sequentially with isopropanol/water solutions at increasing concentrations: 10%vol (denominated as: ip1), 30%vol (ip2), 50%vol (ip3), and 70%vol

(ip4)[6]. At each step 1 ml of eluting medium has been added on sample surfaces for 20 min at room temperature, under static conditions. A final elution step with sodium dodecyl sulphate 0,1%wt (SDS) has been performed to verify the removal of strongly adhered proteins. Following elution, the supernatants have been carefully removed, aliquoted and frozen at –80 °C.

For 1D-electrophoresis the desorbed protein samples have been freeze-dried and resuspended in 20 ml of "sample buffer" (NuPAGETM LDS Sample Buffer, Invitrogen). 6 ml of each resuspended sample have been then loaded on acrylamide SDS-PAGE gels. NUPage® Novex 3-8% (Tris-Acetate) gels have been used for the detection of high molecular weight proteins (40-500 kDa). Each gel has been loaded with a molecular weight protein standard (HiMarkTM, Invitrogen or Protein Marker, Broad Range, BioLabs) and MG63 culture medium as control sample (1:20 in "sample buffer"). SDS-PAGE has been performed in a XCell SureLockTM Mini-Cell (Invitrogen). The 3-8% gels have been run at 150 V, constant voltage. Following electrophoresis, the acrylamide gels have been stained using the Imperial Protein Stain (Pierce), and, to increase the bands profile intensity, it has been successively stained also with ProteoSilver Silver Stain Kit (Sigma). Finally the stained gels have been digitalized by a GEL LOGIC 200 (Kodak) imaging system and the data elaborated by means of the Kodak 1D Image Analysis Software.

Cell culture. Before cell culture, all samples have been sterilized by immersion in ethanol 70% followed by washing with distilled water, then placed in 24 well plates. 1 ml ($1x10^5$ cells/ml) cell suspension of human osteosarcoma derived osteoblasts (MG63, passage 115, obtained from Istituto Zooprofilattico di Brescia) has been seeded in each well. Minimum essential medium (MEM) supplemented with 10% Fetal Bovine Serum (FBS), 1% Penicillin, 1% Glutamax, 1% Vitamins, 1% non-essential amino acids has been used as culture medium. Cells have been incubated at 37ºC in a 5% CO2 atmosphere incubator, changing the medium every 2 days.

Two different samples dimensions have been tested: 5x5 mm^2 and 10x7.5 mm^2.

Cells initial adhesion has been verified by stopping cell culture after one day. Samples fixation has been done using a formaldehyde solution (4% in phosphate buffer solution, PBS) and permeabilization with TritonX (0.2% in PBS). Samples have been stained with rhodamine phalloidin (cell cytoskeleton) and DAPI (cell nucleus) according to the manufacturer protocol (Molecular Probes Inc., Oregon, USA). Finally the morphology of cells has been observed by confocal microscopy (Nikon confocal microscopy A1). The number of cells has been counted taking nine pictures disposed on a 3x3 mm^2 regular grid for each samples. The so obtained images have been analyzed counting the number of nuclei and finally the mean per square centimetres has been calculated.

After three days of culture cells reached confluence on all the samples. Cell sheet detachment has then been achieved in the following ways. Two different methods have been tested: the use of plastic tips tweezers and the use of a forced medium flux produced by a pipette. As control, the same procedure has been tested on confluent cells seeded in a Petri culture well. The viability has been assessed by confocal laser microscopy after staining with fluorescein diacetate–propidium iodide (FDA–PI) (Molecular Probes Inc., Oregon, USA). FDA stains viable cells green, while PI stains necrotic and secondary apoptotic cells red. The assay has been performed according with previously published methods[7]. To test the capability to re-adhere, the cell sheets detached from SAMs have been placed in a new culture well and few microliters of culture medium have been added to maintain the cells alive but, at the same time, avoiding cell sheets to float. New culture medium has been added at regular intervals (1 h) during the first five hours, so that cells could adhere to the bottom of the well. At the end of this first step the sheets have been found completely adherent to the bottom of the well and it has then been possible to add 1 ml of culture medium. After two days, in order to verify cells viability, the cells have been stained with FDA–PI and successively observed at the confocal laser microscopy.

Results and Discussion

The dynamic contact angle measurements (Figure 4.4.1) showed that the selected SAMs covered a broad range of wettability.

The obtained results for OH, COOH, P4EG, NH2, dAzBe, CH3 and F SAMs are consistent with the literature results[1,2,4,5,8,9,10,11]. No data have been found about contact angle measurement on EGNH2.

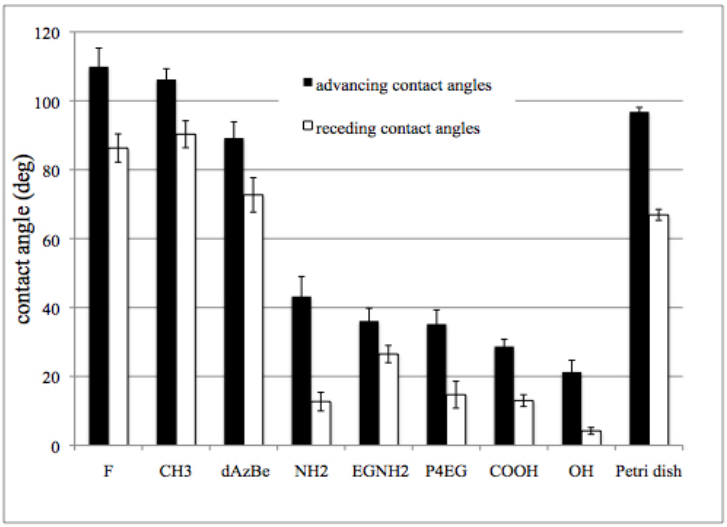

Figure 4.4.1: advancing and receding contact angles for SAMs and the culture substrate (Petri dish).

In particular, OH and COOH displayed a hydrophilic surface (advancing angle $\vartheta a<30°$), while NH2, P4EG and EGNH2 exhibited moderately wettable surfaces ($35°<\vartheta a<45°$). CH3, dAzBe and F presented, instead, hydrophobic characteristics ($\vartheta a\geq 90°$).

The difference between measured advancing and receding contact angle (hysteresis) were in the order of 10-20°, in accordance with the average values reported in the literature for SAMs grown from polycrystalline gold[12]. F and NH2, however, exhibited slightly higher hysteresis

values than usual that can be explained hypothesizing a lower order of the molecules constituting the monolayers.

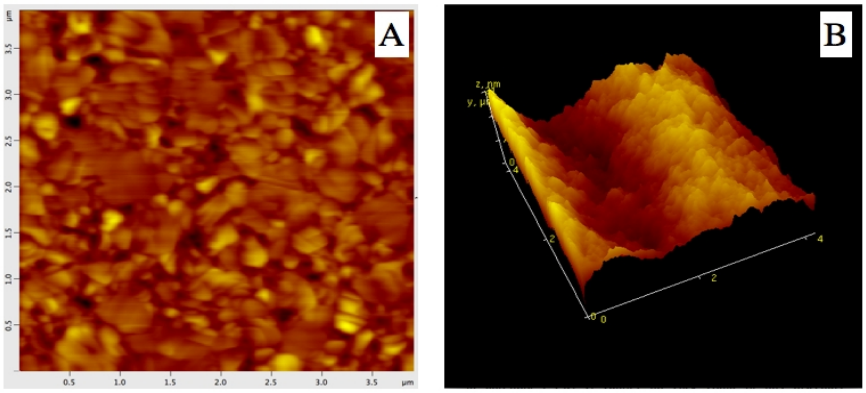

Figure 4.4.2: A: AFM topography displaying the typical appearance of SAM (dAzBe) grown on polycrystalline gold. B: 3D AFM topography of the Petri dish that displays the undulation presents on this surface

The physical appearance of the substrate surface has been observed by AFM and confirmed the polycrystalline nature of the deposited gold (Figure 4.4.2, A). The AFM analysis revealed that the average roughness was relatively low (Figure 4.4.3) with no appreciable differences among SAMs, gold surface and culture Petri dish. In the latter case, beside the average roughness, it has been noticed a quite regular undulation of the surface with a ∼3 μm period (Figure 4.4.2, B), probably as consequence of the cooling process during the fabrication of the material. As regard SAM AFM topography, the results attested an unmodified roughness after the self-assembling. Moreover, the low standard deviation values confirmed the regularity of this kind of surfaces. In this sense, EGNH2 and P4EG represented an exception. The higher standard deviation may be attributed to the soft and hydrated ethylene glycol terminal groups that create a more disordered surface.

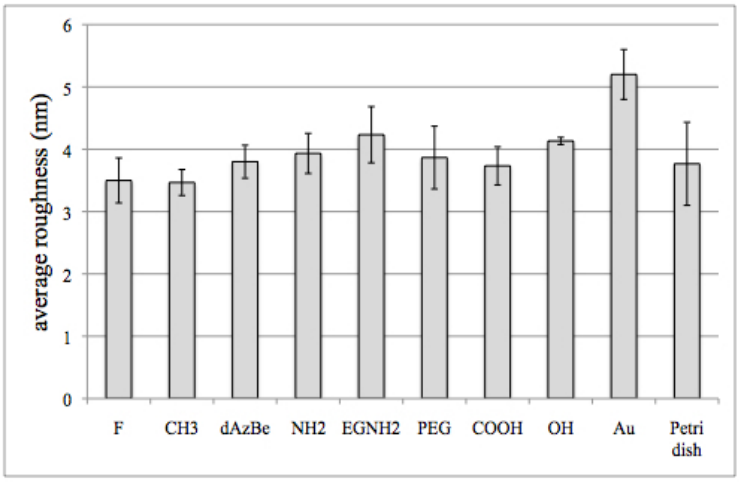

Figure 4.4.3: SAMs and culture substrate (Petri dish) roughness measured by AFM

From these physical characterizations, however, it has not been possible to discern a key factor that may be the cause of cell detachment. The comparison between SAMs and Petri dish roughness revealed similar values but cells detachment has been observed only from the formers while no comparable behaviour has been attested for the latter.

Consequently, surface morphology cannot be considered among the triggering mechanisms of cell detachment.

Even the broad range of wettability measured for the SAMs indicates that the nature of the phenomena is hardly a consequence of chemical interactions between the surfaces and the biological environment.

Figure 4.4.4 summarize the SDS-PAGE profiles of proteins desorbed during the first elution in water. Only these results are shown since they exhibit the most intense and significant signal.

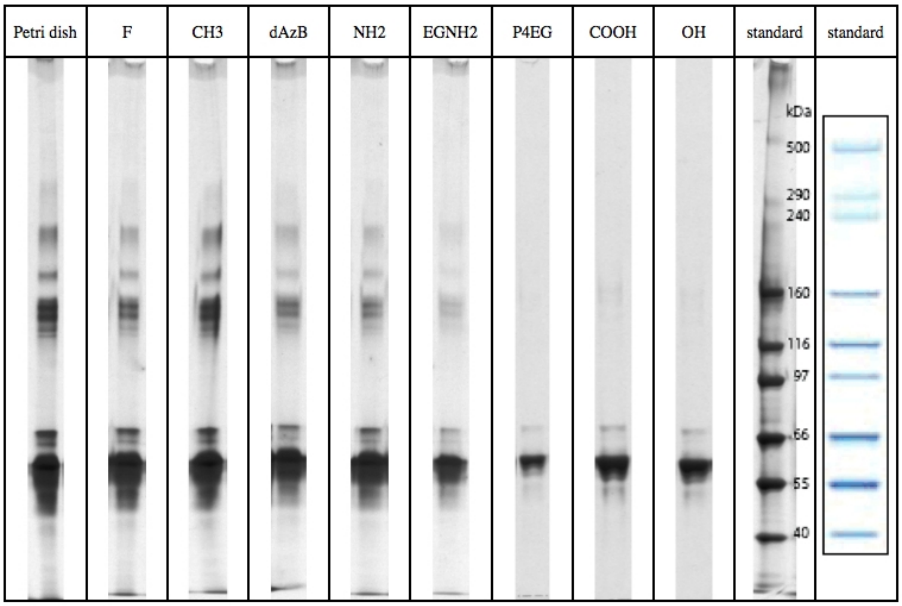

Figure 4.4.4: SDS-PAGE profiles of proteins desorbed by SAMs and the culture substrate (Petri dish) during the first elution in water.

In general, it has been possible to notice that all the samples presented bands of adsorption, even the SAMs with ethylene glycol terminal groups.

This fact is not in disagreement with the literature since it is well known that the antifouling properties of this molecule strongly depend on chains length and density such as on the presence of additional functionalities[3,13,14]. In this case P4EG displayed a markedly low adsorption concentrated at values corresponding to albumin band (at ～60 kDa). On the contrary, EGNH2 presented relatively strong adsorption bands. Although the presence of ethylene glycols groups the intensity of the profile was comparable to OH. Consequently,

despite both P4EG and EGNH2 surfaces presented some kind of resistance to protein adsorption, the ethylene glycol chain length has not been sufficiently long to obtain fully antifouling characteristics. EGNH2, in particular, displayed limited antifouling characteristic probably masked by the amine terminal group.

Wettable surfaces, such as COOH and OH, presented some kind of resistance to proteins adsorption confirming characteristics already reported in the literature[2].

Instead, hydrophobic surfaces displayed a good affinity for proteins, with a maximum of intensity for the methyl terminated SAMs.

From the second elution (data not shown) the amount of proteins drastically decreased for all the samples with only the bands at around 60 kDa clearly recognizable. For the antifouling surfaces (P4EG and EGNH2) no signals have been detected with the exception of a band in the albumin range in the second elution in water. Instead, the less wettable surfaces presented a more marked result compared to hydrophilic SAMs. In particular, the fluorinated SAM displayed the band of adsorption at 60 kDa in the elution with a higher concentration of isopropanol (ip2 and ip3), indicating a strong interaction with these proteins. CH3 terminated SAM showed a less binding strength compared to the previous, with visible bands until ip2. The last hydrophobic molecule, dAzBe, presented results comparable to the fluorinated SAM, with the profile that was more intense in ip2 and ip4. NH2 exhibited less marked bands and concentrated in the second water elution and in ip2.

The obtained results largely confirmed similar analysis previously reported in the literature[1,2,15]. However, as will be clear from the cell culture tests, it seams that protein adsorption influences principally the initial cell adhesion, while long-term MG63 cell culture seems not to be greatly affected by this parameter and, consequently, by SAM chemistry.

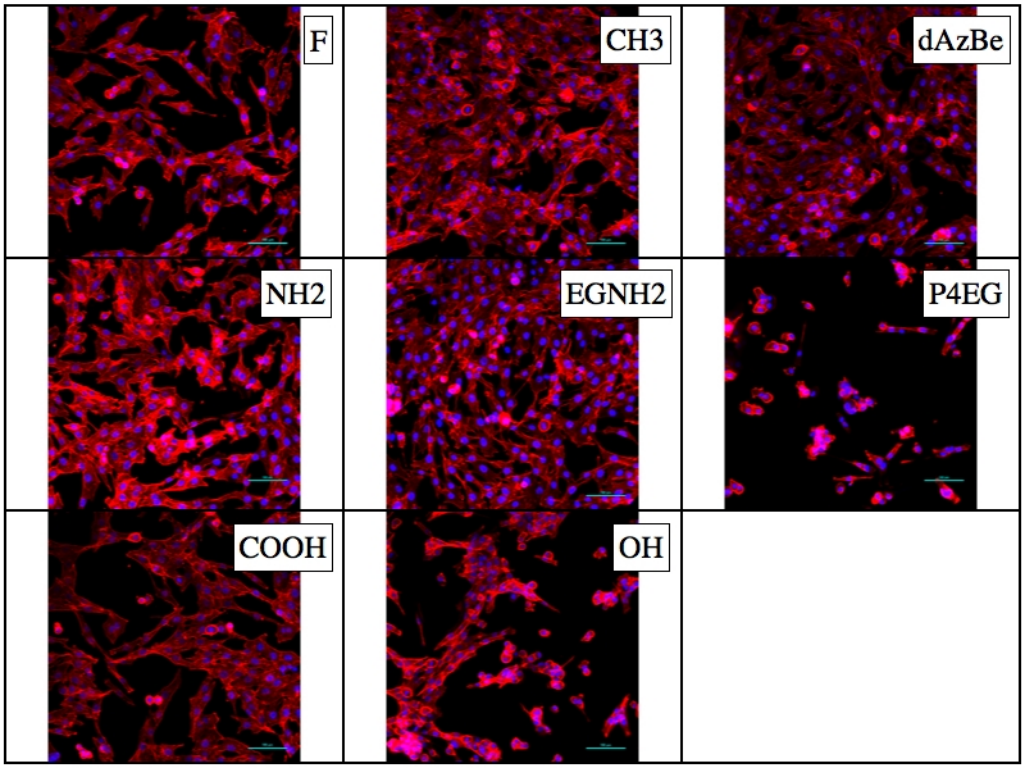

Figure 4.4.5: MG63 cells adhesion on the different SAMs surfaces after 24 hours from the seeding. Cell nuclei (blue spots) cell cytoskeletons (red) are clearly distinguishable.

Some parallel between initial cell adhesion and protein adsorption onto SAMs can be drawn observing Figure 4.4.5. One day after the seeding, osteoblast-like cells presented completely different response toward the various tested surfaces. In general, it has been noticed that cells adhered in greater number on surfaces with a higher amount of adsorbed proteins (Figure 4.4.6). The most hydrophobic surfaces, however, represented some exceptions since the higher protein adsorption, observed for these surfaces, didn't corresponded to a greater cell number. This can be explained considering the fact that also the type and conformation (determined by binding strength) of the adsorbed peptides play a fundamental role in cell adhesion[2].

This general view confirms the literature data attesting that mammalian cells prefer surfaces

with contact angle in the range of 40-80° [1]. In particular, it has been possible to note that the most hydrophilic surfaces (COOH and OH) showed worst results in comparison to amino terminated and dAzBe SAMs. The latter surface, on the contrary, presented the best results with a marked increase of cells in comparison to the initially seeded (28% more).

Even the morphological analysis exhibited some differences. On OH samples, a poor cell adhesion was noticed. Cells displayed a prevalently spherical shape and they tended to form clusters on the surface (Figure 4.4.5). On COOH a gradual increase in cell spreading was observed with more filopodia protruding from cytoplasm periphery and an acicular cell shape. On NH2 and dAzBe cells appeared to well and homogeneously adhere displaying a spread and star-like shape. A physiological morphology has been observed also on hydrophobic surfaces (Figure 4.4.5), even when cell number was relatively low such as on F.

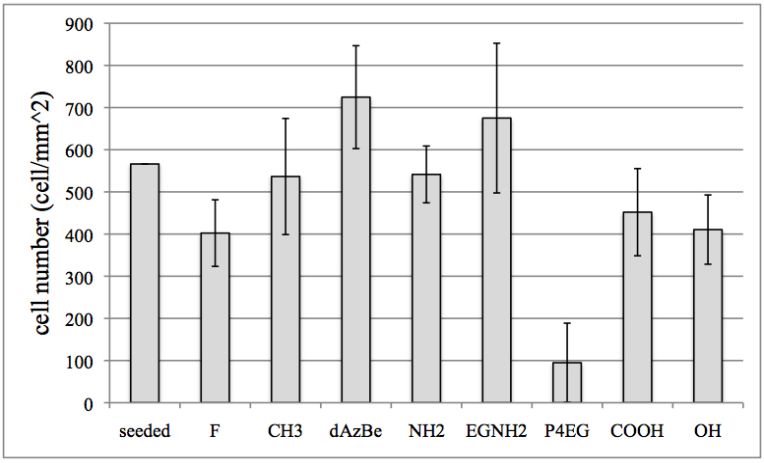

Figure 4.4.6: MG63 cell number per square millimetre 24 hours from the seeding. The initially seeded MG63 cells are represented by the first column

As expected the P4EG terminated SAM displayed the worst initial adhesion. Thanks to the antifouling properties of this molecule, less than 20% of cells survived after one day of culture.

Unexpectedly, the EGNH2 showed good adhesion properties, surpassed only by the diazo-

benzene terminal group. Cell morphology exhibited a parallel behaviour: on P4EG cells maintained a spherical profile and they have been observed to group in small clusters. On the contrary, cells adhering on EGNH2 showed a homogeneous surface coverage and a marked spread with many filopodia protruding from the cells boundary.

The biological response obtained on EGNH2 is really interesting since it seems to confirm the results previously described for protein adhesion: although the molecules present a relatively long ethylene glycol chain the antifouling characteristic appears to be masked by the terminal amino group with the consequence that a good proteins adsorption and a good cells adhesion are observed.

After three days of culture, cells reached confluence on all the SAM surfaces. This fact demonstrates that, within few days, MG63 cell responded with a uniform behaviour toward the different substrates.

Even on hydrophilic and P4EG terminated SAMs, those showing the worst initial adhesion, MG63 were able to finally proliferate and reach confluence.

As in the cases the mixed SAMs, the low adhesion of cells to the substrates and the parallel strong cell-cell interaction led to the possibility to detach the entire layer of cells without noticeable damages. Sheets of cell have been harvested from all the different SAMs.

All cells survived to the detachment process, as viability stain marked (Figure 4.4.7) (only one cell sheet image per ”class” of wettability is presented: CH3 as hydrophobic, NH2 as moderately wettable, EGNH2 as non-fouling, OH as hydrophilic).

The same detachment procedure applied on confluent cells seeded in the control Petri dish induced no cell sheet detachment. In this case cells remained adherent to the dish surface except where the tweezers tips scraped them from the Petri, forming small clusters of cells (Figure 4.4.7, Petri dish).

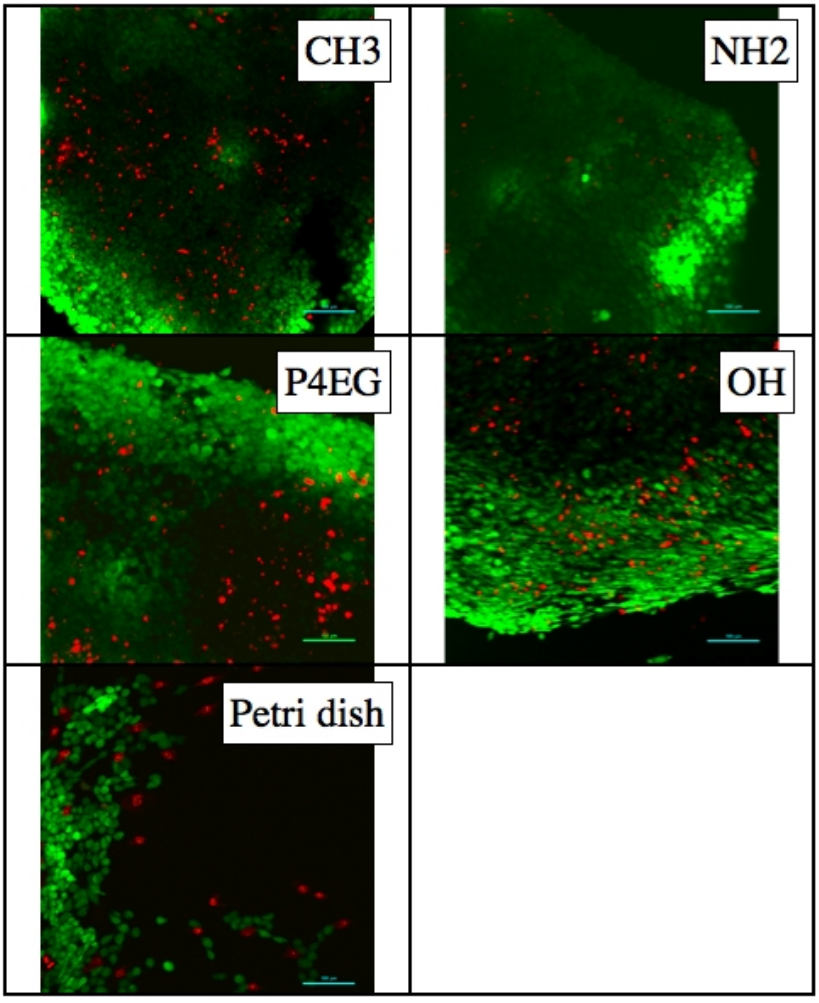

Figure 4.4.7: Cell sheets detached from SAMs and the results obtained trying to detach cells from the culture well (Petri dish). The cells stained in green represent alive cells whereas red cells are dead.

It has not been possible to quantitatively assess the detachment force but, up to the subjective impression of the authors, it seemed that slightly easier detachment occurred from surfaces with antifouling characteristic. However, apart from this impression, no appreciable detachment differences have been noticed.

What appears clear is that, although an apparent good adhesion to some kind of surfaces, as

testified by a spread morphology, this type of cells are, in fact, weakly attached to the SAM surfaces.

Finally, the sheets detached from SAMs were placed in a new culture well to test the adhesion capabilities of the lamina and assess the possibility, for these cell layers, to be loaded in scaffolds.

The test revealed that the cell sheets were able to re-adhere to the well in few hours and after 48h a high rate of viability was observed (Figure 4.4.8). As for the cases described in the previous chapter, the increase in dead cells is caused by limits in passive diffusion. No dead cells are, in fact, recognizable on the border of the sheet. The test results, however, can be considered as positive and confirm the possibility, for these cell sheets, to be loaded in a scaffold and found useful applications for *in vitro* tests.

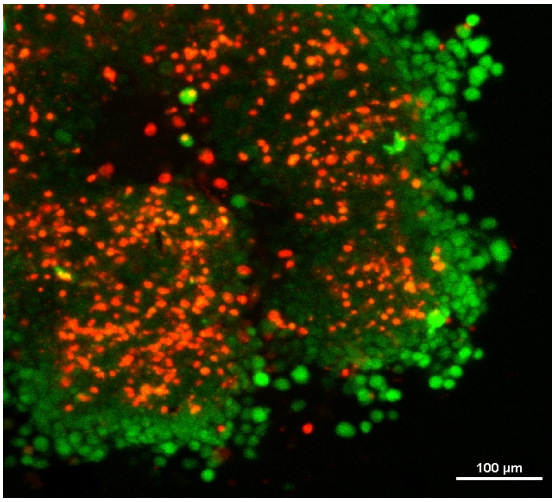

Figure 4.4.8: A MG63 cell sheet re-adhered to a culture Petri dish after 48h. Red spots are dead cells whereas alive cells are in green.

To authors' knowledge "spontaneous" cell detachment has never been reported for SAMs and, in the literature, there are few examples of similar behaviours. Guillaume-Gentil et

al.[17] reported "spontaneous" osteoblast cell sheet detachment from a poly-L-lysine/hyaluronic acid substrate. In this case, however, the progressive decrease in cell adhesion was correlated to an increase in the polyelectrolyte thickness. The detachment mechanism is, then, probably linked to an increasingly hydrated and softer surface that limited cell adhesion.

Despite comparable final results, this explanation cannot be valid for SAMs. The detachment mechanism seems to have a different nature since the adhesion of cells to the substrates appears weak independently of the characteristics of the terminal group. Further studies have to be performed to better understand the cells/SAMs interaction that leads to detachment. In practical terms, however, the results appear interesting in light of the possible applications.

General Conclusions

The force by which cells adhere to the surface of a scaffold is a remarkable feature for the success for a biomedical product. It is known that, for most of the cell lines, a certain degree of adhesion is required to start the process of proliferation and biological activation[18]. Conversely, when the material induces an excessive cell spreading, it is possible to observe undesired phenomena such as reduced cellular functionality[18]. The equilibrium between these two extreme situations represents an optimum in biocompatibility that, nevertheless, varies from case to case.

The field of bone regeneration is one of the most flourishing and active areas of research in the biomedical field and, thus, the study on the cells involved in this process and their adhesion are of considerable scientific interest.

In these terms, osteoblasts are no exception and a broad literature has been published about the understanding of how this type of cell adheres to a surface and the biological response that derive from this process[19,20,21]. During bone artificial regeneration a good cell adhesion has been always sought as a strategic factor for the success of an implant.

However, it is not obvious that a poor adhesion of osteoblasts to a surface would prove to be a

failure. In fact, observing the adhesion behaviour of osteoblast-like cells on SAMs, it has been possible to report the interesting phenomenon described in this chapter.

On the investigated surfaces, MG63 cells displayed different initial adhesion but, once they reached confluence, it was possible to easily recover an undamaged sheet of cells from all the tested SAMs. The authors saw in this process not only the possibility to report an unknown, peculiar, behaviour of osteoblast-like cells while interacting with nano-structured surfaces, but also a possible application for this result.

The chemical/physical characterization of the variously terminated and mixed SAMs showed that, beside a different chemical nature, the selected molecules covered a broad range of wettability. These characteristics led to a wide range of protein desorption behaviours that were largely confirmed by the data reported in the literature. An interesting exception has been represented by the case of EGNH2 where, despite the hexa-ethylene glycol group, a quite marked adsorption of proteins has been found.

Protein adsorption differences, however, demonstrated to be of little, initial, influence for MG63 osteoblast-like cells and confluence has been reached within few days also on antifouling surfaces. Interestingly, it has been noticed that cells at confluence didn't adhere tightly to SAMs and that it was possible to easily detach an undamaged layer of cells, possibly large enough to be used for *in vitro* bone tissue engineering tests. In order to verify this possibility, detached cell sheets where placed in a new culture dish and the re-adhesion capability of cells was positively assessed.

The mechanism by which the MG63 cells are able to adhere and proliferate maintaining such a low adhesion to SAM substrates is not yet clear and no similar results have been obtained with other tested cell lines. Further studies are necessary to understand this phenomenon that, nevertheless, has interesting potentials.

Petri dish modified with thermoresponsive smart polymers are usually reported to be as one of the most effective way to harvest cell sheets[22,23,24], in the case of osteoblast, also other technique has been reported as possible alternative[25].

Although currently restricted to a specific cell line, the SAMs described in this chapter can

reasonably be considered as a possible alternative to these techniques in the production cell sheets of MG63 osteoblast-like cells, especially considering that these surfaces are easily prepared with a good repeatability.

FINAL REMARKS

The research activity described in this work was focused on the synthesis and characterization of substrates for cell sheet engineering. Different strategy has been investigated to obtain surfaces from which cell laminae could be harvested.
In the first part of this report the attention has been addressed to the investigation of PNIPAM, the most exploited polymer for this kind of applications.
The synthesis via ATRP of this polymer has been successfully verified and the smart characteristics of PNIPAM tested by different techniques. In particular, it has been assessed that the dry film thickness growth followed a linear trend, as predicted by controlled/living radical polymerization. AFM measurements demonstrated that the PNIPAM coating underwent the swelled to coiled transition as consequence of a temperature increase.

The effective cell sheet detachment has been assessed with different cell lines. At 37 °C, cells adhered to the PNIPAM-coated surfaces that displayed a positive biocompatibility for all cell lines. In few days cells were able to reach confluence. Then, decreasing temperature below the LCST cells detached in the form of an undamaged sheet as consequence of PNIPAM hydration.

The examination of the cell layers confirmed that cells survived to the lift-off process displaying good cell-cell junctions and a physiological state.

Furthermore, it has been demonstrated that cell sheets, placed in a new culture well, were able to re-adhere. This demonstrated the effectiveness of the process and the possibility to use the cell layers for biomedical applications.

Final Remarks

Subsequently a deep investigation of the outermost region of the PNIPAM brushes has been carried out to verify the real physical state of the surface with which biological environment comes in contact during cell culture.
The collected data on advancing contact angle confirmed the qualitative theoretical modelling reported in the literature for tethered PNIPAM. The Wilhelmy plate test evidenced the appearing of a stick/slip phenomenon never reported before for PNIPAM brushes. A model of this behaviour has been proposed. This has been based on the possibility that the PNIPAM chains can reorient exposing the hydrophilic moieties toward water also at a temperature above the LCST. Furthermore, the possible factors that influence this kinetics phenomenon have been evidenced.

Finally the correlation between tethered brushes thickness and smart characteristics has been examined.

The influence of PNIPAM brush length on different cell lines has been analyzed.

The samples with different brushes thickness have been tested again by means of the Wilhelmy plate technique. While temperature and wetting/de-wetting speed were varied, a decrease in temperature responsiveness has been noticed for thicker PNIPAM-coating. At the same time, an increase in wettability has been observed.

Once again, the stick/slip phenomenon has been observed above the LCST. The new data have been merged with the previously described model observing a good correlation.

In the second part of the work, it has been investigated the possibility to harvest a cell sheet of osteoblast-like cells from SAMs without the need of any active stimuli. This behaviour, although restricted to a specific cell line, can be potentially useful for *in vitro* test devoted to bone tissue engineering.
The interesting phenomenon has been investigated on differently terminating SAMs. The chemical/physical characterization of the various SAMs showed that, due to the different chemical nature, the selected molecules covered a broad range of wettability. This caused a different initial adhesion of MG63 cells but, once the cells reached confluence, it was possible to easily recover an undamaged sheet of cells from all the tested SAMs. Then, despite the

chemical differences, all the tested surfaces displayed the ability to induce a low MG63 adhesion.

Although currently restricted to a specific cell line, this new technique can reasonably be considered as a possible alternative to harvest osteoblast-like cells, especially considering that these surfaces are easily prepared with a good repeatability.

REFERENCES:

References “Preface and Objectives”

[1] Joseph Yang, Masayuki Yamato, Kohji Nishida, Takeshi Ohki, Masato Kanzaki, Hidekazu Sekine, Tatsuya Shimizu, and Teruo Okano, Journal Of Controlled Release : Official Journal Of The Controlled Release Society **116**, 193-203 (2006).

[2] J P Vacanti, Archives Of Surgery (Chicago, Ill. : 1960) **123**, 545-9 (1988).

[3] R Langer and JP Vacanti, Science **260**, 920-926 (1993).

[4] C A Vacanti and J P Vacanti, The Orthopedic Clinics Of North America **31**, 351-6 (2000).

[5] C A Vacanti, L J Bonassar, M P Vacanti, and J Shufflebarger, The New England Journal Of Medicine **344**, 1511-4 (2001).

[6] T Shin'oka, Y Imai, and Y Ikada, The New England Journal Of Medicine **344**, 532-3 (2001).

[7] Melissa Poh, Matthew Boyer, Amy Solan, Shannon L M Dahl, Dawn Pedrotty, Soma S R Banik, J Andrew McKee, Rebecca Y Klinger, Christopher M Counter, and Laura E Niklason, The Lancet **365**, 2122-2124 (2005).

[8] Anthony Atala, Stuart B Bauer, Shay Soker, James J Yoo, and Alan B Retik, The Lancet **367**, 1241-1246 (2006).

References Chapter 1

[1] Masayuki Yamato, Yoshikatsu Akiyama, Jun Kobayashi, Joseph Yang, Akihiko Kikuchi, and Teruo Okano, Progress In Polymer Science **32**, 1123-1133 (2007).

[2] Joseph Yang, Masayuki Yamato, Chinatsu Kohno, Ayako Nishimoto, Hidekazu Sekine, Fumio Fukai, and Teruo Okano, Biomaterials **26**, 6415-22 (2005).

[3] B Ronneberger, W J Kao, J M Anderson, and T Kissel, Journal Of Biomedical Materials Research **30**, 31-40 (1996).

[4] J. M. Schakenraad, M. J. Hardonk, J. Feijen, I. Molenaar, and P. Nieuwenhuis, Journal Of Biomedical Materials Research **24**, 529-45 (1990).

[5] Hak-Joon Sung, Carson Meredith, Chad Johnson, and Zorina S. Galis, Biomaterials **25**, 5735-42 (2004).

[6] René Drucker-Colín and Leticia Verdugo-Díaz, Cellular And Molecular Neurobiology **24**, 301-316 (2004).

[7] Lucian V. Del Priore, Henry J. Kaplan, Tongalp H. Tezel, Nobutsugu Hayashi, Adam S. Berger, and W. Richard Green, American Journal Of Ophthalmology **131**, 472-480 (2001).

[8] Tatsuya Shimizu, Masayuki Yamato, Akihiko Kikuchi, and Teruo Okano, Biomaterials **24**, 2309-2316 (2003).

[9] Teruo Okano, Noriko Yamada, Hideaki Sakai, and Yasuhisa Sakurai, Journal Of Biomedical Materials Research **27**, 1243-51 (1993).

[10] Kazuyuki Nakajima, Shizuyo Honda, Yasuko Nakamura, Fernando López-Redondo, Shinichi Kohsaka, Masayuki Yamato, Akihiko Kikuchi, and Teruo Okano, Biomaterials **22**, 1213-1223 (2001).

[11] M Yamato, M Utsumi, A Kushida, C Konno, A Kikuchi, and T Okano, Tissue Engineering **7**, 473-80 (2001).

[12] Masayuki Yamato and Teruo Okano, Materials Today **7**, 42-47 (2004).

[13] Joseph Yang, Masayuki Yamato, Kohji Nishida, Takeshi Ohki, Masato Kanzaki, Hidekazu Sekine, Tatsuya Shimizu, and Teruo Okano, Journal Of Controlled Release : Official Journal Of The Controlled Release Society **116**, 193-203 (2006).

[14] Marta A. Cooperstein and Heather E. Canavan, Langmuir 091030152049000 (2009).

[15] H.G. Schild, Progress In Polymer Science **17**, 162-249 (1992).

[16] A Kushida, M Yamato, Y Isoi, A Kikuchi, and T Okano, European Cells & Materials **10**, 23-30; discussion 23-30 (2005).

[17] Ai Kushida, Masayuki Yamato, Chie Konno, Akihiko Kikuchi, Yasuhisa Sakurai, and Teruo Okano, Journal Of Biomedical Materials Research **45**, 355-362 (1999).

[18] Heather E Canavan, Xuanhong Cheng, Daniel J Graham, Buddy D Ratner, and David G Castner, Langmuir : The ACS Journal Of Surfaces And Colloids **21**, 1949-55 (2005).

[19] Heather E. Canavan, Xuanhong Cheng, Daniel J. Graham, Buddy D. Ratner, and David G. Castner, Journal Of Biomedical Materials Research. Part A **75**, 1-13 (2005).

[20] Takeshi Ide, Kohji Nishida, Masayuki Yamato, Taizo Sumide, Mika Utsumi, Takayuki Nozaki, Akihiko Kikuchi, Teruo Okano, and Yasuo Tano, Biomaterials **27**, 607-14 (2006).

[21] Yasutaka Hayashida, Kohji Nishida, Masayuki Yamato, Katsuhiko Watanabe, Naoyuki Maeda, Hitoshi Watanabe, Akihiko Kikuchi, Teruo Okano, and Yasuo Tano, Investigative Ophthalmology & Visual Science **46**, 1632-9 (2005).

[22] Katsuhiko Watanabe, Masayuki Yamato, Yasutaka Hayashida, Joseph Yang, Akihiko Kikuchi, Teruo Okano, Yasuo Tano, and Kohji Nishida, Biomaterials **28**, 745-9 (2007).

[23] Joseph Yang, Masayuki Yamato, Tatsuya Shimizu, Hidekazu Sekine, Kazuo Ohashi, Masato Kanzaki, Takeshi Ohki, Kohji Nishida, and Teruo Okano, Biomaterials **28**, 5033-43 (2007).

[24] Kohji Nishida, Masayuki Yamato, Yasutaka Hayashida, Katsuhiko Watanabe, Naoyuki Maeda, Hitoshi Watanabe, Kazuaki Yamamoto, Shigeru Nagai, Akihiko Kikuchi, Yasuo Tano, and Teruo Okano, Transplantation **77**, 379-85 (2004).

[25] Yasutaka Hayashida, Kohji Nishida, Masayuki Yamato, Joseph Yang, Hiroaki Sugiyama, Katsuhiko Watanabe, Yuichi Hori, Naoyuki Maeda, Akihiko Kikuchi, Teruo Okano, and Yasuo Tano, Investigative Ophthalmology & Visual Science **47**, 552-7 (2006).

[26] Tatsuya Shimizu, Masayuki Yamato, Yuki Isoi, Takumitsu Akutsu, Takeshi Setomaru, Kazuhiko Abe, Akihiko Kikuchi, Mitsuo Umezu, and Teruo Okano, Circulation Research **90**, e40 (2002).

[27] Yuji Haraguchi, Tatsuya Shimizu, Masayuki Yamato, Akihiko Kikuchi, and Teruo Okano, Biomaterials **27**, 4765-74 (2006).

[28] Sachiko Sekiya, Tatsuya Shimizu, Masayuki Yamato, Akihiko Kikuchi, and Teruo Okano, Biochemical And Biophysical Research Communications **341**, 573-82 (2006).

[29] Tatsuya Shimizu, Hidekazu Sekine, Yuki Isoi, Masayuki Yamato, Akihiko Kikuchi, and Teruo Okano, Tissue Engineering **12**, 499-507 (2006).

References

[30] Tatsuya Shimizu, Hidekazu Sekine, Joseph Yang, Yuki Isoi, Masayuki Yamato, Akihiko Kikuchi, Eiji Kobayashi, and Teruo Okano, The FASEB Journal : Official Publication Of The Federation Of American Societies For Experimental Biology **20**, 708-10 (2006).

[31] Martin A Cole, Nicolas H Voelcker, Helmut Thissen, and Hans J Griesser, Biomaterials **30**, 1827-50 (2009).

[32] Akihiko Kikuchi and Teruo Okano, Journal Of Controlled Release : Official Journal Of The Controlled Release Society **101**, 69-84 (2005).

References Chapter 2.1

[1] Finklea Harry O., Ravenscroft Melissa S., and Snider Daniel A., Langmuir **9**, 223-227 (1993).

[2] S. J. Stranick, P. S. Weiss, A. N. Parikh, and D. L. Allara, in *39th National Symposium Of The American Vacuum Society* (AVS, Chicago, Illinois (USA), 1993), pp. 739-741.

[3] J Christopher Love, Lara A Estroff, Jennah K Kriebel, Ralph G Nuzzo, and George M Whitesides, Chemical Reviews **105**, 1103-69 (2005).

[4] Bain Colin D., Troughton E. Barry, Tao Yu Tai, Evall Joseph, Whitesides George M., and Nuzzo Ralph G., Journal Of The American Chemical Society **111**, 321-335 (1989).

[5] L. H. Dubois and R. G. Nuzzo, Annual Review Of Physical Chemistry **43**, 437-463 (1992).

[6] J. Christopher Love, Daniel B. Wolfe, Richard Haasch, Michael L. Chabinyc, Kateri E. Paul, George M. Whitesides, and Ralph G. Nuzzo, J. Am. Chem. Soc **125**, 2597-2609 (2003).

[7] Arthur W. Adamson and Alice P. Gast, *Physical Chemistry Of Surfaces* (Wiley - Interscience , 1997), p. 808.

[8] Schneider Thomas W. and Buttry Daniel A., Journal Of The American Chemical Society **115**, 12391-12397 (1993).

[9] Takao Ishida,*,†,‡, Wataru Mizutani,§, Hiroaki Azehara,§,∥, Fuminobu Sato,∥, Nami Choi,⊥, Uichi Akiba,∥, Masamichi Fujihira,∥ and, and Tokumoto§ Hiroshi, Langmuir **17**, 7459-7463 (2001).

[10] Dong Yan,, and Jeremy A. Saunders, and Jennings* G. Kane, Langmuir **19**, 9290-9296 (2003).

[11] Oliver Dannenberger,†,‡, J. Jens Wolff,§ and, and Manfred Buck*,†, Langmuir **14**, 4679-4682 (1998).

[12] and Laurent Huron, Ellis* Thomas H., and Kruus Erik, Langmuir **13**, 5335-5340 (1997).

[13] Frank Schreiber, Progress In Surface Science **65**, 151-256 (2000).

[14] Masihul Hasan, Donald Bethell, and Mathias Brust, Journal Of The American Chemical Society **124**, 1132-3 (2002).

References

[15] Jae-Gook Lee, Junseok Lee, and John T Yates, Journal Of The American Chemical Society **126**, 440-1 (2004).

[16] Bareman James P. and Klein Michael L. , The Journal Of Physical Chemistry **94**, 5202-5205 (1990).

[17] Melinda K. Ferguson,, and Emily R. Low, and Morris* John R., Langmuir **20**, 3319-3323 (2004).

[18] R. Valiokas, M. Oestbolm, S. Svedhem, and S. C. T. Svensson, The Journal Of Physical Chemistry B **106**, 10401-10409 (2002).

[19] Sun Li and Crooks Richard M., Langmuir **9**, 1951-1954 (1993).

[20] Jun Nara, Shin'ichi Higai, Yoshitada Morikawa, and Takahisa Ohno, The Journal Of Chemical Physics **120**, 6705-11 (2004).

[21] N. Camillone III, C. E. D. Chidsey, P. Eisenberger, P. Fenter, J. Li, K. S. Liang, G.-Y. Liu, and G. Scoles, The Journal Of Chemical Physics **99**, 744-747 (1993).

[22] Irmgard Wenzl,, Chi Ming Yam,, and David Barriet, and Lee* T. Randall, Langmuir **19**, 10217-10224 (2003).

[23] Byeongwon Park,†, Michael Chandross,, Mark J. Stevens,* and, and Grest Gary S., Langmuir **19**, 9239-9245 (2003).

[24] Mar Wen and Klein Michael L. , Langmuir **10**, 188-196 (1994).

[25] M Toerker, Surface Science **445**, 100-108 (2000).

References Chapter 2.2

[1] M.R. Aguilar, C. Elvira, A. Gallardo, B. Vázquez, and J.S. Román, in *Topics In Tissue Engineering Vol. 3*, N. Ashammakhi, R. Reis, and E. Chiellini (2007), pp. 1-27.

[2] R Dagani, Chemical And Engineering News **73**, 30-33 (1995).

[3] I Y Galaev, M N Gupta, and B Mattiasson, CHEMTECH **26**, 19-25 (1996).

[4] Teruo Okano, Advances In Polymer Science **110**, 179-197 (1993).

[5] Mitsuhiro Shibayama and Toyoichi Tanaka, Advances In Polymer Science **109**, 1-62 (1993).

[6] H Brønsted and J Kopecek, in *Polyelectrolyte Gels: Properties, Preparation, And Applications*, S. Harland Ronald and Robert K Prud"homme (American Chemical Society, Washington DC, USA, 1992), pp. 285-304.

[7] V A Kabanov, Polymer Science **36**, 143-156 (1994).

[8] I Y Galaev and B Mattiasson, Trends In Biotechnology **17**, 335-40 (1999).

[9] E Gil and S Hudson, Progress In Polymer Science **29**, 1173-1222 (2004).

[10] Shouei Fujishige, K. Kubota, and I. Ando, The Journal Of Physical Chemistry **93**, 3311-3313 (1989).

[11] X Zhang, R Zhuo, and Y Yang, Biomaterials **23**, 1313-8 (2002).

[12] H.G. Schild, Progress In Polymer Science **17**, 162-249 (1992).

[13] Mitsuhiro Ebara, Masayuki Yamato, Motohiro Hirose, Takao Aoyagi, Akihiko Kikuchi, Kiyotaka Sakai, and Teruo Okano, Biomacromolecules **4**, 344-9 (2003).

[14] F Eeckman, European Polymer Journal **40**, 873-881 (2004).

[15] Martin A Cole, Nicolas H Voelcker, Helmut Thissen, and Hans J Griesser, Biomaterials **30**, 1827-50 (2009).

[16] W Brown, K Schillen, and S Hvidt, Journal Of Physical Chemistry **96**, 6038-6044 (1992).

[17] Es Ron and Le Bromberg, Advanced Drug Delivery Reviews **31**, 197-221 (1998).

[18] Y Qiu and K Park, Advanced Drug Delivery Reviews **53**, 321-39 (2001).

[19] Byeongmoon Jeong, Sung Wan Kim, and You Han Bae, Advanced Drug Delivery Reviews **54**, 37-51 (2002).

[20] N Nath and A Chilkoti, Journal Of American Chemical Society **123**, 8197–8202 (2001).

[21] Kathleen Di Zio and David A Tirrell, Macromolecules **36**, 1553–1558 (2003).

[22] Yuichi Ohya, Megumi Toyohara, Mitsuhiro Sasakawa, Hidetoshi Arimura, and Tatsuro Ouchi, Macromolecular Bioscience **5**, 273-276 (2005).

[23] Zaki Megeed, Ryan M Winters, and Martin L Yarmush, Biomacromolecules **7**, 999-1004 (2006).

[24] D E Meyer, G A Kong, M W Dewhirst, M R Zalutsky, and A Chilkoti, Cancer Research **61**, 1548-1554 (2001).

[25] D E Meyer, B C Shin, G A Kong, M W Dewhirst, and A Chilkoti, Journal Of Controlled Release **74**, 213-224 (2001).

[26] S Dai, P Ravi, K C Tam, B W Mao, and L H Gan, Langmuir **19**, 5175-5177 (2003).

[27] Sarah Sanjuan and Yvette Tran, Macromolecules **41**, 8721-8728 (2008).

[28] Joerg Lahann and Robert Langer, MRS Bulletin **30**, 185-188 (2005).

[29] Sang Yeob Park and You Han Bae, Macromolecular Rapid Communications **273**, 269-273 (1999).

[30] M K Chourasia and S K Jain, Journal Of Pharmacy & Pharmaceutical Sciences **6**, 33-66 (2003).

[31] W T Godbey and A G Mikos, Journal Of Controlled Release : Official Journal Of The Controlled Release Society **72**, 115-25 (2001).

[32] J. M. Sansiñena, V. Olazábal, T. F. Otero, C. N. Polo Da Fonseca, and Marco-A. De Paoli, Chemical Communications 2217-2218 (1997).

[33] J A M Sondag-Huethorst and L G J Fokkink, Langmuir **10**, 4380-4387 (1994).

[34] Nicholas L Abbott and George M Whitesides, Langmuir **10**, 1493-1497 (1994).

[35] Joerg Lahann, Samir Mitragotri, Thanh-Nga Tran, Hiroki Kaido, Jagannathan Sundaram, Insung S Choi, Saskia Hoffer, Gabor A Somorjai, and Robert Langer, Science (New York, N.Y.) **299**, 371-374 (2003).

[36] Xuemei Wang, Andrei B Kharitonov, Eugenii Katz, and Itamar Willner, Chemical Communications 1542-1543 (2003).

[37] Xueme Wang, Eugenii Katz, and Itamar Willner, Electrochemistry Communications **5**, 814-818 (2003).

References

[38] K. Ichimura, Science **288**, 1624-1626 (2000).

[39] a Hoffman and P Stayton, Progress In Polymer Science **32**, 922-932 (2007).

[40] a Kumar, a Srivastava, I Galaev, and B Mattiasson, Progress In Polymer Science **32**, 1205-1237 (2007).

[41] J Rodriguezhernandez, F Checot, Y Gnanou, and S Lecommandoux, Progress In Polymer Science **30**, 691-724 (2005).

References Chapter 2.3

[1] K Matyjaszewski and A H Mueller, Progress In Polymer Science **31**, 1039-1040 (2006).

[2] Krzysztof Matyjaszewski and James Spanswick, Materials Today **8**, 26-33 (2005).

[3] Mitsuru Kato, Masami Kamigaito, Mitsuo Sawamoto, and Toshinobu Higashimura, Macromolecules **28**, 1721–1723 (1995).

[4] Jin-Shan Wang and Krzysztof Matyjaszewski, Journal Of American Chemical Society **117**, 5614–5615 (1995).

[5] Tomislav Pintauer and Krzysztof Matyjaszewski, Coordination Chemistry Reviews **249**, 1155-1184 (2005).

[6] J Qiu, B Charleux, and K Matyjaszewski, Progress In Polymer Science **26**, 2083-2134 (2001).

[7] H L Hsieh and R P Quirk, *Anionic Polymerization: Principles And Practical Applications* (Marcel Dekker, New York, 1996).

[8] K Matyjaszewski and M Sawamoto, *Cationic Polymerization Mechanisms Synthesis And Applications* (Marcel Dekker, New York, 1996), pp. 265-380.

[9] Tomislav Pintauer, Blayne McKenzie, and Krzysztof Matyjaszewski, ACS Symposium SerieS **854**, 130–147 (2003).

[10] Daniel A Singleton, Daniel T III Nowlan, Nazeem Jahed, and Krzysztof Matyjaszewski, Macromolecules **36**, 8609–8616 (2003).

[11] Hanns Fischer, Macromolecules **30**, 5666–5672 (1997).

[12] Hanns Fischer, Journal Of Polymer Science, Part A: Polymer Chemistry **37**, 1885-1901 (1999).

[13] M Souaille and H Fischer, Macromolecules **33**, 7378–7394 (2000).

[14] W Braunecker and K Matyjaszewski, Journal Of Molecular Catalysis A: Chemical **254**, 155-164 (2006).

[15] K Matyjaszewski and J Xia, Chemical Reviews **101**, 2921–2990 (2001).

References

[16] Jérôme Gromada, James Spanswick, and Krzysztof Matyjaszewski, Macromolecular Chemistry And Physics **205**, 551-566 (2004).

[17] G Moineau, Ph Dubois, R Jérôme, T Senninger, and Ph Teyssié, Macromolecules **31**, 545–547 (1998).

[18] Jérôme Gromada and Krzysztof Matyjaszewski, Macromolecules **34**, 7664-7671 (2001).

[19] W Jakubowski and K Matyjaszewski, Macromolecules **38**, 4139-4146 (2005).

[20] Wojciech Jakubowski, Ke Min, and Krzysztof Matyjaszewski, Macromolecules **39**, 39-45 (2006).

[21] K Matyjaszewski and K A Davis, Advances In Polymer Science **159**, 2-166 (2002).

[22] K Matyjaszewski, Progress In Polymer Science **30**, 858-875 (2005).

[23] Krzysztof Matyjaszewski, Wojciech Jakubowski, Ke Min, Wei Tang, Jinyu Huang, Wade A Braunecker, and Nicolay V Tsarevsky, Proceedings Of The National Academy Of Sciences **103**, 15309-15314 (2006).

References Chapter 3.1

[1] Stephan Schmidt, Hubert Motschmann, Thomas Hellweg, and Regine von Klitzing, Polymer **49**, 749-756 (2008).

[2] H.G. Schild, Progress In Polymer Science **17**, 162-249 (1992).

[3] Howard G. Schild and David A. Tirrell, The Journal Of Physical Chemistry **94**, 4352-4356 (1990).

[4] I DIMITROV, B TRZEBICKA, A MULLER, A DWORAK, and C TSVETANOV, Progress In Polymer Science **32**, 1275-1343 (2007).

[5] Solon Mias, Jan Sudor, and Henri Camon, Microsystem Technologies **14**, 691-695 (2007).

[6] Young Mooa Lee and Jin Kie Shim, Polymer **38**, 1227-1232 (1997).

[7] T. NONAKA, K. HASHIMOTO, and S. KURIHARA, Journal Of Applied Polymer Science **66**, 209-216 (1997).

[8] Ryo Yoshida, Katsumi Uchida, Yuzo Kaneko, Kiyotaka Sakai, Akihiko Kikuchi, Yasuhisa Sakurai, and Teruo Okano, Nature **374**, 240-242 (1995).

[9] Martin A Cole, Nicolas H Voelcker, Helmut Thissen, and Hans J Griesser, Biomaterials **30**, 1827-50 (2009).

[10] E Gil and S Hudson, Progress In Polymer Science **29**, 1173-1222 (2004).

[11] Charles McCormick, Stacey Kirkland, and Adam York, Polymer Reviews **46**, 421-443 (2006).

[12] M.R. Aguilar, C. Elvira, A. Gallardo, B. Vázquez, and J.S. Román, in *Topics In Tissue Engineering Vol. 3*, N. Ashammakhi, R. Reis, and E. Chiellini (2007), pp. 1-27.

[13] Yuzo Kaneko, Satoki Nakamura, Kiyotaka Sakai, Takao Aoyagi, Akihiko Kikuchi, Yasuhisa Sakurai, and Teruo Okano, Macromolecules **31**, 6099-6105 (1998).

[14] T OKANO, Y BAE, H JACOBS, and S KIM, Journal Of Controlled Release **11**, 255-265 (1990).

[15] S Chun, Journal Of Controlled Release **38**, 39-47 (1996).

[16] I Y Galaev and B Mattiasson, Trends In Biotechnology **17**, 335-40 (1999).

[17] N. Nath and A. Chilkoti, Advanced Materials **14**, 1243-1247 (2002).

[18] Hideko Kanazawa, Kazuo Yamamoto, Yoshikazu Matsushima, Nobuharu Takai, Akihiko Kikuchi, Yasuhisa Sakurai, and Teruo Okano, Analytical Chemistry **68**, 100-105 (1996).

[19] Marta A. Cooperstein and Heather E. Canavan, Langmuir (2009).

[20] T Okano, Biomaterials **16**, 297-303 (1995).

[21] M Yamato, Biomaterials **21**, 981-986 (2000).

[22] Masayuki Yamato, Minako Okuhara, Fumiko Karikusa, Akihiko Kikuchi, Yasuhisa Sakurai, and Teruo Okano, Journal Of Biomedical Materials Research **44**, 44-52 (1999).

[23] Peter Kingshott and Hans J Griesser, Journal Of Physical Chemistry B **4**, 403-412 (1999).

[24] G. Graziano, F. Catanzano, and G. Barone, Journal Of Thermal Analysis And Calorimetry **57**, 329-341 (1999).

[25] K. Binder, J. Baschnagel, M. Müller, W. Paul, and F. Rampf, Macromolecular Symposia **237**, 128-138 (2006).

[26] Sergio Mendez, John G Curro, John D Mccoy, and Gabriel P Lopez, Macromolecules **38**, 174-181 (2005).

[27] E. B. Zhulina, O. V. Borisov, V. A. Pryamitsyn, and T. M. Birshtein, Macromolecules **24**, 140-149 (1991).

[28] Vladimir a. Baulin and Avi Halperin, Macromolecular Theory And Simulations **12**, 549-559 (2003).

[29] S. Balamurugan, Sergio Mendez, Sreelatha S. Balamurugan, Michael J. O'Brie, and Gabriel P. López, Langmuir **19**, 2545-2549 (2003).

[30] Guangming Liu and Guangzhao Zhang, The Journal Of Physical Chemistry. B **109**, 743-7 (2005).

[31] Guangzhao Zhang, Macromolecules **37**, 6553-6557 (2004).

[32] H. Yim, M. S. Kent, S. Mendez, G. P. Lopez, S. Satija, and Y. Seo, Macromolecules **39**, 3420-3426 (2006).

[33] H. YIM, M. S. KENT, S. SATIJA, S. MENDEZ, S. S. BALAMURUGAN, S. BALAMURUGAN, and G. P. LOPEZ, Journal Of Polymer Science. Part B. Polymer Physics **42**, 3302-3310 (2004).

[34] X Zhu, C Yan, F M Winnik, and D Leckband, Langmuir : The ACS Journal Of Surfaces

And Colloids **23**, 162-9 (2007).

[35] Yoshikatsu Akiyama, Akihiko Kikuchi, Masayuki Yamato, and Teruo Okano, Langmuir **20**, 5506-5511 (2004).

[36] F J Xu, S P Zhong, L Y L Yung, E T Kang, and K G Neoh, Biomacromolecules **5**, 2392-403 (2004).

[37] Taiji Yakushiji and Kiyotaka Sakai, Langmuir : The ACS Journal Of Surfaces And Colloids **14**, 4657-4662 (1998).

[38] Yoshiyuki G. Takei, Takashi Aoki, Kohei Sanui, Naoya Ogata, Yasuhisa Sakurai, and Teruo Okano, Macromolecules **27**, 6163-6166 (1994).

[39] P Heinz, F Brétagnol, I Mannelli, L Sirghi, a Valsesia, G Ceccone, D Gilliland, K Landfester, H Rauscher, and F Rossi, Langmuir : The ACS Journal Of Surfaces And Colloids **24**, 6166-75 (2008).

[40] Kyle N Plunkett, Xi Zhu, Jeffrey S Moore, and Deborah E Leckband, Langmuir : The ACS Journal Of Surfaces And Colloids **22**, 4259-66 (2006).

[41] Xiangdong Feng, Jun Liu, Peter C. Rieke, and Glen E. Fryxell, Macromolecules **31**, 7845-7850 (1998).

[42] Alexander E Ivanov, Johan Ekeroth, Lars Nilsson, Bo Mattiasson, Björn Bergenståhl, and Igor Yu Galaev, Journal Of Colloid And Interface Science **296**, 538-44 (2006).

[43] Yoshiyuki G. Takei, Takashi Aoki, Kohei Sanui, Naoya Ogata, Yasuhisa Sakurai, and Teruo Okano, Macromolecules **27**, 6163-6166 (1994).

[44] a Kumar, a Srivastava, I Galaev, and B Mattiasson, Progress In Polymer Science **32**, 1205-1237 (2007).

References Chapter 3.2

[1] Krzysztof Matyjaszewski, Wojciech Jakubowski, Ke Min, Wei Tang, Jinyu Huang, Wade a Braunecker, and Nicolay V Tsarevsky, Proceedings Of The National Academy Of Sciences Of The United States Of America **103**, 15309-14 (2006).

[2] Rongyue Zhang, Gengliang Yang, Peiyong Xin, Li Qi, and Yi Chen, Journal Of Chromatography. A **1216**, 2404-11 (2009).

[3] Monique Martina, Gayathri Subramanyam, James C Weaver, Dietmar W Hutmacher, Daniel E Morse, and Suresh Valiyaveettil, Biomaterials **26**, 5609-16 (2005).

[4] Huilin Tu, Carla E Heitzman, and Paul V Braun, Langmuir : The ACS Journal Of Surfaces And Colloids **20**, 8313-20 (2004).

[5] Ellina Kesselman, Ory Ramon, Ronen Berkovici, and Yaron Paz, Polymers For Advanced Technologies **13**, 982-991 (2002).

[6] Kai Zhang, Hongtu Li, Shuang Zhao, Wei Wang, Shuwei Wang, Yaxin Xu, Wenzhi Yu, and Jingyuan Wang, Polymer Bulletin **57**, 253-259 (2006).

[7] Satoru Kidoaki, Shoji Ohya, Yasuhide Nakayama, and Takehisa Matsuda, Langmuir **17**, 2402-2407 (2001).

[8] By Darren M Jones, James R Smith, Wilhelm T S Huck, and Cameron Alexander, Advanced Materials **14**, 1130-1134 (2002).

[9] Jong-bum Kim, Merlin L Bruening, and Gregory L Baker, Journal Of American Chemical Society **112**, 7616-7617 (2000).

[10] T Takezawa, Y Mori, and K Yoshizato, Bio/technology (Nature Publishing Company) **8**, 854-6 (1990).

[11] Tatsuya Shimizu, Masayuki Yamato, Akihiko Kikuchi, and Teruo Okano, Biomaterials **24**, 2309-16 (2003).

[12] Noriko Yamada, Teruo Okano, Hideaki Sakai, Fumiko Karikusa, Yoshio Sawasaki, and Yasuhisa Sakurai, Die Makromolekulare Chemie, Rapid Communications Die Makromolekulare Chemie, Rapid Communications **11**, 571-576 (1990).

[13] Marta A. Cooperstein and Heather E. Canavan, Langmuir (2009).

[14] T Okano, Biomaterials **16**, 297-303 (1995).

[15] Eun Chul Cho, Yong Deuk Kim, and Kilwon Cho, Polymer **45**, 3195-3204 (2004).

[16] Aya Mizutani, Akihiko Kikuchi, Masayuki Yamato, Hideko Kanazawa, and Teruo Okano, Biomaterials **29**, 2073-81 (2008).

[17] H.G. Schild, Progress In Polymer Science **17**, 162-249 (1992).

[18] Valeri P. Tolstoy, Irina V. Chernyshova, and Valeri A. Skryshevsky, *Hand Book Of Infrared Spectroscopy Of Ultrathin Films* (A JOHN WILEY & SONS, INC., 2003), p. 710.

[19] Kyle N Plunkett, Xi Zhu, Jeffrey S Moore, and Deborah E Leckband, Langmuir : The ACS Journal Of Surfaces And Colloids **22**, 4259-66 (2006).

[20] T Farhan and W Huck, European Polymer Journal **40**, 1599-1604 (2004).

[21] P a Ramires, a Giuffrida, and E Milella, Biomaterials **23**, 397-406 (2002).

[22] Heather E Canavan, Xuanhong Cheng, Daniel J Graham, Buddy D Ratner, and David G Castner, Langmuir : The ACS Journal Of Surfaces And Colloids **21**, 1949-55 (2005).

[23] Heather E Canavan, Xuanhong Cheng, Daniel J Graham, Buddy D Ratner, and David G Castner, Journal Of Biomedical Materials Research. Part A **75**, 1-13 (2005).

[24] Vladimir a. Baulin and Avi Halperin, Macromolecular Theory And Simulations **12**, 549-559 (2003).

[25] G. Graziano, F. Catanzano, and G. Barone, Journal Of Thermal Analysis And Calorimetry **57**, 329-341 (1999).

[26] Sergio Mendez, John G Curro, John D Mccoy, and Gabriel P Lopez, Macromolecules **38**, 174-181 (2005).

[27] K. Binder, J. Baschnagel, M. Müller, W. Paul, and F. Rampf, Macromolecular Symposia **237**, 128-138 (2006).

[28] S. Balamurugan, Sergio Mendez, Sreelatha S. Balamurugan, Michael J. O'Brie, and Gabriel P. López, Langmuir **19**, 2545-2549 (2003).

[29] Guangming Liu and Guangzhao Zhang, The Journal Of Physical Chemistry. B **109**, 743-7 (2005).

[30] Guangzhao Zhang, Macromolecules **37**, 6553-6557 (2004).

[31] Yoshiyuki G. Takei, Takashi Aoki, Kohei Sanui, Naoya Ogata, Yasuhisa Sakurai, and Teruo Okano, Macromolecules **27**, 6163-6166 (1994).

[32] Taiji Yakushiji and Kiyotaka Sakai, Langmuir : The ACS Journal Of Surfaces And Colloids

14, 4657-4662 (1998).

[33] Xiangdong Feng, Jun Liu, Peter C. Rieke, and Glen E. Fryxell, Macromolecules **31**, 7845-7850 (1998).

[34] P Heinz, F Brétagnol, I Mannelli, L Sirghi, a Valsesia, G Ceccone, D Gilliland, K Landfester, H Rauscher, and F Rossi, Langmuir : The ACS Journal Of Surfaces And Colloids **24**, 6166-75 (2008).

[35] Alexander E Ivanov, Johan Ekeroth, Lars Nilsson, Bo Mattiasson, Björn Bergenståhl, and Igor Yu Galaev, Journal Of Colloid And Interface Science **296**, 538-44 (2006).

[36] F Schmitt, C Park, J Simon, H Ringsdorf, and J Israelachvili, Langmuir : The ACS Journal Of Surfaces And Colloids **14**, 2838-2845 (1998).

[37] Koji Abe, Hiroshi Takiguchi, Kaoru Tamada, and Au-thiol Sam, Langmuir : The ACS Journal Of Surfaces And Colloids **16**, 2394-2397 (2000).

[38] D Y Kwok and A W Neumann U, Advances In Colloid And Interface Science **81**, 167-249 (1999).

[39] J.D. Andrade, L.M. Smith, and D.E. Gregonis, in *Surface And Interfacial Aspects Of Biomedical Polymers* (Plenum press, New York, 1985), pp. 249-292.

[40] Vincent P Gilcreest, William M Carroll, Yuri A Rochev, Irena Blute, Kenneth A Dawson, and Alexander V Gorelov, Langmuir 10138-10145 (2004).

[41] M. Morra, E. Occhiello, and F. Garbassi, Journal Of Colloid And Interface Science **149**, 84-91 (1992).

[42] M. Morra, E. Occhiello, and F. Garbassi, Colloid & Polymer Science **271**, 696-704 (1993).

[43] A. H. Hogt, D. E. Gregonis, J. D. Andrade, W. S. Kim, J. Dankert, and J. Feijen, J. Colloid Interface Sci. **106**, 289 (1985).

[44] J. D. Andrade, S. M. Ma, R. N. King, and D. E. Gregonis, J. Colloid Interface Sci. **72**, 488 (1979).

[45] F. J. Holly and F. M. Refojo, in *Hydrogels For Medical And Related Applications*, J. D. Andrade (ACS Syrup. Series, Washington, D.C., 1976), p. 252.

[46] H. Yasuda, in *Plasma Polymerization* (Academic Press, Orlando, 1985), p. 352.

[47] Shan-yang Lin, Ko-shao Chen, and Liang Run-chu, Polymer **40**, 2619-2624 (1999).

References Chapter 3.3

1 X. Zhu, C. Yan, F. M. Winnik, and D. Leckband, *Langmuir : the ACS journal of surfaces and colloids*, 2007, 23, 162-9.

2 H. Yim, M. S. Kent, S. Mendez, G. P. Lopez, S. Satija, and Y. Seo, *Macromolecules*, 2006, 39, 3420-3426.

3 H. Yim, M. S. Kent, S. Mendez, S. S. Balamurugan, S. Balamurugan, G. P. Lopez, and S. Satija, *Macromolecules*, 2004, 37, 1994-1997.

4 M. A. Cole, N. H. Voelcker, H. Thissen, and H. J. Griesser, *Biomaterials*, 2009, 30, 1827-50.

5 Y. Akiyama, A. Kikuchi, M. Yamato, and T. Okano, *Langmuir*, 2004, 20, 5506-5511.

6 F. J. Xu, S. P. Zhong, L. Y. Yung, E. T. Kang, and K. G. Neoh, *Biomacromolecules*, 2004, 5, 2392-403.

7 J. Qiu, B. Charleux, and K. Matyjaszewski, *Progress in Polymer Science*, 2001, 26, 2083-2134.

8 F. A. Scholl, *The Journal of Cell Biology*, 2000, 151, 495-506.

9 K. N. Plunkett, X. Zhu, J. S. Moore, and D. E. Leckband, *Langmuir : the ACS journal of surfaces and colloids*, 2006, 22, 4259-66.

10 T. Farhan and W. Huck, *European Polymer Journal*, 2004, 40, 1599-1604.

11 S. Kidoaki, S. Ohya, Y. Nakayama, and T. Matsuda, *Langmuir*, 2001, 17, 2402-2407.

12 A. Mizutani, A. Kikuchi, M. Yamato, H. Kanazawa, and T. Okano, *Biomaterials*, 2008, 29, 2073-81.

13 H. Tu, C. E. Heitzman, and P. V. Braun, *Langmuir : the ACS journal of surfaces and colloids*, 2004, 20, 8313-20.

14 A. Kikuchi and T. Okano, *Journal of controlled release : official journal of the Controlled Release Society*, 2005, 101, 69-84.

References

15 T. Shimizu, M. Yamato, A. Kikuchi, and T. Okano, *Biomaterials*, 2003, 24, 2309-16.

16 T. Okano, *Advances in Polymer Science*, 1993, 110, 179-197.

17 T. Okano, *Biomaterials*, 1995, 16, 297-303.

References Chapter 4.1 - 4.2 – 4.3

[1] E. Katz, M. Lion-Dagan, and I. Willner, Journal Of Electroanalytical Chemistry **408**, 107-112 (1996).

[2] Shengfu Wang and Dan Du, Sensors **2**, 41-49 (2002).

[3] Hun-gi Hong and Wonchoul Park, Langmuir : The ACS Journal Of Surfaces And Colloids 2485-2492 (2001).

[4] V Budavari, Electrochimica Acta **48**, 3499-3508 (2003).

[5] E Katz and I Willner, Electrochemistry Communications **8**, 879-882 (2006).

[6] Muhammad N Yousaf, Eugene W L Chan, and M Mrksich, Angew. Chem. Int. Ed. **39**, 1943-1946 (2000).

[7] Muhammad N Yousaf, Benjamin T Houseman, and Milan Mrksich, Angew. Chem. Int. Ed. **40**, 1093-1096 (2001).

[8] Woon-Seok Yeo, Muhammad N Yousaf, and Milan Mrksich, Journal Of The American Chemical Society **125**, 14994-5 (2003).

[9] W Russell Everett and Ingrid Fritsch-faules, Analytica Chimica Acta **307**, 253-268 (1995).

[10] E Ostuni, Colloids And Surfaces B: Biointerfaces **15**, 3-30 (1999).

[11] P R Anil Kumar, H K Varma, and T V Kumary, Acta Biomaterialia **1**, 545-52 (2005).

[12] Brian Stevens, Yanzhe Yang, Arunesh Mohandas, Brent Stucker, and Kytai Truong Nguyen, Journal Of Biomedical Materials Research. Part B, Applied Biomaterials **85**, 573-82 (2008).

[13] António J Salgado, Olga P Coutinho, and Rui L Reis, Macromolecular Bioscience **4**, 743-65 (2004).

[14] Manabu Akahane, Akifumi Nakamura, Hajime Ohgushi, Hideki Shigematsu, Yoshiko Dohi, and Yoshinori Takakura, J Tissue Eng Regen Med **2**, 196-201 (2008).

[15] Yefang Zhou, Fulin Chen, Saey Tuan Ho, Maria Ann Woodruff, Tit Meng Lim, and

References

Dietmar W Hutmacher, Biomaterials **28**, 814-24 (2007).

[16] Noriko Yamada, Teruo Okano, Hideaki Sakai, Fumiko Karikusa, Yoshio Sawasaki, and Yasuhisa Sakurai, Die Makromolekulare Chemie, Rapid Communications Die Makromolekulare Chemie, Rapid Communications **11**, 571-576 (1990).

[17] Y.S. Kim, J.Y. Lim, H.J. Donahue, and T.L. Lowe, Tissue Eng. **11**, 30-40 (2005).

[18] E Tziampazis, J Kohn, and P V Moghe, Biomaterials **21**, 511-20 (2000).

[19] D W Branch, B C Wheeler, G J Brewer, and D E Leckband, Biomaterials **22**, 1035-47 (2001).

[20] Peter Kingshott and Hans J Griesser, Journal Of Physical Chemistry B **4**, 403-412 (1999).

[21] Wageesha Senaratne, Luisa Andruzzi, and Christopher K Ober, Biomacromolecules **6**, 2427-48 (2005).

[22] Yusuke Arima and Hiroo Iwata, Biomaterials **28**, 3074-82 (2007).

[23] H J Griesser, R C Chatelier, T R Gengenbach, G Johnson, and J G Steele, Journal Of Biomaterials Science. Polymer Edition **5**, 531-54 (1994).

References Chapter 4.4

[1] Yusuke Arima and Hiroo Iwata, Biomaterials **28**, 3074-82 (2007).

[2] N Faucheux, R Schweiss, K Lützow, C Werner, and T Groth, Biomaterials **25**, 2721-30 (2004).

[3] Christian Hoffmann and Günter E M Tovar, Journal Of Colloid And Interface Science **295**, 427-35 (2006).

[4] Inês C Gonçalves, M Cristina L Martins, Mário A Barbosa, Esmaeel Naeemi, and Buddy D Ratner, Journal Of Biomedical Materials Research. Part A **89**, 642-53 (2009).

[5] Colin A Scotchford, Christopher P Gilmore, Elaine Cooper, Graham J Leggett, and Sandra Downes, Journal Of Biomedical Materials Research **59**, 84-99 (2002).

[6] Antonella Motta, Claudio Migliaresi, Andrew W Lloyd, Stephen P Denyer, and Matteo Santin, Journal Of Bioactive And Compatible Polymers **17**, 23-35 (2002).

[7] Monique Martina, Gayathri Subramanyam, James C Weaver, Dietmar W Hutmacher, Daniel E Morse, and Suresh Valiyaveettil, Biomaterials **26**, 5609-16 (2005).

[8] E Ostuni, Colloids And Surfaces B: Biointerfaces **15**, 3-30 (1999).

[9] D Barriet, Current Opinion In Colloid & Interface Science **8**, 236-242 (2003).

[10] T. Ederth, K. Tamada, P. M. Claesson, R. Valiokas, R. Colorado, M. Graupe, O. E. Shmakova, and T. R. Lee, Journal Of Colloid And Interface Science **235**, 391-397 (2001).

[11] S. D. Evans, S. R. Johnson, H. Ringsdorf, L. M. Williams, and H. Wolf, Langmuir **14**, 6436-6440 (1998).

[12] J Christopher Love, Lara A Estroff, Jennah K Kriebel, Ralph G Nuzzo, and George M Whitesides, Chemical Reviews **105**, 1103-69 (2005).

[13] Chi Ming Yam, Maxence Deluge, David Tang, Amit Kumar, and Chengzhi Cai, Journal Of Colloid And Interface Science **296**, 118-30 (2006).

[14] Inês C Gonçalves, M Cristina L Martins, Mário a Barbosa, Esmaeel Naeemi, and Buddy D Ratner, Journal Of Biomedical Materials Research. Part A **89**, 642-53 (2009).

[15] V Tegoulia, Colloids And Surfaces B: Biointerfaces **24**, 217-228 (2002).

[16] N Faucheux, R Schweiss, K Lützow, C Werner, and T Groth, Biomaterials **25**, 2721-30 (2004).

[17] O. Guillaume-Gentil, T. Zambelli, Y. Akiyama, M. Yamato, T. Okano, and J. Vörös, in (UZH ETH, Zurich, 2008).

[18] Susan E. LaFlamme and Andrew Kowalczyk, *Cell Junctions: Adhesion, Development, And Disease* (WILEY-VCH Verlag GmbH & Co. KGaA, Weinheim, 2008), p. 301.

[19] Felicity R A J Rose and Richard O C Oreffo, Biochemical And Biophysical Research Communications **292**, 1-7 (2002).

[20] António J Salgado, Olga P Coutinho, and Rui L Reis, Macromolecular Bioscience **4**, 743-65 (2004).

[21] Brian Stevens, Yanzhe Yang, Arunesh Mohandas, Brent Stucker, and Kytai Truong Nguyen, Journal Of Biomedical Materials Research. Part B, Applied Biomaterials **85**, 573-82 (2008).

[22] Joseph Yang, Masayuki Yamato, Kohji Nishida, Takeshi Ohki, Masato Kanzaki, Hidekazu Sekine, Tatsuya Shimizu, and Teruo Okano, Journal Of Controlled Release : Official Journal Of The Controlled Release Society **116**, 193-203 (2006).

[23] Joseph Yang, Masayuki Yamato, Tatsuya Shimizu, Hidekazu Sekine, Kazuo Ohashi, Masato Kanzaki, Takeshi Ohki, Kohji Nishida, and Teruo Okano, Biomaterials **28**, 5033-43 (2007).

[24] Marta A. Cooperstein and Heather E. Canavan, Langmuir 091030152049000 (2009).

[25] Yefang Zhou, Fulin Chen, Saey Tuan Ho, Maria Ann Woodruff, Tit Meng Lim, and Dietmar W Hutmacher, Biomaterials **28**, 814-24 (2007).

ACKNOWLEDGMENTS

First of all, I would like to thank my advisors Prof. Claudio Milgiaresi an Dr. Antonella Motta, for giving me the possibility to work on an interesting argument in stimulating environment.

A special thanks goes to the peoples of “BIOtech”, “laboratorio Polimeri e Compositi”, Bernardo and Prof. Fontanari, for the help, the support and the happiness they gave me in these years.

I would like also to acknowledge all the researches and Professors I met during my PhD and who helped with measurements and discussions the evolution of the my work:

Dr. Tullio Toccoli (Ellipsometry), Prof. Salvatore Iannotta, Dr. Luca Minati and Dr. Giorgio Speranza (XPS), Dr. Claudio Della Volpe (contact angle measurements), Dr. Emanuela Callone (NMR), and all the one I surely forgot in these short acknowledgments.
Thank you all